

**FRICION HYDRO PILLAR RIVETING PROCESS OF TI-6Al-4V
TITANIUM SHEET**

D.S. Tsikayi

2015

FRICTION HYDRO PILLAR RIVETING PROCESS OF TI-6Al-4V
TITANIUM SHEET

By:

DAVIES SHAMISO TSIKAYI

Submitted in fulfilment of the requirements for the degree of Masters in
Technology Engineering: Mechanical to be awarded at the Nelson Mandela
Metropolitan University
Port Elizabeth
South Africa

March 2015

Supervisor: Prof. D. G. Hattingh

Declaration

I, Davies Shamiso Tsikayi (s209080067), hereby declare that the dissertation for Students qualification to be awarded is my own work and that it has not previously been submitted for assessment or completion of any postgraduate qualification to another University or for another qualification

Signature:

Date:

Acknowledgements

First of all, I would like to express my sincere gratitude to Prof. D. G. Hattingh for the supervision and unconditional support during this research masters. It would not have been possible without your assistance and vast knowledge in the field of Friction Processing.

I would like to thank the staff of NMMU metallurgy lab and eNtsa, “a Technology Innovation Agency station” for their technical and administrative support especially: Lucinda Lindsay and Nadine Marupen (administrative assistance), Glynn Erasmus and Marlon Koopman for their help in sample preparation as well as Amish Lalla, Melikhaya Nohonyaza and Jaromir Cizek for providing me assistance in the manufacturing of the test samples.

To my fellow researchers, Willem Pentz, Madindwa Mashinini, Dreyer Bernard, Raymond Pothier and Nthatisi Koloi, thank you for the help and constructive criticism.

Further special mention goes to my family, my mom, brother and sister who have always believed in me and supported me financially. I dedicate this dissertation to my late father who passed away in 2007. He made me the man I am today and because of his hard work, I got this far.

I would like to also thank my girlfriend Ayanda Kheswa, for her continued support and encouragement during the finalisation of my dissertation. To my friends Sipiwe Dhlamini, Clement Moyo, Tafadzwa Nembaware and Ralph Tizora, thank you.

Lastly, to the Lord Almighty, I am because YOU ARE. Thank You Lord.

I can do all things through Christ who strengthens me.

(Philippians 4:13)

Abstract

Friction Hydro Pillar Riveting Process of Ti-6Al-4V

Titanium sheet

D.S. Tsikayi

Faculty of Engineering, the Built Environment and Information Technology

Nelson Mandela Metropolitan University

PO BOX 77000, Port Elizabeth, South Africa

Dissertation for

Magister Technologiae: Engineering Mechanical

March 2015

Mechanical fasteners are used extensively in the joining of two or more metal plates or sheets. Riveted joints have been the joints of choice mainly for the Aerospace Industry. However for this research, Friction Hydro Pillar Processing has been used to develop and characterise a new riveting technique termed Friction Hydro Pillar Riveting (FHPR). Two overlapping 3.17 mm Ti-6Al-4V sheets were joined together using $\varnothing 6$ mm rivet which was friction processed. This research has focussed on the initial development of Friction Hydro Pillar Riveting thereby establishing a basic understanding of the influences of main process parameters, rotational speed and axial force - and also joint configurations. The results showed that with a decrease in the bottom hole chamfer angle, there was resulting overall increase in the rivet joint pull off strength. From the best performing joint configuration in pull off tests, shear tests were conducted whilst a blind hole FHPR joint was also done and tested in pull off and shear strength. The shear test fracture surfaces exhibited ductile failure. The microstructure of the joints was thus evaluated. From parent material, heat affected zone and to weld zone there was a variation in the microstructure analysed. The hardness profiles showed increased hardness in the weld zone which partly explained the shear results. The hardness increase was mainly due to grain refinement in the weld zone by the Friction Hydro Pillar Riveting process.

Contents

Declaration	i
Acknowledgements	ii
Abstract	iii
List of Figures	vi
List of Tables	viii
CHAPTER 1: PROJECT OVERVIEW	1
1.1 Introduction	1
1.2 Objective	2
1.3 Problem Statement	2
1.4 Sub-Problems	2
1.5 Hypothesis	3
1.6 Motivation	3
1.7 Delimitations	4
1.8 Significance of Research	5
1.9 Research Methodology	5
CHAPTER 2: LITERATURE REVIEW	8
2.1 Introduction	8
2.2 Mechanical Fasteners: Bolts and Rivets	8
2.3 Titanium alloys	9
2.4 Failure Modes of Metals	12
2.5 Friction Processing	13
2.5.1 Riveting by Friction	14
2.5.2 Rotary Friction Welding	15
2.5.3 Friction Stud Welding	18
2.5.4 Friction Hydro Pillar Processing (FHPP)	19
2.5.5 Process Parameter Control in FHPP	22
2.6 Summary	26
CHAPTER 3: EXPERIMENTAL SET-UP AND PRELIMINARY WORK	27
3.1 Introduction	27
3.2 Friction Processing platforms used	27

3.3	Volume Fill Calculation	31
3.4	Weld Setup (PDS and Weldcore3 platforms)	33
3.5	Material Specifications for sheet and bar	35
3.6	Mechanical Evaluation	36
3.7	Process Development: FHPR of Ti-6Al-4V	38
3.8	Summary	55
CHAPTER 4: RESULTS AND DISCUSSION		56
4.1	Introduction	56
4.2	FHPR process model.....	58
4.3	Macrostructural analysis	66
4.4	Pull off Test.....	68
4.5	Shear testing.....	73
4.6	Hardness analysis.....	80
4.7	Microstructure analysis	84
4.8	Effect of rotational speed on FHPR joints	89
4.9	Summary	94
CHAPTER 5: CONCLUSION AND FUTURE WORK.....		96
5.1	Introduction	96
5.2	Discussion and Conclusion	96
5.3	Future work.....	98
REFERENCES		100
APPENDIX A: LOADCELL CALIBRATION		103
APPENDIX B: PAPER SUBMITTED TO THE ADVANCED METALS INITIATIVE, LIGHT METALS CONFERENCE		104
APPENDIX C: VISUAL IMAGES OF JOINTS		111
APPENDIX D: PROCESS CURVES (15°, 30° AND 45° JOINTS)		112
APPENDIX E: MICROSTRUCTURE VARIATION (30° AND 45° JOINTS)		114

List of Figures

Figure 1-1: A typical rivet joint as applied in the Aerospace industry [9]	3
Figure 1-2: The FHPP process [10]	4
Figure 1-3: FHPP as a joining method [11]	4
Figure 1-4: Outline of Research methodology	7
Figure 2-1: Riveting on fuselage structure [15]	9
Figure 2-2: Applications of Titanium in the Aircrafts [19].....	11
Figure 2-3: Friction Riveting [a) Positioning and clamping of joining partners, b) Insertion of rotating rivet, c) Rotation braking and subsequently rivet forging and d) Cooling and joint consolidation [27].	14
Figure 2-4: Friction Plunge Riveting 1) rotating rivet, 2) rivet penetration into plates and 3) Plates joined together [28]	15
Figure 2-5: Definition of stages on the friction torque curve of RFW [31].....	16
Figure 2-6: First stage of RFW (low and high pressure) [31].....	17
Figure 2-7 Low a) and High b) Friction Pressure Friction Stud Weld joints [33] ...	19
Figure 2-8: Basic principle of FHPP (i) Consumable stud, (ii)Plasticised zone (iii) pillar of extruded material [34].....	20
Figure 2-9: FHPP weld input and outputs flow diagram [35].....	21
Figure 2-10: Parameter Influence [2]	22
Figure 2-11 torque curve stages 1 to 7 of FHPP [37].....	25
Figure 3-1: PDS Platform set up	28
Figure 3-2: Weldcore 3 Friction Processing platform	29
Figure 3-3: Schematic of loadcell.....	31
Figure 3-4: Schematic of rivet and volume to be filled before the start of the joining process	31
Figure 3-5: Schematic of FHPR process.....	33
Figure 3-6: Lack of adequate shielding	34
Figure 3-7: Adequate shielding	34
Figure 3-8: Weldcore 3 shielding mechanism	35
Figure 3-9: Pull off test set up	36
Figure 3-10: Single shear specimen	37
Figure 3-11: Schematic of sheets for Matrix A	38
Figure 3-12: Macrographs A01 and A02	39

Figure 3-13: Adjustment to insert and backing plate	40
Figure 3-14: Experimental analysis diagram	41
Figure 3-15: Cylindrical and chamfered rivet geometries	42
Figure 3-16: Friction Torque curve	42
Figure 3-17: Torque (Up to 1 second)	43
Figure 3-18: Process torque response curves	47
Figure 3-19: Process energy relationship to rotational speed	48
Figure 3-20: Influence of rotational speed on torque response	49
Figure 3-21: Hardness profile representation of half the sheet and rivet.....	50
Figure 3-22: Horizontal hardness profile of 4000 and 5000rev/min joints	50
Figure 3-23: Full joint of 4000 rev/min and 5000 rev/min	51
Figure 3-24: A clear separation line between plasticised material and rivet.....	51
Figure 3-25: Increase in stopping/ braking time, PDS platform	53
Figure 3-26: Rotational speed relationship to stopping time, PDS platform	54
Figure 3-27: Rotational speed relationship to stopping time, PDS platform vs. Weldcore 3 platform.....	54
Figure 4-1: Geometry of the plate with varying chamfer angles and the blind hole	57
Figure 4-2: Rivet design for final matrix using the Weldcore 3 platform	58
Figure 4-3: FHPR process curve for Bottom hole chamfer (15°).....	60
Figure 4-4: Torque curve stages	60
Figure 4-5: Same process parameter FHPR joints process torque	64
Figure 4-6: Process energy vs. Joint Type.....	65
Figure 4-7: 45° bottom hole chamfer macrograph.....	66
Figure 4-8: Macrographs of FHPR joints with varying angles and the blind hole .	67
Figure 4-9: Blind hole 5000rev/min macrograph	67
Figure 4-10: Pull off test results	68
Figure 4-11: Pull off fracture surfaces	70
Figure 4-12: Energy absorbed at differing angles; Pull off test; (* data discussed in this section).....	72
Figure 4-13: Energy absorbed and process energy relationship.....	73
Figure 4-14: Shear testing sample	74
Figure 4-15: Shear test results: 15° bottom hole chamfer.....	75

Figure 4-16: Shear test results: Blind hole geometry	75
Figure 4-17: Blind hole, Rivet pulling off the bottom sheet.....	76
Figure 4-18: 15° bottom hole chamfer fracture surface	78
Figure 4-19: Blind hole shear fracture surface	79
Figure 4-20: Crack initiation on the Ti-6Al-4V FHPR joined	80
Figure 4-21: Micro-hardness 15° bottom hole chamfer, bottom and centre	81
Figure 4-22: Micro-hardness blind hole, bottom and centre	83
Figure 4-23: Parent sheet material (a. SEM X1900 and b. Optical Microscope) ..	84
Figure 4-24: Parent rivet material (a. SEM X1900 and b. Optical Microscope)	84
Figure 4-25: 15° bottom hole chamfer microstructure analysis	85
Figure 4-26: Blind hole: (5000rev/min) microstructure analysis	86
Figure 4-27: 15° Bottom hole chamfer microstructure; SEM x1900	88
Figure 4-28: Blind hole (5000rev/min) microstructure SEM x1900.....	89
Figure 4-29: Blind hole 5000rev/min macrograph of pulled off rivet.....	90
Figure 4-30: Blind hole 2500rev/min macrograph of pulled off rivet.....	90
Figure 4-31: Blind Hole, Rotational speed influence on torque curve	91
Figure 4-32: Pull off results of 2500rev/min and 5000rev/min.....	92
Figure 4-33: 2500rev/min Blind hole	93
Figure 4-34: Hardness profile of varied rotational speed blind hole joints	94

List of Tables

Table 2-1: Optimum Process Parameters [33].....	19
Table 3-1: PDS and Weldcore 3 platform capabilities	29
Table 3-2: Example of upset distance calculation	32
Table 3-3: Chemical composition specification % wr	35
Table 3-4: Single Shear Specimen Geometry	37
Table 3-5: Matrix A.....	38
Table 3-6: Matrix B.....	40
Table 3-7: Process Energy at up to 1 second	43
Table 3-8: Geometry utilised	44
Table 3-9: Rotational speed influence.....	46
Table 3-10: Gradient (Process Energy to Rotational Speed)	49
Table 3-11: Influence of increasing axial force on braking time	52

Table 3-12: Stopping time at different rotational speed.....	53
Table 4-1: FHPR of Ti-6Al-4V Final Matrix.....	57
Table 4-2: Process Parameters that in FHPR	62
Table 4-3: Visual appearance of same process parameter joints	63
Table 4-4: Upset distance analysis	64
Table 4-5: Calculated process energy	65
Table 4-6: Pull off results	69
Table 4-7: Shear testing results calculated using an unprocessed rivet diameter	76

List of Abbreviations

ASTM	American Society for Testing and Materials
AWS	American Welding Society
FP	Friction Processing
FHPP	Friction Hydro Pillar Processing
FRW	Friction Welding
FSW	Friction Stir Welding
FTPW	Friction Taper Plug Welding
FTSW	Friction Taper Stud Welding
HAZ	Heat Affected Zone
HMI	Human Machine Interface
NMMU	Nelson Mandela Metropolitan University
MPa	Mega Pascal
SEM	Scanning Electron Microscope
TWI	The Welding Institute of the United Kingdom

Glossary of terms

Alloying element: An element added to and remaining in metal that changes its structure and properties

Braking phase: Sudden increase in torque response as rotation of consumable tool slows from welding speed to stop

Consumable tool: This is the tool used in specific friction welding processes that is rotated against a workpiece or inside a hole. The tool material is deposited and bonds to the parent material

Down or axial force: The force applied to the FP tool during the welding process in the direction of the axis of rotation of the tool. Also referred to as the z direction force or z-force on the FP platform

Faying surface: The mating surface of a member that is in contact with another member to which it is to be joined

Flash: The material that is displaced from the friction weld interface. See also 'weld flash'

Flash formation: Excess plasticised material ejected during friction processing.

Forging force: A compressive force applied to the faying surfaces after the friction phase of the welding cycle is completed

Friction Hydro Pillar Processing: Friction welding process whereby a consumable tool or stud is rotated concentrically inside a blind hole under an axial load thereby filling the hole and creating a strong bond with the parent plate

Friction Stir Welding: Solid state welding process whereby abutting parts are joined together by rotating a non-consumable tool along the interface

Friction Taper Stud Welding: Solid state welding process used to join similar or dissimilar material by rotating a tapered consumable rod co-axially in a taper-

Glossary of terms

sided cavity, of equal or slightly larger included angle than the tool, whilst under an applied load so as to generate a plasticised layer thereby forming a bond.

Macrograph: A graphic reproduction of a prepared surface of a specimen at a magnification not exceeding 10x.

Macrostructure: The structure of metals as revealed by macroscopic examination of the etched surface of a polished specimen.

Microstructure: The structure of a prepared surface of a metal as revealed by a microscope at a magnification exceeding 10x.

Parameter: The minimum and maximum parameters will describe the operating range of a variable.

Parent material: Pertains to material in its as manufactured form and condition.

Plastic deformation: Deformation that remains or will remain permanent after release of the stress that caused it

Plasticised material: Material that is displaced when its yield strength is exceeded and cannot return to its original form.

Sidewall: The surface of the hole along which bonding usually occurs during FHPP

Solid state welding: A group of welding processes which produce coalescence at temperatures essentially below the melting point of the materials being joined.

Spindle speed: The speed of the tool holding device (chuck), measured in revolutions per minute (rev/min)

Glossary of terms

Torque stages: The trends of torque responses which are a measure of the resistance to rotation and have identifiable phases

Tool rotational speed: This is the rotary speed of the tool. This can be quoted as rotation speed (rev/min), peripheral velocity (m/s), or angular velocity (rad/s)

Upset: Bulk deformation resulting from the application of pressure in friction welding. Is measured as a percent increase in interface area or as a reduction in length

Upset distance: The total loss of axial length of the workpieces from the initial contact to the completion of the weld. Can be separated into the upset during friction phase, friction upset; and the upset during the forge phase, forge upset

Chapter 1: Project Overview

1.1 Introduction

Friction Processing (FP) has been researched extensively over the past decade but Rotary Friction Welding (RFW) has been in existence for over a decade in the manufacturing industry [1]. This type of welding has numerous advantages which include:

- Low production time,
- High joint efficiency,
- Fast, repeatable, economic process that does not require an operator with welding skills.
- Flash formed when welding carries out most surface impurities and oxides out from the weld zone.

Some of the better known solid state welding techniques include Friction Stir Welding (FSW), Friction Taper Stud Welding (FTSW) and Friction Hydro Pillar Processing (FHPP) [1] [2].

RFW is one of the most common types of friction processing. During the RFW process, two work pieces are joined together under force/load [2]. The first piece is rotated against the second stationary work-piece; thereby generating frictional heat at the inner surface. The joint area is plasticised as a result of the increase in temperature. The rotational speed of the spindle is stopped and the end force is increased to forge and consolidate the weld [1] [3].

Friction Hydro Pillar Processing (FHPP) and Friction Taper Stud (FSTW) are both solid state processes where a consumable tool is co-axially rotated in a hole under a continuously applied axial force. These two processes were developed by TWI in the early 1990's [1] [4]. Nelson Mandela Metropolitan University (NMMU) through eNtsa, (a technology station) and the Friction Processing Research Unit (FPRU) have over the past decade dedicated numerous research attempts to the field of friction processing. These two units are headed by

Distinguished Professor D. G. Hattingh, who has contributed greatly to this field of FP.

This research aims to employ techniques of FHPP to develop a process of Friction Hydro Pillar Riveting (FHPR) in order to investigate the quality of the joint that will be formed between the rivet and the sheets.

1.2 Objective

This project aims to develop and analyse a process of riveting titanium (Ti-6Al-4V) lap joints based on the principle of FHPP. The project will further explore the feasibility and suitability of the FHPR process as an alternative for the current Aerospace Rivet practises.

1.3 Problem Statement

Currently, there are no developments or successful implementations of FHPR using FHPP as the basis for joining two similar/ metals. This research is required to develop a relationship between process parameters, metallurgical and mechanical properties - and to determine the commercial feasibility of this process.

1.4 Sub-Problems

- Sub-Problem 1

Determine the stud diameter, length and the shape of the rivet head and establish the optimum stud geometry and process parameters through preliminary welds.

- Sub-Problem 2

Determine how the interaction of the stud and the backing plate material at the start of the welding process influences the material flow in order to understand the material flow and the formation of the bottom rivet head.

- Sub-Problem 3

Quantify the influence of different process parameters on the joint integrity.

- Sub-Problem 4

Determine suitable material for the backing plate and look at varying the backing plate configuration from using a consumable backing plate to using a non-consumable backing plate with a layer of Magnesium Oxide (aids in non-sticking of the rivet head to the backing plate).

1.5 Hypothesis

Friction Hydro Pillar Riveting will have improved joint strength in shear allowing it to be a replacement or an alternative to the current riveting techniques used on Ti-6Al-4V sheets.

1.6 Motivation

The rivet joint is one of the current viable methods for fastening thin-walled sheet-metal parts permanently [5]. Rivets have many advantages, such as providing for a simple joining process, reliable joining intensity and high working efficiency, and are thus used extensively in the aircraft industry. Due to the type and thickness of plates/sheets used in aircraft skins and other components, welding processes tend to damage thin fuselage skin structures and the skins are not easily welded [5] [6] [7].

FP has been used to overcome some of the shortcomings of convectional joining and fusion welding methods [8]. FHPR will be developed as an alternative to the current riveting method. A lap configuration joint on the fuselage of an aeroplane is shown in Figure 1-1.

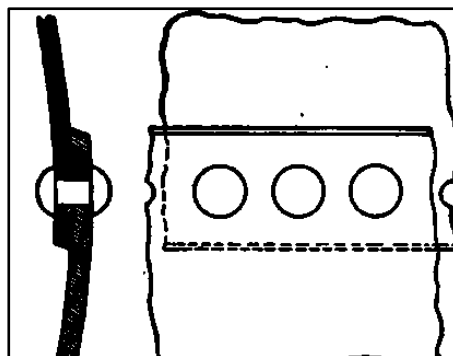


Figure 1-1: A typical rivet joint as applied in the Aerospace industry [9]

FHPP involves rotating a consumable tool co-axially in what is essentially a slightly tapered hole or a circular split mould whilst under an applied axial force, in order to generate frictional heat which leads to plasticisation of the rod as shown in Figure 1-2 [1] [2] [4].

Please note: FHPP will be discussed in detail in section 2.5.4.

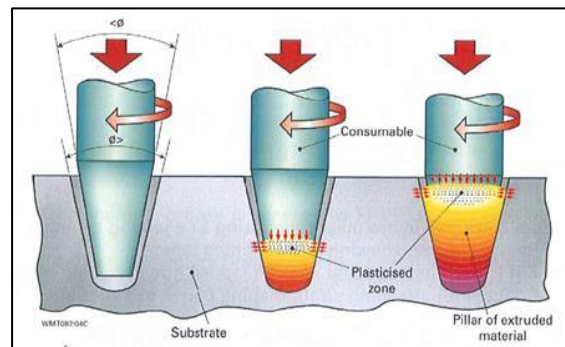


Figure 1-2: The FHPP process [10]

FHPP has the potential to compete with stud and slot welding, bolting or riveting and as shown in Figure 1-3, it can be used as a joining method. For this research, the characteristics of FHPP are utilised so as to develop a method of Friction Riveting [11].

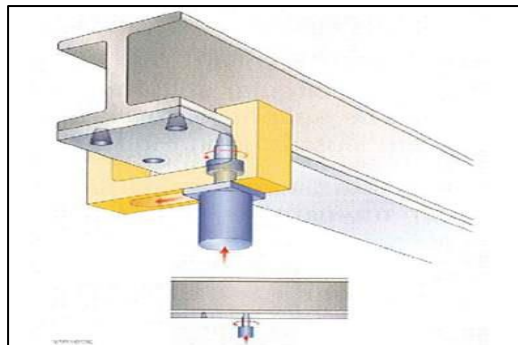


Figure 1-3: FHPP as a joining method [11]

1.7 Delimitations

- Friction Hydro Pillar Riveting will only be developed on 3.17 mm Ti-6Al-4V sheets.
- Only sheets with pre-drilled holes will be used for this research purpose.

- The process parameters will be depended on the PDS platform machine capability (maximum spindle rotational speed and axial force of 9000 rev/min and 94.8 kN respectively).

1.8 Significance of Research

This research seeks to contribute towards the following:

- **Industry:**

The knowledge generated from this research will allow for the development of a new viable option for joining materials to be used in the Aerospace industry as also many other applications: this will provide better structural stability compared to the currently available methods.

- **The Nelson Mandela Metropolitan University [NMMU]:**

It will help develop a new process for Friction Riveting and establishing it as a viable research field and thereby further international collaboration of the established FPRU within eNtsa.

1.9 Research Methodology

The research methodology is shown in Figure 1-4 which details the steps followed which are:

Step 1:

A literature survey on FSTW, FHPP, FPW and RFW or any other similar processes that may indicate any key information on FP will be conducted. This survey will also include the following:

- A review of both the type of material to be used as backing plate and of the type of configuration for good process results;
- Details of components to be designed, including the stud and integrated shielding mechanism;

- Information about the development of a clamping methodology for lap joints of thin sheets of titanium;

Step 2:

Development of a preliminary weld matrix to analyse process parameter influence on the envisaged FHPR Ti-6Al-4V joints will be conducted.

Step 3:

The influence of stud geometry, process parameters and backing plate configuration will be examined during the preliminary welding stage.

Step 4:

A final weld matrix will be established this will consist of the determined process parameters which will include samples for shear and pull off tests.

Step 5:

A report will be generated based on the static (shear and pull off testing) and metallurgical analysis conducted as illustrated in Figure 1-4.

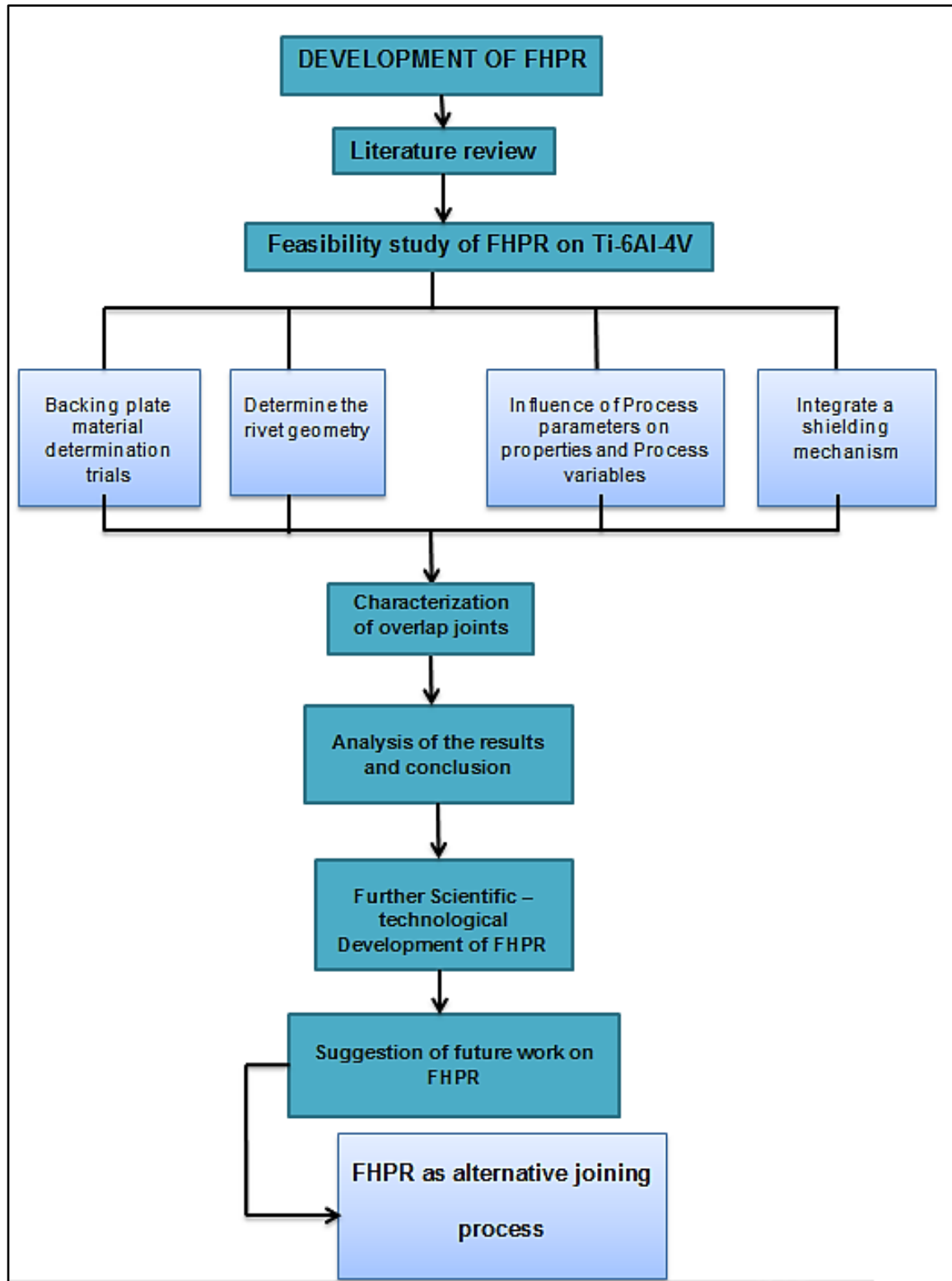


Figure 1-4: Outline of Research methodology

Chapter 2: Literature Review

2.1 Introduction

As proposed in Chapter 1, the advent of Friction Hydro Pillar Riveting (FHPR) is based on the principles of Friction Hydro Pillar Processing (FHPP): therefore the literature discussed here-within looks at the fundamentals of FHPP in developing FHPR. Other forms of Friction Welding are Rotary Friction Welding, Friction Taper Stud Welding and Friction Stud Welding: these are also discussed in this Chapter. The aerospace industry has a vast need for lighter and easily automated processes to join metal plates and sheets in sub-assemblies and for the manufacture of aerospace components [12] [13].

2.2 Mechanical Fasteners: Bolts and Rivets

Mechanical fasteners are used extensively in the joining of aerospace components, sheets and plates. The most common types of mechanical fasteners used in the aerospace industry are rivets and bolts [14]. The biggest advantages of mechanical fasteners are that they produce joints of high efficiency especially in high strength alloys: in addition they maintain excellent mechanical properties and corrosion resistance [7]. The other advantages of mechanical fasteners are as follows:

- They provide a simple joining process.
- The cost of installation tools is less than welding techniques.
- Little or no operator skill is required. Committal

However, the joint design limitation of mechanical fastening has led to the development of welding processes to replace mechanical fasteners. In the Aerospace industry, mechanical fasteners still stand out compared to conventional welding techniques due to their fatigue and corrosion properties. Welding is intricate or complicated especially for thin sheets and requires specialised skills [6] [7].

Bolts and rivets are the most extensively used and well known types of mechanical fasteners. Bolt designs generally consist of a bolting connection

supporting loads in shear or tension and compression (where a high tensile strength bolt is used to apply a high compression load between structural component members) [7]. Rivets in turn mainly support loads in shear. Bolting provides joints that are strong, reliable and are easily disassembled, whilst rivet joints are permanent joints and difficult to disassemble. Rivet joints are shown in a sub-assembly of a passenger aircraft in Figure 2-1.

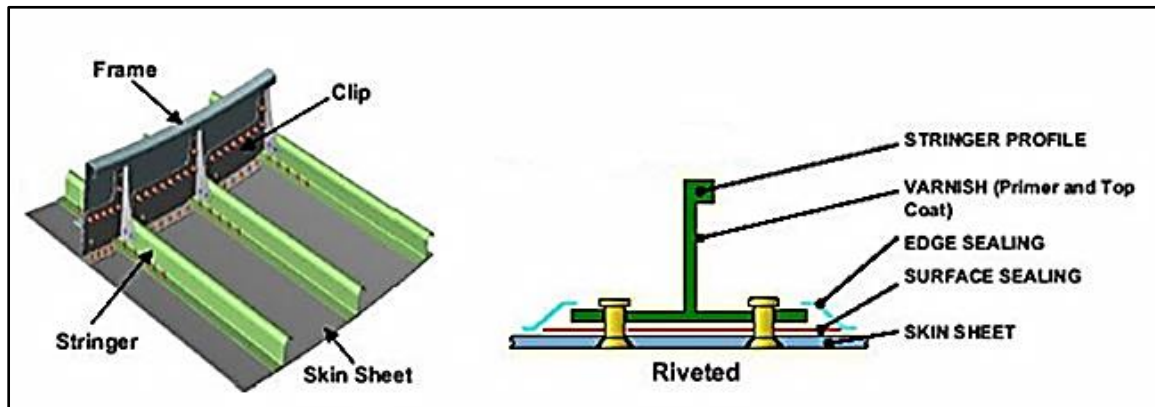


Figure 2-1: Riveting on fuselage structure [15]

The most common type of rivets are blind and solid (button head) rivets, with the latter termed high strength rivets, whilst the former are used mainly for their aerodynamic qualities. Blind rivets are mainly made via a hammer or squeeze mechanism. Most common blind rivets are made from aluminium 2000, 5000 and 6000 series materials. Another method of riveting is the Self Piercing Riveting method (SPR). SPR consists of a semi-tubular rivet driven into two or more sheets or plates while supported by an anvil, i.e. a shaped die supports the underside [7]. A known problem with titanium rivets is that of the rivet heads cracking because of their strain rate sensitivity and a high yield, as discussed from Deng et al [16].

2.3 Titanium alloys

Titanium, which was discovered in 1790, is named after the Titans, the powerful children of the supreme rulers of the Universe in Greek mythology. Titanium started being purified only in the early 1900s. Nowadays Titanium is readily available and competes directly with stainless steels, copper alloys, etc. Titanium

experiences allotropic transformation at approximately 900 degrees Celsius whilst it has a melting temperature in the excess of 1660 degrees Celsius [12] [17]. The Titanium is a high strength, low weight and corrosion resistant material. These properties make it acceptable for use in a wide range of applications such as aerospace, oil and gas extraction and in the medical and other industries. The most common type of titanium alloy is Ti-6Al-4V known as the workhorse of the aerospace industry which uses at least 50% of the available titanium alloy (Ti-6Al-4V): Figure 2-2 shows some of its applications [12]. Due to its high strength to weight ratio, titanium is the metal of choice for the highly stressed wing sections and also the fuselage-wing connections on aeroplanes [18].

American government funded research on titanium as a strategic metal for use in aerospace for spacecraft and missile manufacture. In Aerospace, the Lockheed's SR-71 Blackbird spy plane, first flown in 1964, was predominantly made of titanium (at least 93% of its parts were titanium) [12].

Titanium alloys have proved to be a metal of choice due to the following reasons [12]:

- High corrosive resistance (superior resistance to chlorides, seawater and sour and oxidising acidic media).
- Bio compatible material.
- Non-magnetic property.
- Low specific gravity.
- High specific strength

Titanium is almost half the weight of steel and has the capability to withstand higher temperatures than both steel and aluminium respectively [18].

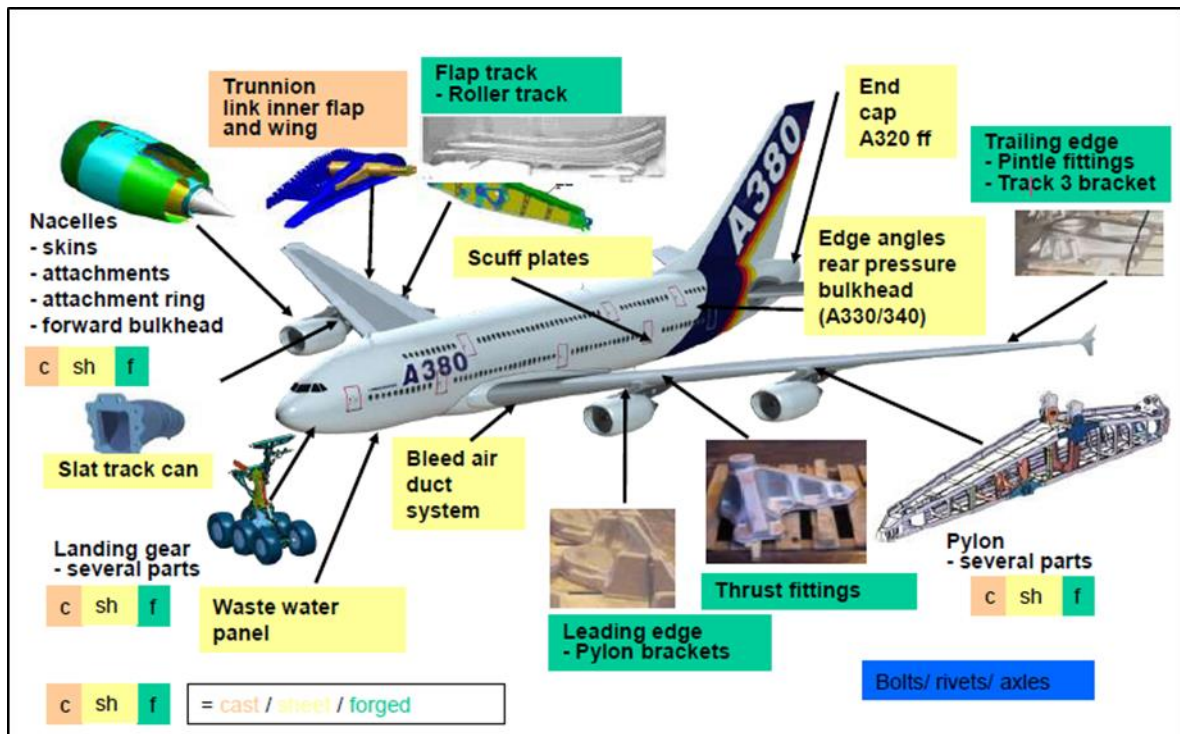


Figure 2-2: Applications of Titanium in the Aircrafts [19]

Titanium applications have increased with each new generation of commercial airplanes. The Boeing 777 used titanium in areas that had earlier used Carbon Fibre Reinforced Plastics (CFRP) structures because of the need to minimise galvanic corrosion [20]. For this application beta-annealed Ti-6Al-4V Eli was used because it provides maximum damage tolerance properties for titanium alloys. Due to its many advantages, especially Ti-6Al-4V, it has been used in many applications although it is costly compared to aluminium and steel. For example, Ti-6Al-4V is used in wide ranging applications which include the following (refer to Figure 2-2) [18]:

- Aerospace industries, i.e. in engines due to its high temperature resistance.
- Marine industries due to its high corrosive resistance.
- Chemical and biomedical applications.
- Sports equipment due to it being lightweight.
- Power generation and nuclear waste storage.
- Medical implants because of biocompatibility.

The titanium alloy (Ti-6Al-4V) consists mainly of the alpha (α) and beta phase (β). The alpha-beta phase in titanium means that the structure is a mixture of the hexagonal closed packed (alpha) and body centred cubic structures (beta) [17] [18]. A matter of challenge is the weldability of titanium. According to RMI Titanium Company specifications, Grade 5 and 23 exhibit fairly good weldability properties [18]. According to Arcam [21], Ti-6Al-4V has a chemical composition of (wt. %) Al 6, V 4.04, Fe 0.19, N 0.018, O 0.18 and remaining Ti. The alpha stabilisers are Al, O and N while Fe is a beta stabiliser [22]. Ti-6Al-4V alloy can easily be fabricated allowing the mill products to be made into all shapes. Ti-6Al-4V Eli (extra-low-interstitial) has controlled interstitial elements (oxygen, nitrogen and carbon) to improve ductility and fracture toughness [17] [18].

Processing of titanium requires a shielding gas to avoid contamination by oxidation. Oxidation of titanium, for example in FSW will weaken the weld quality. In RFW and FTSW of titanium, no shielding has been required for these processes assuming that all impurities are expelled out as flash [17] [23].

According to the Military Handbook [14], to determine the strength of mechanically fastened joints, it is necessary to know the strength of the individual fasteners. Failure in joints occurs mostly due to tensile and shearing failure of the fasteners, or by bearing and tearing of the sheet or plate. The handbook also specifies the acceptable shear strength for fasteners, i.e. rivets for the aerospace industry. The efficiency of a riveted joint is defined as the ratio of the strength of the joint to the strength of a solid plate in one pitch of the joint [14].

2.4 Failure Modes of Metals

Metals fail in different modes and for different reasons. There are only four principle fracture modes, i.e. dimple rupture, cleavage, fatigue and decohesive rupture, as described by the Metals Handbook on Fractography [24]. Dimple rupture is when overload is the principal cause of fracture. This type of failure exhibits cuplike depressions which occur as a result of microvoid coalescence. This process occurs when microvoids nucleate at regions of localised strain discontinuities i.e. second phase particles, inclusions, grain boundaries and

dislocation pile-ups. The common feature of dimple rupture is the elongated cuplike structure [24].

Cleavage failure is a low energy fracture compared to a dimple rupture. It propagates along well defined low index crystallographic planes which are called cleavage planes. Due to a possible mismatch of the low index planes across grain and sub-grain boundaries, a distinct cleavage fracture surface is produced. The produced surface exhibits cleavage steps, river patterns, feather markings and chevron patterns and tongues [24].

Fatigue failure is failure due to repeated cyclic loading. As stated by the Metals Handbook on Fractography [24], fatigue fracture occurs in three stages which are:

- I. Stage 1 involves the crack initiation,
- II. Stage 2 is the propagation along the entire length,
- III. And lastly, there is catastrophic failure.

A fracture that does not exhibit dimple-like failure and little or no bulk plastic deformation is known as decohesive rupture. It is mainly rupture along the grain boundaries which contains the lowest melting point constituents of alloys [24].

2.5 Friction Processing

Friction processing, or Friction welding as it is commonly known, is a solid state joining process. It is termed a solid state joining process due to the entire process not exhibiting any molten material [2]. The process involves frictional heat being generated by rotating or moving workpieces relative to each other under an axial force. Due to the rubbing, frictional heat is generated, leading to the plasticisation of material. The plasticised material is displaced from the rubbing or faying/contacting surfaces. The plasticised material mixes and then as rotation is stopped, a forging force is applied allowing for the consolidation of the plasticised material whilst it cools. As stated earlier, the commonly known types of Friction Processing are FHPP, RFW, FSW and Friction Stud Welding which are discussed in section 2.5.3 [2] [25] [26].

2.5.1 Riveting by Friction

During the past decade there have been developments made in the area of riveting using friction. The following are some of the examples:

2.5.1.1 Friction riveting

The Friction Riveting technique was developed by Amancio [27] for polymeric-metallic joints as an alternative spot joining process which is reliable, environmentally compatible and economically viable. It involves a rotating cylindrical metallic rivet which is inserted in a thermoplastic base plate thereby leading to a temperature increase. When insertion depth is achieved, this leads to an increase in heat input which becomes higher than the heat outflow due to the polymer's low thermal conductivity. The increase in temperature leads to the rivet tips plasticising. Then rotation is abruptly stopped and forging begins, forming the rivet head as shown below in Figure 2-3 [27].

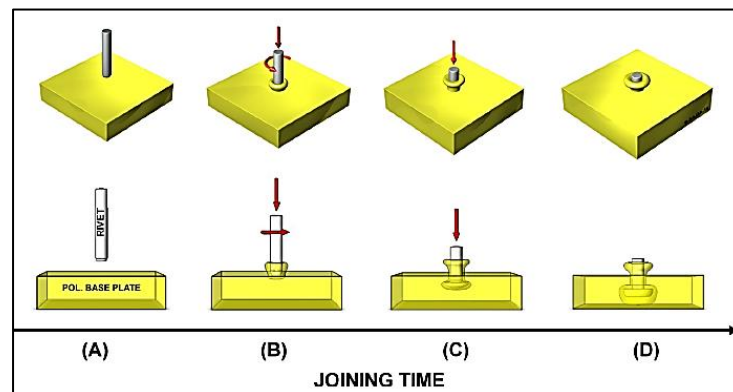


Figure 2-3: Friction Riveting [a] Positioning and clamping of joining partners, b) Insertion of rotating rivet, c) Rotation braking and subsequently rivet forging and d) Cooling and joint consolidation [27].

2.5.1.2 Friction Plunge Riveting (W. Thomas and Nicholas)

Friction Plunge Riveting was invented and patented in 2002 by I. Stol, W. Thomas and P. Threadgill. Stol et al [28] termed Friction Plunge Riveting as a joining method for metal components with a rivet having a hardness that is substantially similar or higher to at least one of the components. Friction Plunge riveting is a force-plunge, pierce, penetrate into and metallurgical bond two or more metal

parts lapped or stacked together. Figure 2-4 shows the process of Friction Plunge Riveting.

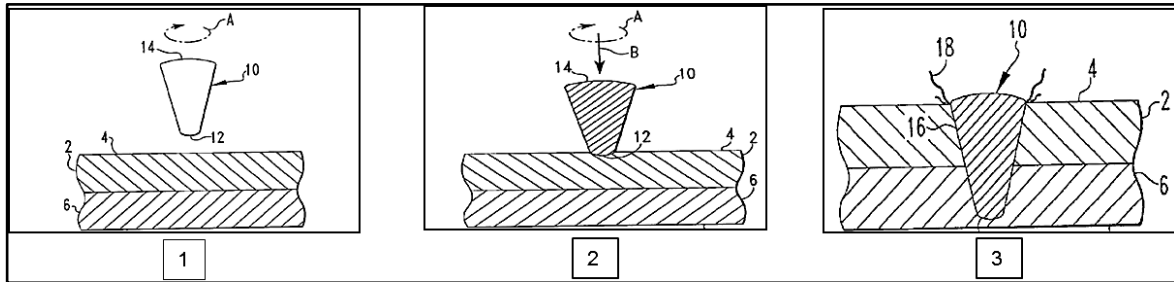


Figure 2-4: Friction Plunge Riveting 1) rotating rivet, 2) rivet penetration into plates and 3) Plates joined together [28]

2.5.1.3 Friction Stir Blind Riveting

A riveting technique called Friction Stir Blind Riveting was developed for one-sided joining of aluminium alloys. It involves a blind rivet rotating at high speed which is brought into contact with the work-piece, thereby generating frictional heat between the plate and the rivet. The generated frictional heat softens the work-piece's material, thus enabling the rivet to be driven into the work-piece, and thereby forming a rivet joint [29].

2.5.2 Rotary Friction Welding

RFW has been in existence for the last century, with the first known patent applied for in 1891, according to the American Welding Society. As with all FP techniques, RFW involves the joining process occurring at the plasticisation temperature: therefore it is termed a solid state process [30]. The Welding Institute (TWI) has done extensive research on FP and they have termed the process whereby a rotating shaft is joined to a stationary shaft under an axial force as RFW. Due to the process not exceeding the melting temperature of the material being welded, it has metallurgical benefits compared to conventional welding methods [31].

Kimura et al [31] divided the welding cycle of RFW into four stages on the basis of the friction torque curve for a similar material joint as shown in Figure 2-1. According to Kimura et al [31], the first stage comprises the contacting of the faying surfaces and then friction torque reaches an initial peak from zero. In the

second stage, the friction torque reaches equilibrium, and then it reaches the third steady state stage. The fourth stage is the forging (upset) stage. In this stage, friction torque increases when a motor brake is applied and then drops to zero when the rotation is stopped.

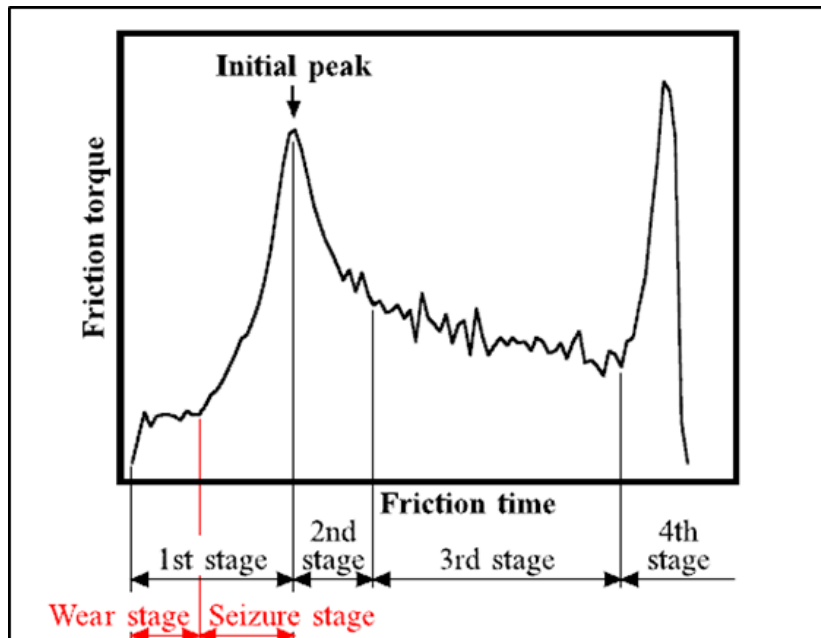


Figure 2-5: Definition of stages on the friction torque curve of RFW [31]

Kimura et al [31] went on to explain the difference between the low and high pressure in the first stage of RFW as shown in Figure 2-5. The main difference between the low and high pressure, is that for low pressure wear occurs over the whole area before seizure occurs as opposed to the high pressure welds as illustrated in Figure 2-6.

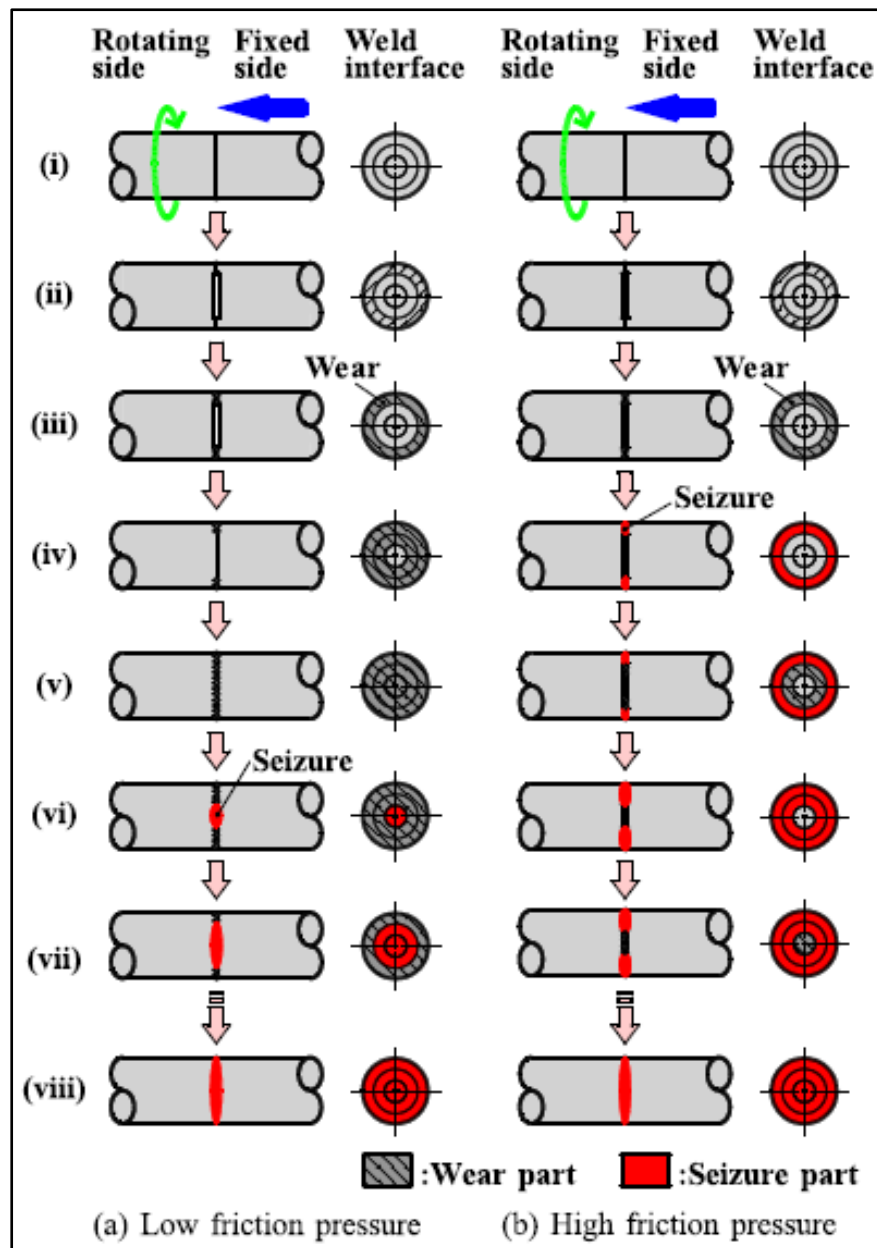


Figure 2-6: First stage of RFW (low and high pressure) [31]

Avinash, Chaitanya, Giri, Upadhy and Muralidhara [32] conducted RFW of Ti-6Al-4V shafts to determine microstructure and mechanical behaviour. From their research, they concluded that the tensile strength of joints was affected by rotational speed. At a rotational speed of 1500 rev/min, the weld microstructure appeared to be continuous with similar grain size. Avinash et al [32], conducted tensile tests on the welded specimens (the matrix had differing rotational speeds of 1000, 1500 and 2000 rev/min) and it was observed that the 1500 rev/min joint

had the highest tensile strength compared to the 1000 and 2000 rev/min joints [32].

Sahin and Akata [3] investigated the process parameters of RFW and they discovered that the most significant parameters were rotational speed, friction time, friction force and forging force. Their test matrix had a variation of friction force and friction time whilst all the other process parameters were kept constant. With an increase of friction force, the tensile strength of the RFW joints increased to about 96% of the weaker parent material.

2.5.3 Friction Stud Welding

Friction Stud Welding is another type of friction processing and was first applied in 1992 at an underwater scenario where a 12.5mm stud was welded to keel of a ship by the American Naval Sea Systems Command [30]. From this investigation, it was found that Friction Stud Welding had properties that exceeded that of conventional welding in terms of hardness and hammer bend tests.

More recently in 2009, Samuel [33] investigated the feasibility of Friction Stud Welding on tanks using a Ø6 mm AISI 304L stainless steel stud. From the research work some of the conclusions made were as follows:

- Low friction pressure increases the temperature at the weld interface. The stud forms a large convex weld nugget between stud and plate as illustrated Figure 2-7 a.
- Increasing the upset distance past the required upset, leads to an increase in the amount of process energy required to complete the welding process.
- Rotational speed has limitations where very low or high rotational speeds have a significant effect on the joint's mechanical properties.

A low and high pressure welds of Friction Stud Welding using AISI 304L stainless steel stud are shown in Figure 2-7.

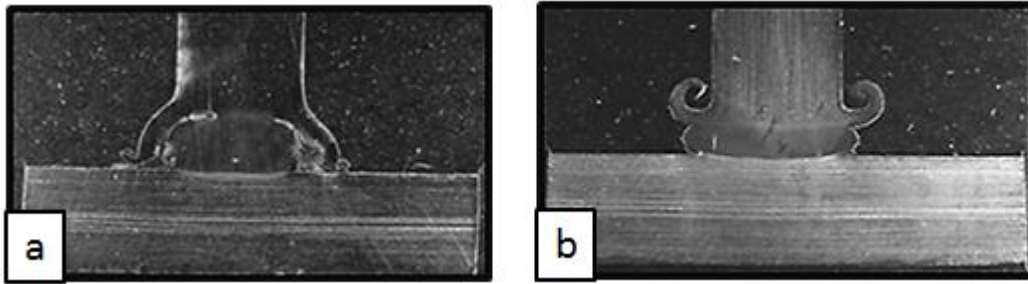


Figure 2-7 Low a) and High b) Friction Pressure Friction Stud Weld joints [33]

Table 2-1 shows the optimum process parameter setting found by Samuel [33] for Friction stud welding of $\text{\O}6\text{mm}$ AISI 304L stainless steel with respect to fracture force, elongation to failure, backing plate temperature and total process energy.

Table 2-1: Optimum Process Parameters [33]

Burn off (mm)	1
Friction Pressure (MPa)	76
Forging Pressure (MPa)	90
Rotational speed (rev/min)	5034

2.5.4 Friction Hydro Pillar Processing (FHPP)

FHPP was developed and patented by The Welding Institute (TWI) in 1991 as a method of repairing and joining material sections [25]. The TWI inventors, Thomas and Nicholas described of FHPP [4] as, “a technique that involves rotating a consumable stud rod co-axially in a hole whilst under an applied axial force as shown in Figure 1-2 and Figure 2-8, tapered and straight hole geometry respectively.”

When rotation starts at the interface between the stud and hole, temperature at the interface increases. This allows material to plasticise and shear off [34] [35]. Some of the material is pushed to the sides as a result of a decrease in resistance to the axial force. The consumption of the stud continues rapidly, forming shear layers. The first shear layer forms at the base of the following shear layer as the first cools and recrystallises, and the process is repeated until the last shear layer is formed. According to Bullbring [35] the thickness of each shear is dependent

on the temperature profile, the cross sectional area and the mechanical properties of the stud.

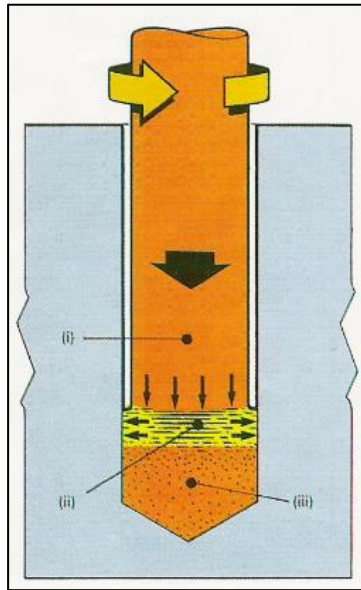


Figure 2-8: Basic principle of FHPP (i) Consumable stud, (ii)Plasticised zone (iii) pillar of extruded material [34]

Originally, the FHPP process was developed mainly for the repair of steel structures in the construction and offshore industry. Ambrozaick [26] reports that the main advantage of FHPP would be the improvement of safety and the reduced cost of on-shore tapping.

The main difference between FTSW and FHPP is that the FTSW cross sections show that the consumable stud plasticises only in the contact area near to the side wall while FHPP involves the plasticisation of the whole stud with the formation of a pillar of shear layers to fill the hole. Bullbring [35] details the two main factors (process parameters and geometry of stud and hole) and their effects on FHPP as shown in Figure 2-9 [26].

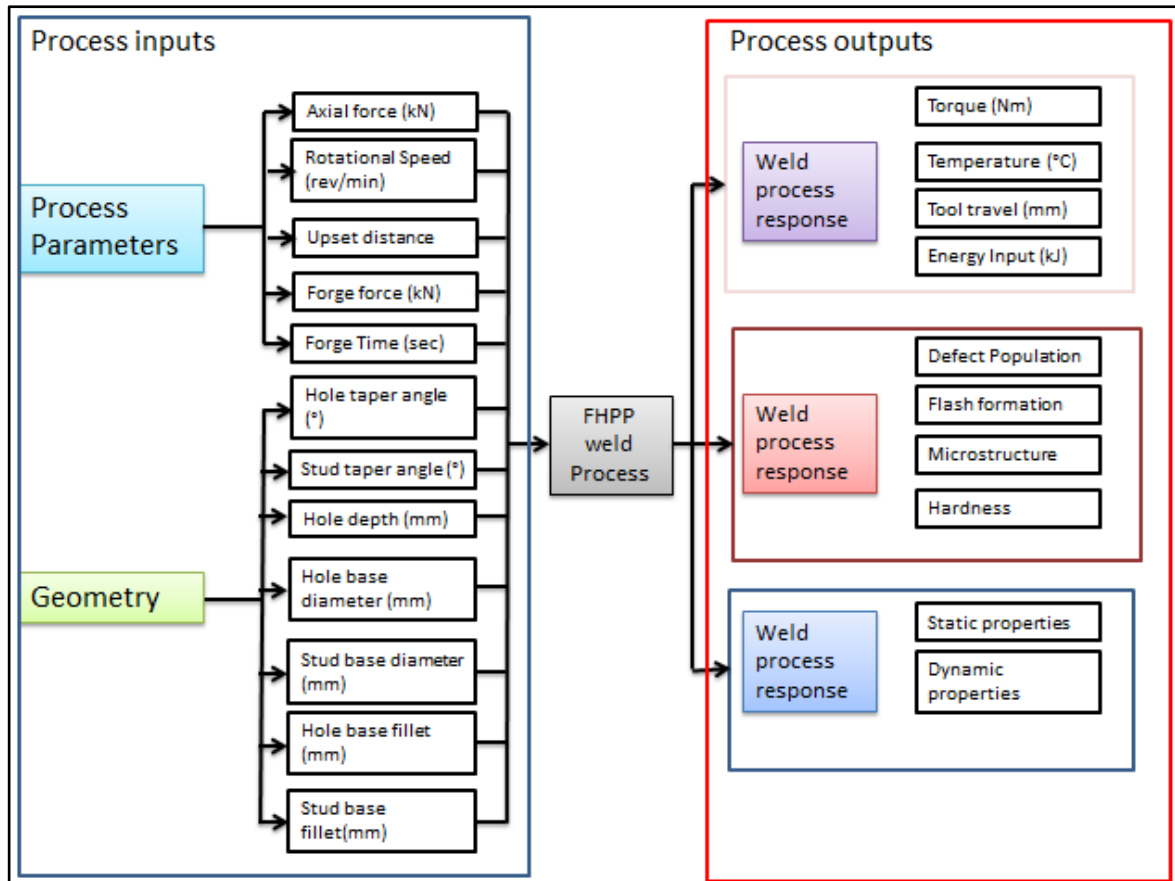


Figure 2-9: FHPP weld input and outputs flow diagram [35]

Another phenomenon of interest with FHPP is the idea that each material has its optimum material flow. Nicholas [1] points out that materials which do not exhibit adequate flow characteristics often respond better to a tapered joint design than a straight hole geometry [25].

The main advantage of FHPP, as with all FP techniques, is that the process is solid state based. This means that the process does not occur above the melting temperature, thereby ensuring fewer metallurgical defects. The other advantages of FHPP are:

- Its suitability for joining of dissimilar materials which are not easily weldable by conventional welding techniques.
- Compared to conventional methods, no filler material, flux or shielding is required except for titanium welding where oxidation occurs.
- The process is easily automated for mass production at lower costs.

Although the FHPP has many advantages, the feasibility and cost of specialised equipment for process implementation is very high, whilst also having geometry limitations, i.e. with regard to stud diameter and length [4] [26] [36] .

2.5.5 Process Parameter Control in FHPP

The main process parameters of FHPP are axial force, rotational speed, upset distance and forging force - similar to what is required for the RFW process. Each parameter plays a role in making a successful joint, depending on the type of application. Meyer [2] highlights the influence of these process parameters graphically as illustrated in Figure 2-10 which can be used to control FHPP. At NMMU, the term, “burn off” has been replaced by “upset distance” since burn off implies there is “some” degree of melting in the process.

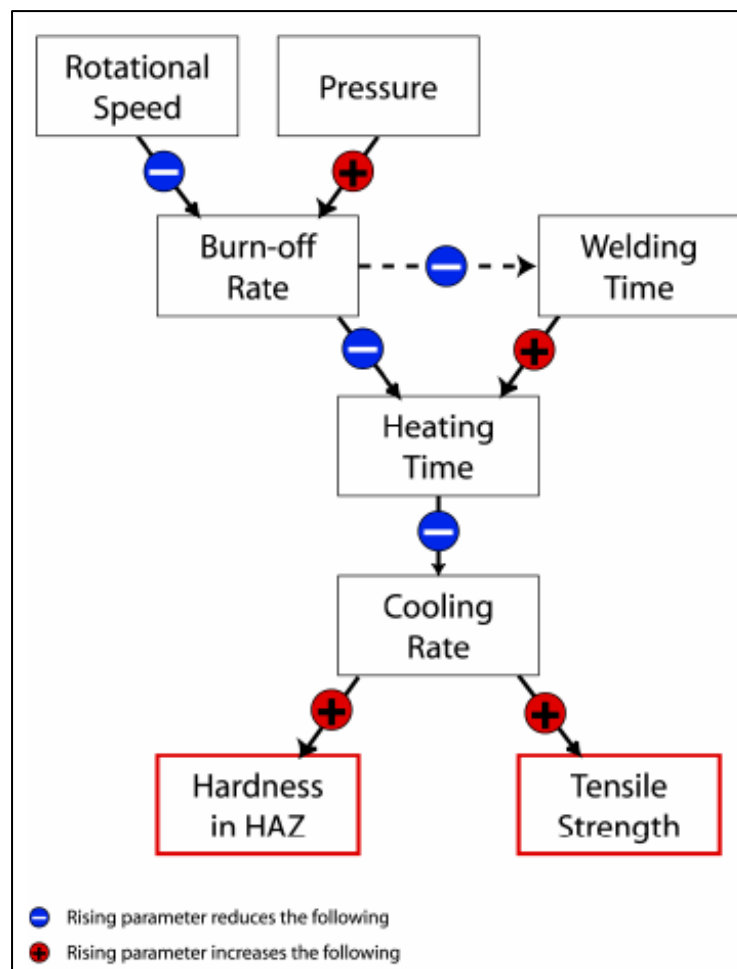


Figure 2-10: Parameter Influence [2]

2.5.5.1 Rotational Speed

Meyer [2], in FHPP rotational speed is the least sensitive process parameter. For every material, there is a certain optimum rotational speed and the idea of increasing rotational speed should be applied only after careful consideration [2]. In RFW, a minimum peripheral velocity of 1.27 m/s is required for sufficient bonding between the two work pieces. The minimum peripheral velocity for FHPP depends mainly on the material and geometry being utilised, joined or repaired. Rotational speed equates to peripheral velocity at the interface/faying surfaces of the pieces being joined together [3].

A higher rotational speed reduces the upset distance rate: this involves longer heating time, leading to low tensile strength and hardness. Low heating time allows for the propagation of thermal energy along the axial direction of the workpieces, thereby leading to a greater volume of material being displaced [35].

From the feedback data acquired, the process torque of FHPP is analysed which points to a difference existing between high and low rotational speed welds. High rotational speed FHPP welds have significantly low torque compared to slow rotational speed welds. This is due to deep tearing at the interface with low rotational speed welds being replaced by a polishing action, which in turn leads to closely packed shear layers, as well as the aforementioned longer heating times. An increase in rotational speed will show a wider heat affected zone exhibiting the difference in the heat input into the weld and also high cooling rates compared to a low rotational speed weld [2] [35].

2.5.5.2 Axial force

Axial force plays an important role in keeping the contacting or faying surfaces together or intimate. By keeping the faying surfaces together, detrimental substances are kept out of the weld zone while some of the impurities are pushed out of the hole as flash. Ambroizaick [26] states that the required axial force for FHPP is mainly dependent on the type of material being welded together and the joint geometry.

Axial force also has an influence on weld time, weld energy input rates and temperature gradient. A high axial force reduces the weld time due to an increase in plunge depth rate (upset distance rate) which allows for the weld to be completed faster in volume displacement governed welds [35] [26].

2.5.5.3 Upset distance

In FHPP, upset distance is the amount of stud material that is required to fill the hole with plasticised material. Upset distance is mainly dependent on the size of the hole and the stud being welded - and can be determined from mathematical calculations or experimentation. The amount of upset distance should be determined by taking into consideration that it has a different effect on shallow holes as compared to deep holes. For shallow holes, upset distance plays a significant role in the joining of stud-plasticised material to the sidewalls of the entire hole, while for deeper holes, it has a greater effect close to the top of the hole. For upset distance governed welds, the weld time is controlled by the amount of upset distance (considering axial force and rotational speed are kept constant) [2] [35].

Upset distance also governs the amount of volume fill % (under-fill % and overfill %). Under-fill refers to the upset distance being less than the required volume fill at 100%, whilst overfill is above the 100% volume fill (considering the hole geometry to be filled by plasticised material). With overfill secondary and primary flash is visualised on the completed FHPP weld. A slight overfill compensates for the forging and cooling stage in FHPP [35].

2.5.5.4 Forging force

Forging force is applied at the end of the weld when rotation has been stopped. It has three benefits as stated by Ambroizack [26], which are as follows:

- To break large inclusions.
- Refines grains.
- And reduces the probability of producing unwanted Widmanstatten structures which may affect the cooling rate.

By refining the grain size, the forging force increases hardness and ultimate tensile strength. In RFW, Kimura et al achieved 100% tensile joint efficiency without forging but there is still a need for forging force in FHPP as stated earlier [31].

2.5.5.5 Torque curve stages in FHPP

As discussed earlier, as with RFW, FHPP friction torque curve can be used to identify the stages of FHPP. Pentz [37] has identified the stages of FHPP rotor steel (26NiCrMoV145) as shown in Figure 2-11.

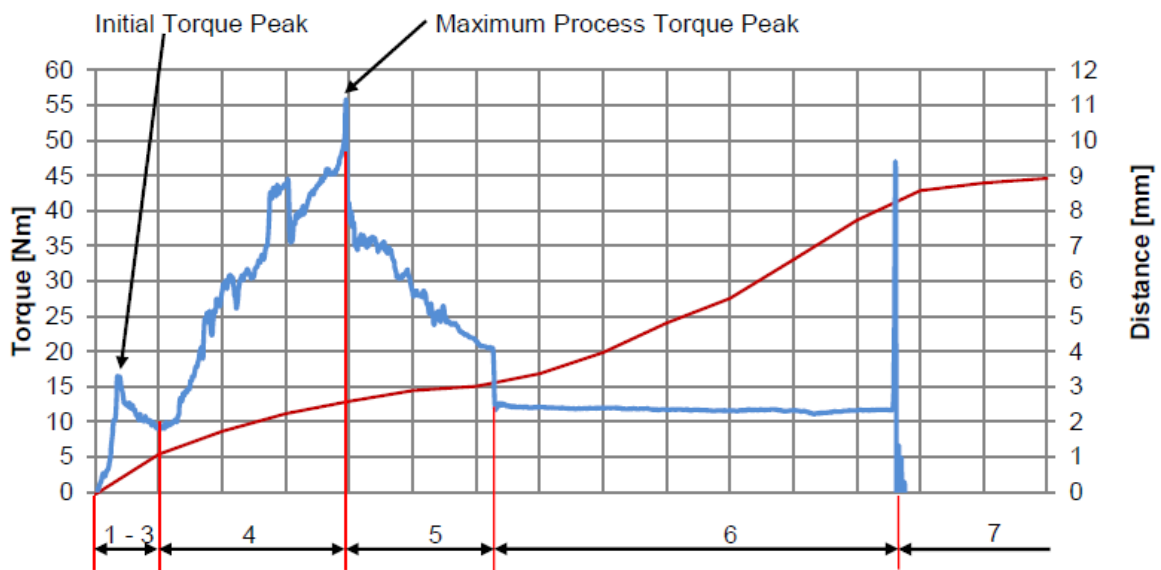


Figure 2-11 torque curve stages 1 to 7 of FHPP [37]

Pentz [37] outlined the stages of the torque curve and divided them into seven stages. From stage 1 to 3, the wear and seizure are shown to be similar to RFW with the initial torque. As soon as stage 3 is finished, there is an increase in torque, thereby signalling the beginning of stage 4 which Pentz explains as a gradual increase in torque due to the weld interface shear area increasing. Stage 5 is the opposite of stage 4 where the shear area decreases, hence leading to a torque decrease. From stage 6 onwards, the hole has been adequately filled: therefore the torque is steady until the motor brakes to stop the process leading to the beginning of forging.

2.6 Summary

This chapter has characterised FHPP and its process variables, as well as mechanical fasteners and their applications. The influence of different process parameters was discussed, with explanations of how these process parameters have an effect on weld quality and mechanical behaviour.

The torque curve of the FHPP and RFW is used as an important piece of information. It allows the process to be characterised and can be used as a quality control measure, thereby eliminating the need to do an in-depth mechanical and metallurgical analysis when conducting welds of the same process variables and parameters. From the torque curve, calculation of total process energy can be done: this will be used greatly in FHPR development.

Types of riveting using friction as medium for generating heat - thereby forming a mechanical lock - are also discussed in this chapter. As seen in the literature survey, the types of friction riveting found are more similar to Friction Spot Welding. As with Friction Spot Welding, the type of friction riveting discussed here focuses more on motor industry applications.

Chapter 3: Experimental Set-Up and Preliminary work

3.1 Introduction

In this chapter, the platforms used and the process developed through a preliminary development of Friction Hydro Pillar Riveting will be introduced. The Friction Processing platforms that are utilised are characterised. The design of the rivet/ stud and sheet to be utilised in the experimental set up is detailed, together with the integration of a shielding mechanism. Methods of testing and characterising the FHPR joints are discussed. The preliminary work focuses on the influence of different process parameters, variables and material behavioural tendencies that are identified and described through a physical (visual) and macrostructural analysis.

3.2 Friction Processing platforms used

FHPR was initially done using a NMMU developed 'Process Development System' (loosely termed PDS), the Friction Processing machine was purposely designed for process research on FSW and FHPP. The PDS platform was designed to allow the operator to input the process parameters and output data to be acquired as feedback. The PDS platform (refer to Figure 3-1) is the latest welding platform at NMMU which was designed mainly for FHPP and FSW.

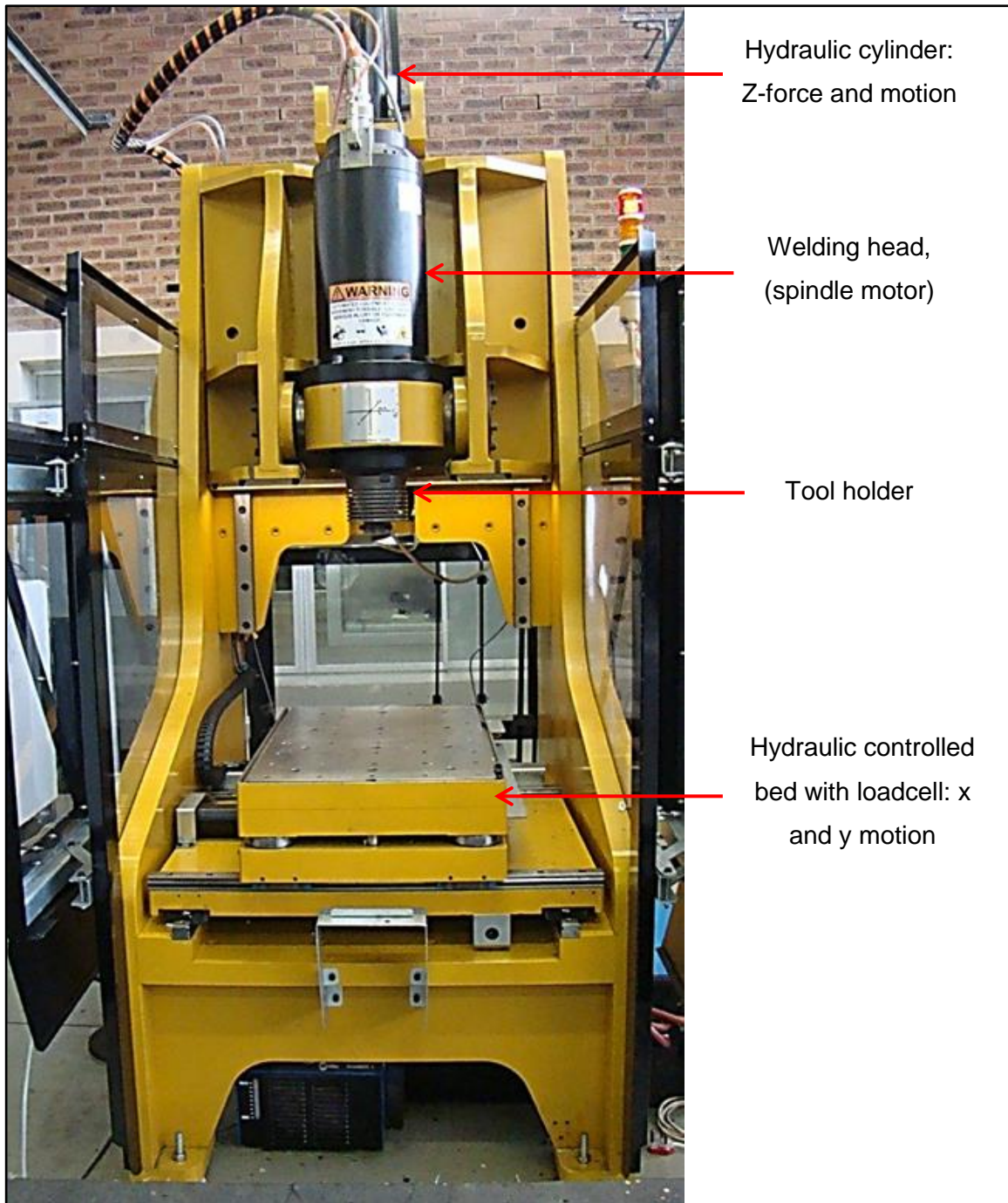


Figure 3-1: PDS Platform set up

The PDS platform has a welding bed which can move in the x and y directions by means of hydraulic actuation. The welding bed is coupled with piezoelectric sensors which are used for the measuring of process feedback during FP. From the output data, overall time for the joining process, total upset distance, average welding force and rotational speed can be determined. Due to complications with the torque measuring component of the PDS platform, a loadcell with torque

measuring capabilities was coupled to the PDS platform for this research. The loadcell allows for the recording of torque data that is used to calculate total process energy of FP welds. The PDS platform capabilities are listed in Table 3-1.

Table 3-1: PDS and Weldcore 3 platform capabilities

Process Parameter	PDS Range	Weldcore 3
Rotational Speed	0-12000 rev/min	0-5250 rev/min
Axial force	0-98.4 kN	0-40 kN

The platform was later changed to the small Weldcore 3 platform, which is third in line in the generation of developed Weldcore platforms at NMMU. The Friction Processing Weldcore 3 platform is shown in Figure 3-2. The reason for this change will be discussed in the preliminary development stage of FHPR.

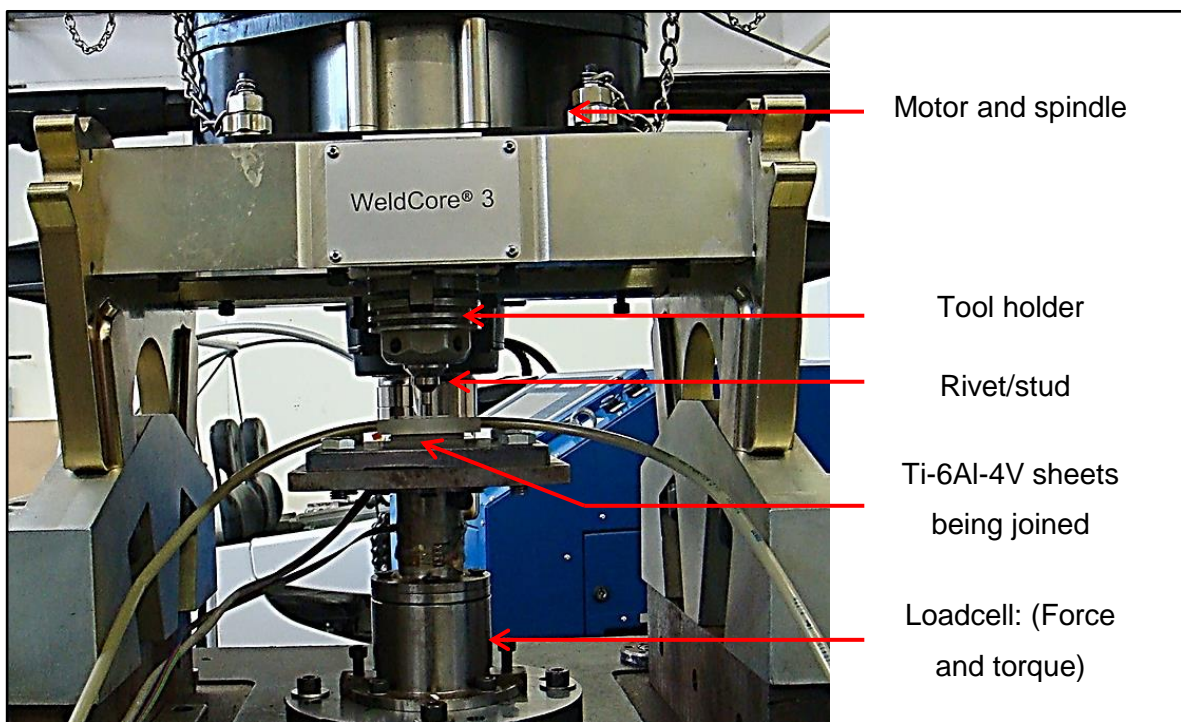


Figure 3-2: Weldcore 3 Friction Processing platform

The Weldcore 3 platform (refer to Figure 3-2) works on the same principles as the PDS platform: however the main difference is that it has a maximum rotational speed of 5250 rev/min. One of the Weldcore 3's major advantages is its ability to

stop quicker than the PDS platform: this will be discussed in detail in later sections.

Both platforms, i.e. The PDS and Weldcore 3, make use of the Human Machine Interface (HMI) to monitor and control process parameters before and during welding. Before the start of each weld, input process parameters - as discussed earlier - are programmed into the HMI weld programme which is then used to control and monitor the whole joining process.

Unlike the PDS platform, which can measure axial force and torque feedback using sensors on its welding bed, the Weldcore 3 uses a purposely designed external loadcell. The Weldcore 3 machine does not have a bed which could have been used for feedback data measuring. The loadcell used for the Weldcore 3 platform, was designed and used by Samuel [33] in the Friction stud welding of AISI 304L stainless steel. Figure 3-3 shows a schematic of the loadcell that has been utilised.

As the loadcell had been idle for a while, force and torque measurements were verified through a series of recalibration tests and thereby the loadcell was deemed to be in good working order. The torque data was recorded using a Spider 8 amplifier, whilst the force component was logged using the HMI. The data logged by the Spider 8's Catman software was in voltage and was converted to torque (Nm), using excel (refer to Appendix A: Loadcell calibration).

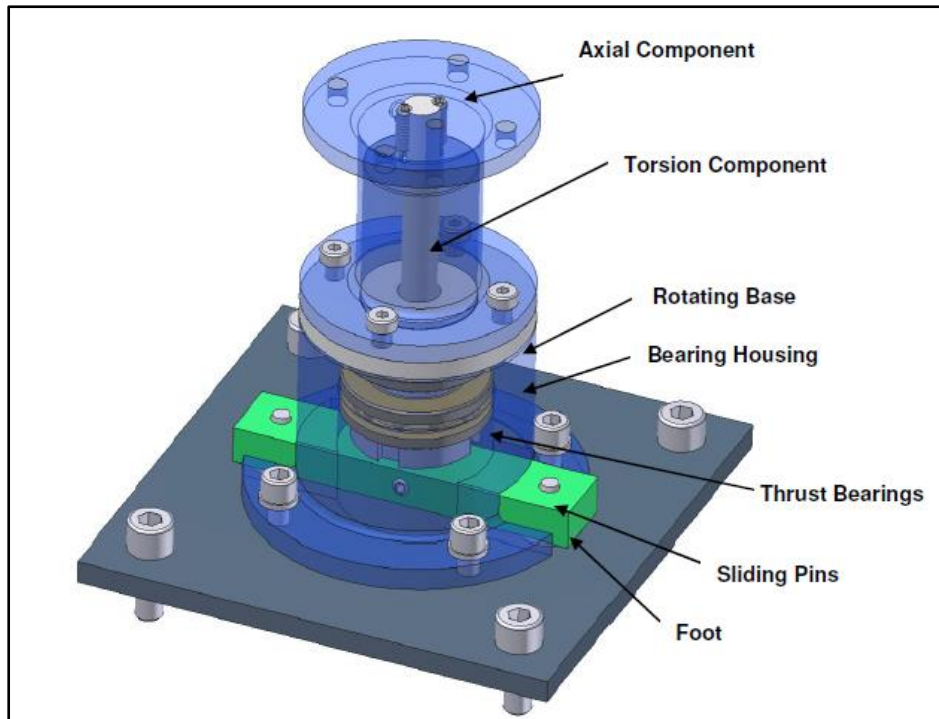


Figure 3-3: Schematic of loadcell

3.3 Volume Fill Calculation

Upset distance as discussed in an earlier section, is the distance that the rivet plunges/upsets to allow for adequate filling of the bottom hole chamfer before the top of the rivet head is forced into the rivet location hole of the top sheet. Upset distance was calculated by equating the volume to be filled to the amount of stud/rivet length as shown in Figure 3-4 and Table 3-2.

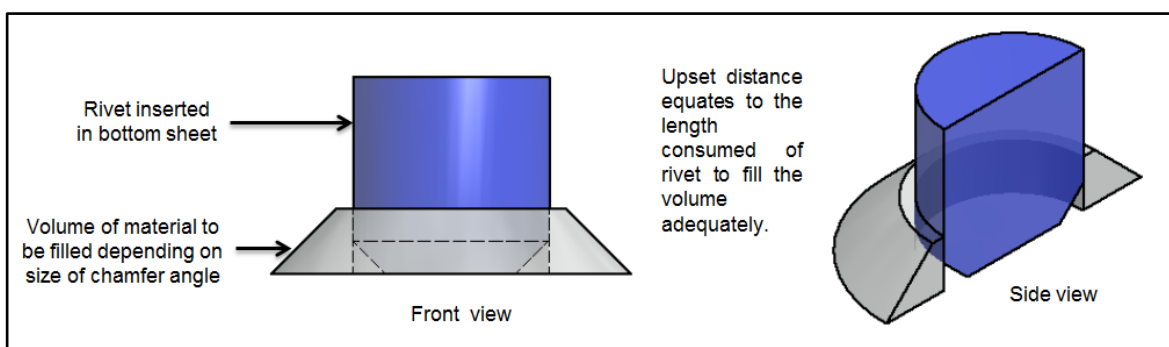
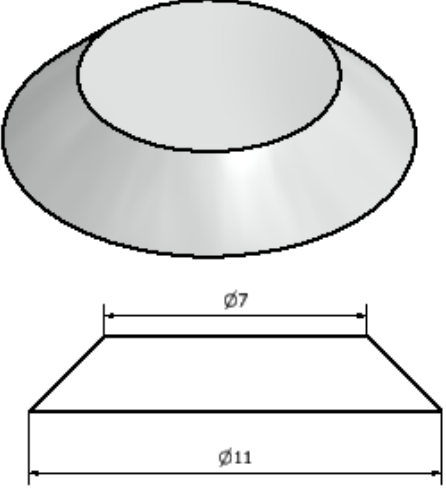
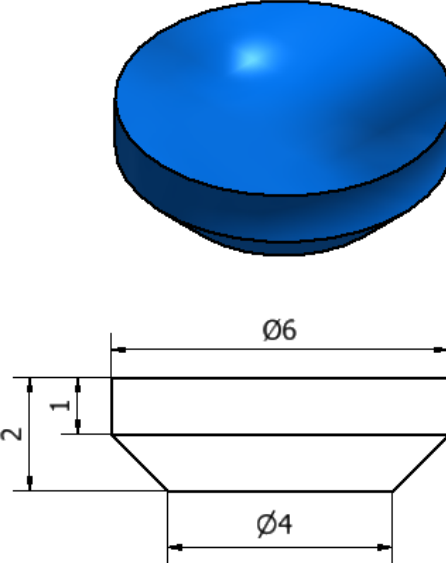


Figure 3-4: Schematic of rivet and volume to be filled before the start of the joining process

Table 3-2: Example of upset distance calculation

Description	Volume Calculation
<p>i) 45° chamfer hole</p> 	<p><u>Volume of frustum</u></p> $V_f = \frac{\pi}{3} h (R^2 + r^2 + (R * r))$ $V_f = \frac{\pi}{3} * 2 \left(\left(\frac{11}{2} \right)^2 + \left(\frac{7}{2} \right)^2 * (5.5 * 3.) \right)$ <p><u>Vfrustum = 129.329mm³</u></p>
<p>ii) Rivet (in hole before the start of the weld)</p> 	<p><u>Volume of rivet with chamfer</u></p> $V = \left(\frac{\pi}{4} D^2 \right) + \left(\frac{\pi}{3} h (R^2 + r^2 + (Rr)) \right)$ $V = 28.274 + 19.897$ <p><u>V = 48.171mm³</u></p>
<p>iii) 100% Volume fill: Upset distance, Ud</p>	$Ud = \frac{V_{frustum} - V_{rivet}}{A_{rivet}}$ $Ud = \frac{129329 - 48.171}{\frac{\pi}{4} * 6^2}$ <p><u>100% Volume fill: Ud = 2.87mm</u></p>

3.4 Weld Setup (PDS and Weldcore3 platforms)

Utilised setup in the FHPR development is shown in Figure 3-5. The set up consists of the rivet, sheets to be joined and a Haynes backing support plates (discussed in the following sections).

Note: The design of the rivet and hole geometry is discussed per matrix.

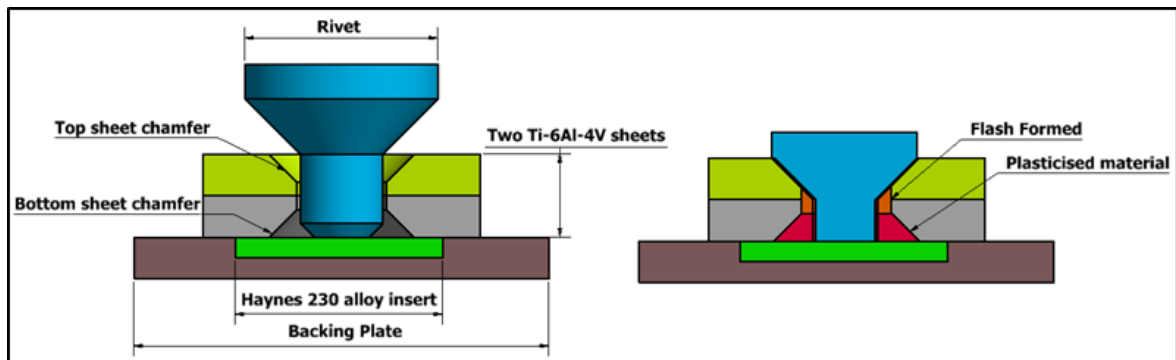


Figure 3-5: Schematic of FHPR process

3.4.1 Backing Support Material

The purpose of the backing support/plate was to act as a support face or anvil for forming the bottom head of the rivet, with no sticking occurring between the faying surfaces. For this research, material chosen for the backing plate was Haynes 230 alloy. Mashinini [23] employed Haynes 230 alloy for his research on FSW of Ti-6Al-4V and its properties allowed for it to be used for FHPR but in a different setup configuration to FSW (refer to Figure 3-5). Haynes 230 alloy is commonly used as a backing material in FSW of Ti-6Al-4V due to the material's high melting point and its ability to withstand high forces at elevated temperatures, thereby allowing for the non-sticking of the titanium rivet at the faying (contacting) surface.. Available Haynes 230 alloy was thus machined into inserts that were used in the FHPR process as shown by the set up configuration in Figure 3-5.

3.4.2 Shielding Mechanism

Titanium is a very reactive material and at temperatures above 650°C it is essential to shield it from oxidation. The amount of oxidation at these elevated temperatures should not exceed 200ppm. A shielding mechanism was developed and integrated into the weld experimental set up. The first shielding mechanism

used did not shield the FHPR joining process from oxidation adequately and a blue oxide layer was present on the flash formed as shown in Figure 3 8.

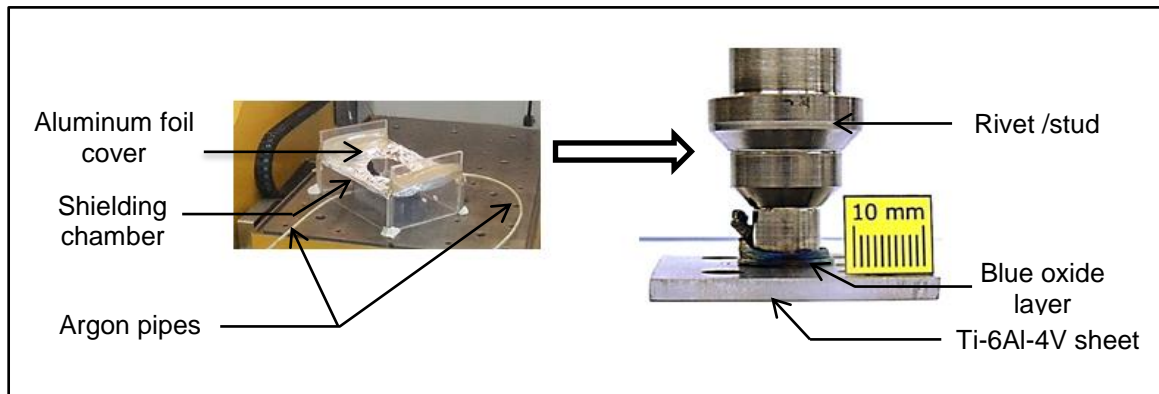


Figure 3-6: Lack of adequate shielding

Another shielding mechanism was designed and manufactured as shown in Figure 3 7 and Figure 3 8 for both PDS and Weldcore 3 platforms respectively. The integrated shielding mechanism for the Weldcore 3 platform was smaller due to the reduction of stud/rievet size: this therefore led to a reduced tool length sticking out after the joining process. With this reduced tool length, rubbing of the platform tool holder whilst rotating with the shielding mechanism would have occurred. A scenario of this nature would have been dangerous for the operator and for people in the vicinity, as the shielding mechanism could be thrown around.

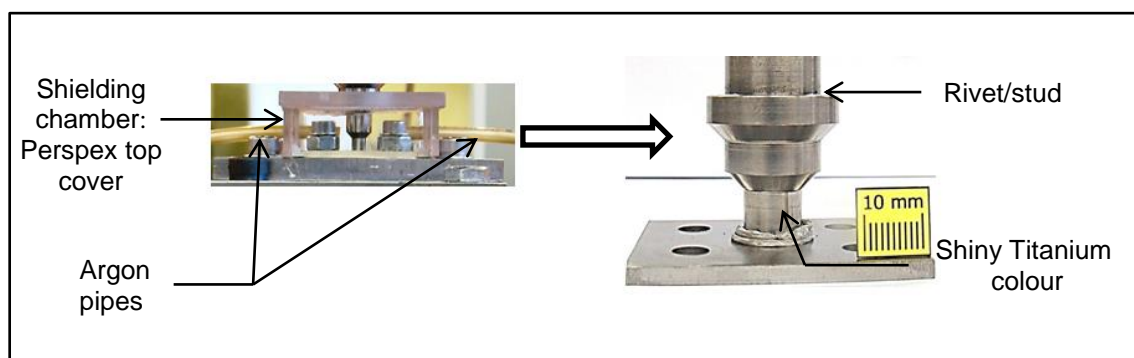


Figure 3-7: Adequate shielding

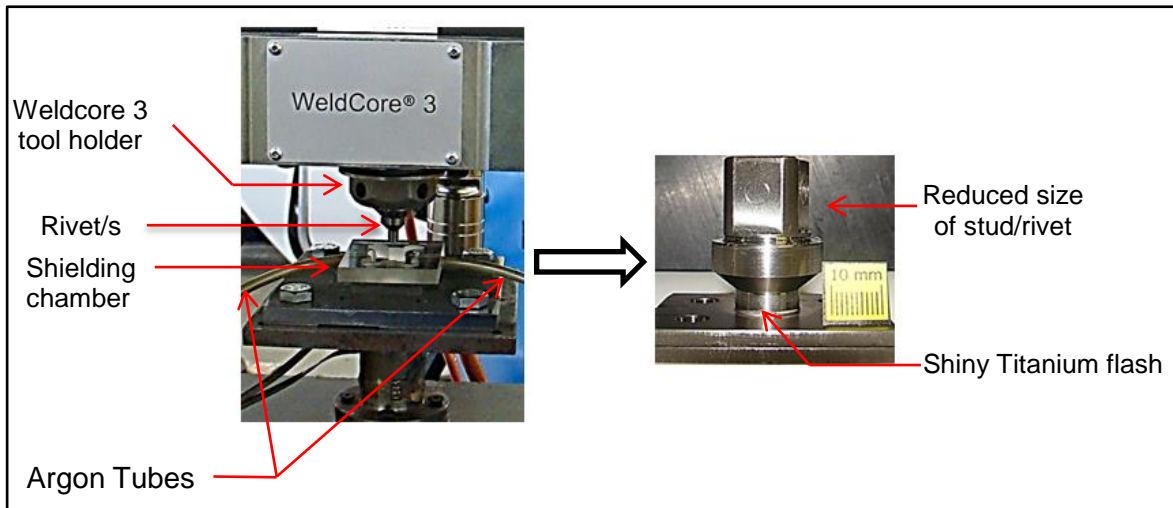


Figure 3-8: Weldcore 3 shielding mechanism

3.5 Material Specifications for sheet and bar

Material used in this investigation was 3.17mm Ti-6Al-4V alloy and Ti-6Al-4V Extra Low Interstitials (Eli) bar for the rivets.

Table 3-3: Chemical composition specification % wr

	Ti-6Al-4V	Ti-6Al-4V Eli
Aluminum, Al	6%	6%
Vanadium, V	4%	4%
Carbon, C	0.03%	0.03%
Iron, Fe	0.1%	0.1%
Oxygen, O	0.15%	0.1%
Nitrogen, N	0.01%	0.01%
Hydrogen, H	0.003%	<0.003%
Titanium, Ti	Balance	Balance

As stated by the Arcam EBM system [21], Ti-6Al-4V ELI (Grade 23) is similar to Ti-6Al-4V (Grade 5) as shown in Table 3-3, except that Ti6Al4V ELI contains reduced levels of oxygen, nitrogen, carbon and iron. ELI is short for “*Extra Low Interstitials*” and these lower interstitials provide improved ductility and better fracture toughness for the Ti6Al4V ELI material [21]. The ultimate tensile strength of Ti-6Al-4V and Ti-6Al-4V Eli grade is 1020MPa and 970MPa respectively [21].

3.6 Mechanical Evaluation

3.6.1 Pull Off test setup

The objective of the pull off test was to quantify the ability of the FHPR joint to fasten sheets together when a force parallel to the rivet is applied. The pull off test was performed based on ASTM D7332 (the standard test method for measuring resistance of fastener pull off in fibre reinforced polymer matrix composites), which was used in helping design and develop a pull off test method for the FHPR joints as illustrated in Figure 3-9.

The testing machine for the pull off test “Instron” was equipped with a 100kN loadcell and the speed of the machine (extension) was set at 5mm/min. The ambient temperature of the room was at 25°C and remained the same throughout the entire specimen testing.

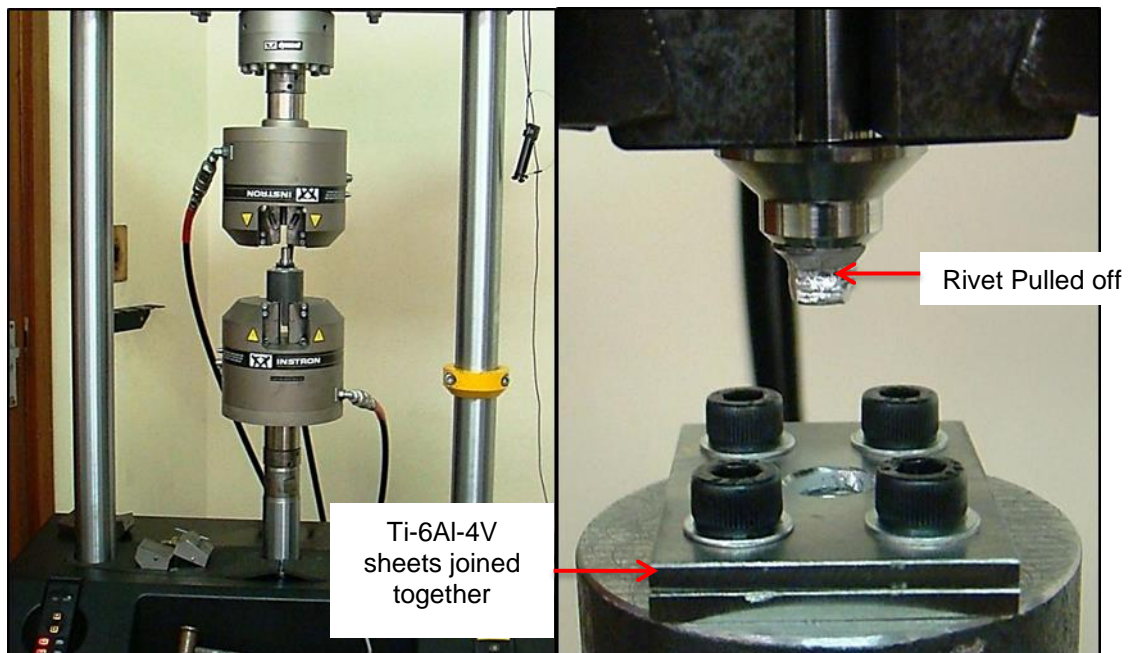


Figure 3-9: Pull off test set up

3.6.2 Shear testing

The shear test was conducted to evaluate the shear strength capacity of the rivet. The single shear specimens were specifically designed for the FHPR process as shown in Figure 3-10 with reference to an Organisation of International Standard (ISO) specification on Mechanical joining. The shear test was done using the

same machine as the pull off test keeping the 100 kN loadcell and the speed of the machine constant (i.e. as with the pull off testing).

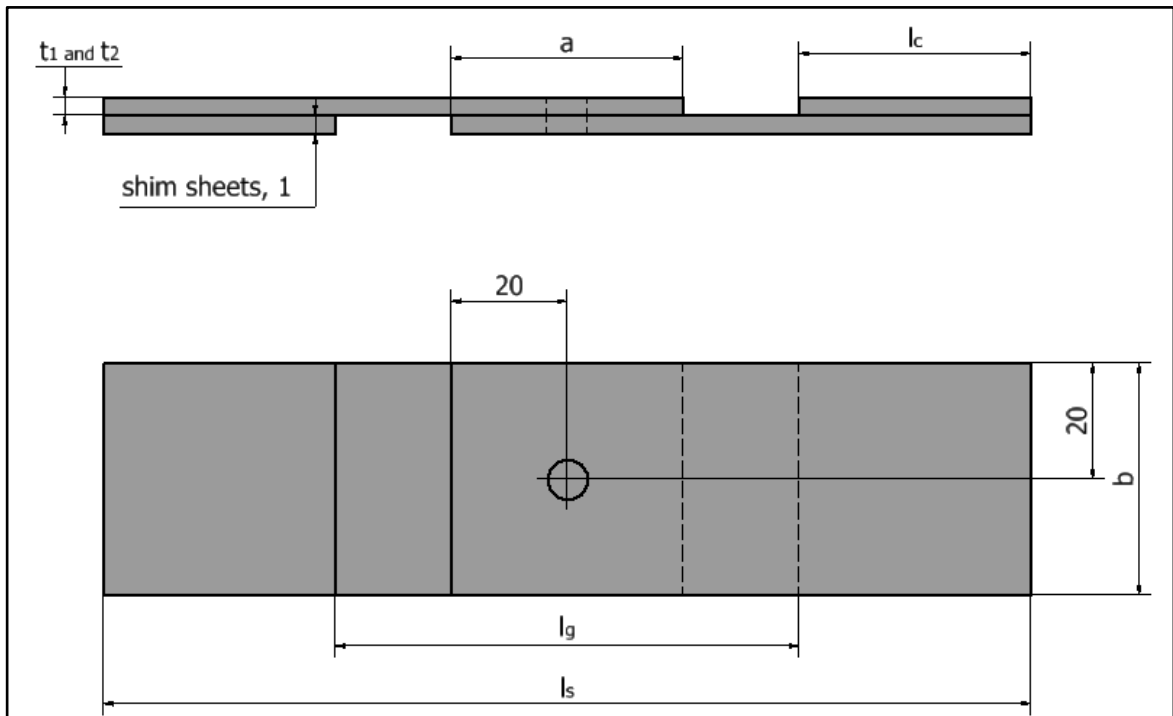


Figure 3-10: Single shear specimen

Table 3-4 shows the single shear sample dimensions.

Table 3-4: Single Shear Specimen Geometry

	Dimension (mm)
Overlap, a	40
Sample width, b	40
Length of clamp area, l_c	40
Total length of specimen, l_s	160
Specimen length between clamps, l_g	80
Sheet length, l_t	100
sheet thickness, t_1 and t_2	3.17
Shim sheets, 1 (same material as sheet)	3.17

3.7 Process Development: FHPR of Ti-6Al-4V

The objective of the preliminary work was to gain an understanding of FP and the influence of different process parameters on the joint formation. Initially the effect of axial force on joint formation was investigated using two Ti-6Al-4V sheets with the bottom sheet hole having a chamfer where the rivet head would be formed. The process also involved the determination of a rotational speed that would allow for material to flow and fill the bottom sheet chamfer adequately.

3.7.1 FHPR Matrix A

Based on available literature, matrix A was established as illustrated in Table 3-5. Material flow characteristics with a change in axial force were quantified, with rotational speed kept constant at 5000 rev/min (peripheral velocity of 2.4 m/s). The axial force was set at 2 kN, 4 kN and 6 kN with the forge force set at 1.5 times the axial force. The initial hole geometry that was used is shown in Figure 3-11 while the dimensions of the rivet are provided in Table 3-5.

Table 3-5: Matrix A

Joint	Axial Force (kN)	Forge Force (kN)	Rotational speed (rev/min)	Volume Fill %	Rivet \varnothing (mm)
A01	2	4	5000	120	9
A02	4	6	5000	120	9
A03	6	9	5000	120	9

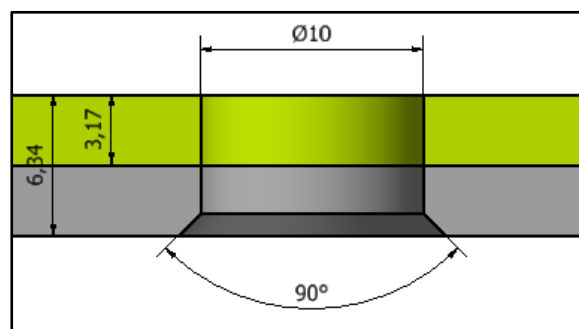


Figure 3-11: Schematic of sheets for Matrix A

Figure 3-12 shows the macrostructure of A01 and A02 with exception of A03.

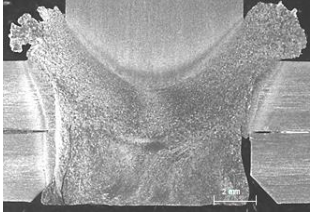
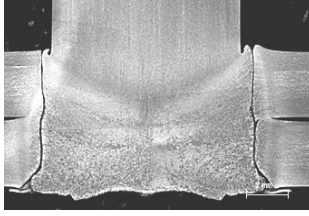
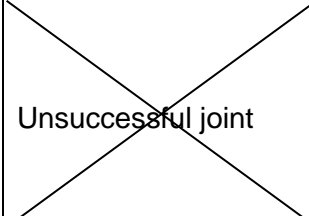
Joint No.	A01	A02	A03
Macrograph			 Unsuccessful joint

Figure 3-12: Macrographs A01 and A02

Discussion: Matrix A: A01, A02 and A03 were the first joints of the FHPR process and the following were deduced:

A01: From the macrograph, it is the author's opinions that due to a very low axial force (2 kN), the faying surfaces could not be kept intimate enough, thus leading to the rivet collapsing. The flash showed that most of the plasticised material was pushed up and bonding is visible from the middle up with an associated increase in forging force (4 kN).

A02: It would appear that bonding was achieved between the sheet and the rivet. The plasticised material was sheared off during solidification and this could have been avoided by stopping the process more quickly. Both rivet and sheet got 'soft' - therefore no bond was formed.

A03: Due to the high axial force and forging force of 6 kN and 9 kN respectively for A03, plasticised material was pushed between the backing plate and the bottom sheet being joined therefore the joint was deemed not successful and would not be discussed any further.

From this work it was noticed that for a successful FHPR joint, the Haynes 230 insert needed to be slightly sticking out and not flush with the backing plate as shown in Figure 3-13. This would eliminate the problem experienced in joint A03 and to a lesser extent A02 where plasticised material flows underneath between the bottom sheet and backing plate.

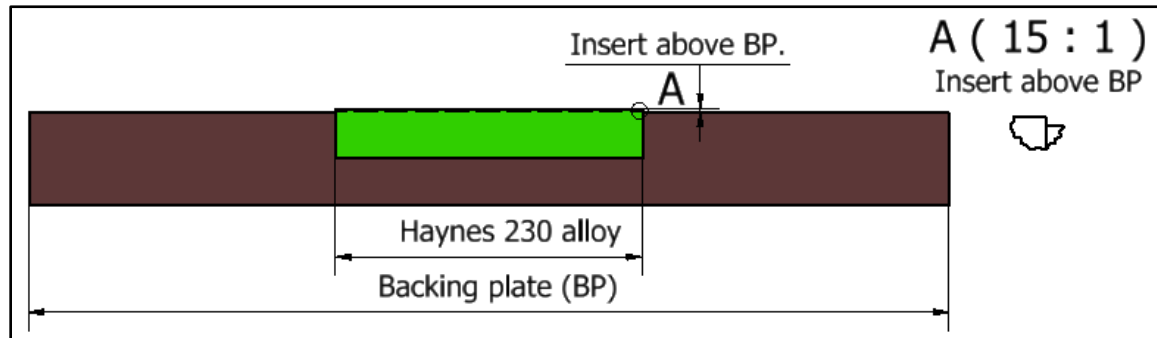


Figure 3-13: Adjustment to insert and backing plate

3.7.2 FHPR Matrix B

The objective of matrix B was to understand the effect of tool geometry and the influence of rotational speed on the formation of the FHPR joint. Important considerations that had been highlighted in matrix A were used to develop matrix A. As had been shown by weld A02, which was done at an axial force of 4 kN, it was decided that the following joint trials would be done at axial force and forging force of 4 kN and 6 kN respectively. The influence of process parameters with emphasis on rotational speed was investigated in order to understand material flow during the plasticisation phase. An understanding of joint performance from a macrostructural and hardness point of view was established. The total process energy was calculated in relation to rotational speed using the generic power formula discussed in this section. The developed matrix is illustrated in Table 3-6.

Table 3-6: Matrix B

Description	Joint Number,	Rotational speed (rev/min)	Axial Force [kN]	Forge Force (kN)	Volume Fill %]
Tool development	B01	5000	4	6	120
	B02	5000	4	6	120
Rotational speed analysis	B03	2000	4	6	120
	B04	4000	4	6	120
	B05	5000	4	6	120
	B06	7000	4	6	120
Full geometry (2 sheets)	B07	Same as B04			
	B08	Same as B05			

3.7.2.1 Rivet/Tool development and analysis

For the tool development, two geometries were investigated in order to gain an understanding of the material flow and the characteristic influence of the slight geometry change in the FHPR process. Based on prior knowledge gained in the preceding joint trials (A01 to A03), a set of parameters was used and kept constant for both joints investigated. The geometry of the two rivets was that of a chamfered rivet (45 degrees and 1 mm chamfer) compared to that of a cylindrical rivet with the diameter kept constant at 6 mm as shown in Figure 3-15. The hypothesis upon which this was based was that there would be minimal difference in terms of process energy and process time for both the cylindrical and chamfered rivets. This would be explained by the volume fill % which would be kept constant at 120% whilst upset distance was adjusted accordingly to accommodate the difference in geometry. These two joints were processed at the same rotational speed of 5000 rev/min. The experimental procedure is illustrated in Figure 3-14.

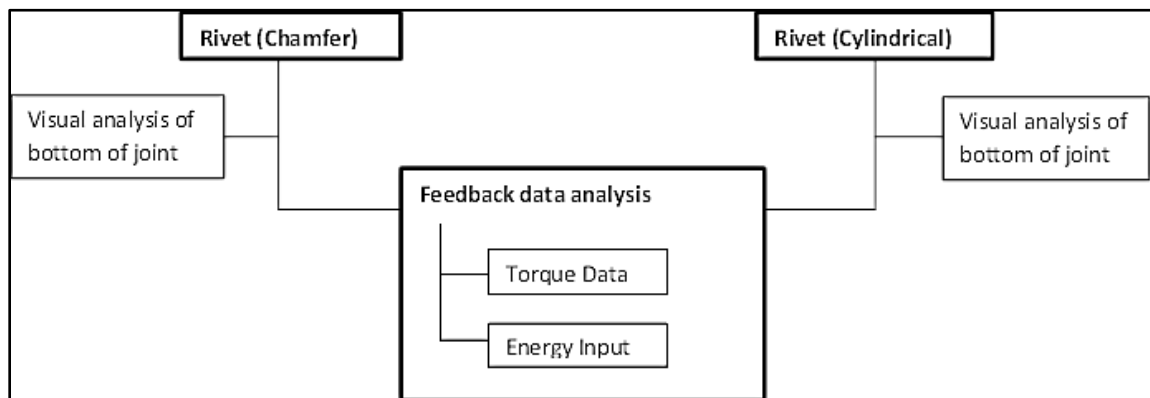


Figure 3-14: Experimental analysis diagram

The configuration and bottom appearance of the joined sheet is shown in Figure 3-15.

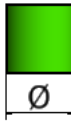
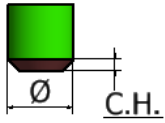


Rivet type (bottom)	Cylindrical (B01)	Chamfered (B02)
Geometry		
Diameter 1 (mm)	6	4
Chamfer height (mm)	0	1
Volume fill (%)	120	120
Joint bottom Appearance after FHPR process		

Figure 3-15: Cylindrical and chamfered rivet geometries

In terms of visual appearance there was no difference between the two joints as both sufficiently filled the bottom chamfer. The total friction time of the chamfered rivet was marginally less than that of the cylindrical rivet, i.e. by 0.4 seconds. As shown in Figure 3-16, the decrease in the total friction time of the chamfered rivet is attributed to the decrease in the contact area at the faying surfaces in the wear and seizure stage of FHPR (i.e. at the start of the FHPR joining process).

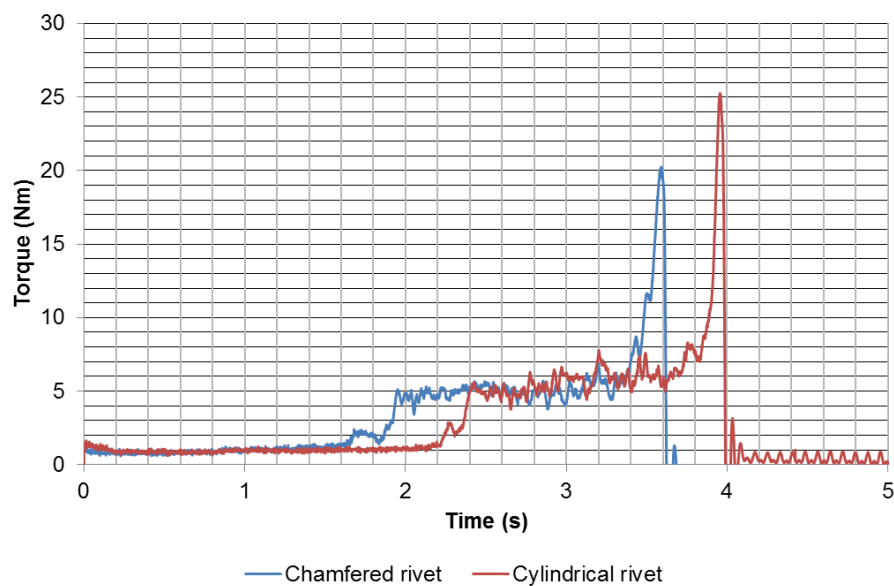


Figure 3-16: Friction Torque curve

Due to the decrease in the volume of material being heated up, the amount of process energy decreases, thus leading to the rapid completion of the first stage (wear and seizure) of the chamfered rivet. With the decrease in area of the chamfered rivet compared to the cylindrical, the torque is lower at the start of the joining process, and then increases until the two torque curves are almost on top of each other, signalling the end of the gradual depletion of the chamfer - as shown in Figure 3-17. The process energy was calculated up to 1 second which is the approximate point where the torque for both geometries was almost equal.

From these results it was concluded that there is a marginal difference in terms of the effect rivet geometry has on the process energy and process time to affect the overall FHPR process, as shown in Table 3-7 and Figure 3-17.

Table 3-7: Process Energy at up to 1 second

Rivet Geometry	Process energy at 1 second (kJ)
Cylindrical	589.2
Chamfered	537.1

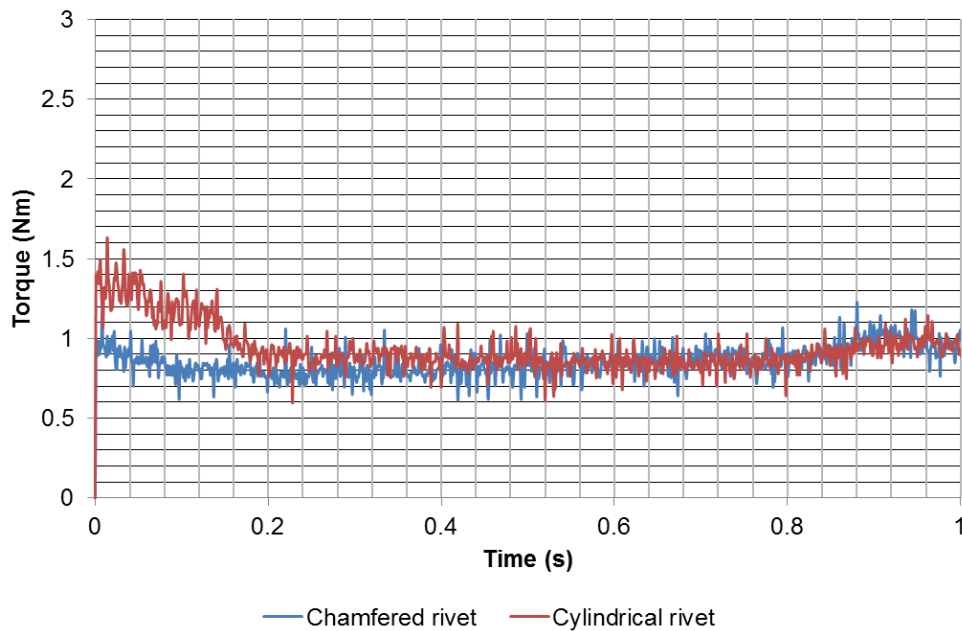
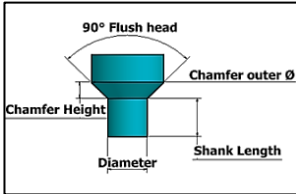
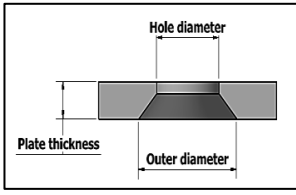


Figure 3-17: Torque (Up to 1 second)

3.7.2.2 Process parameter evaluation: Rotational speed

As was emphasised in the literature review, rotational speed is an important process parameter in FHPP and its influence on the joint formation of FHPR joints was of interest. The influence of rotational speed was therefore investigated in order to understand material flow during the plasticisation phase. The set up used in this matrix was that of a single bottom sheet (instead of a double sheet configuration). The dimensions and geometry of the rivet and sheet are shown in Table 3-8.

Table 3-8: Geometry utilised

Configuration	Description	Size (mm)	Comments
90 degree Flush rivet 	Diameter	6	Machined to size Ti-6Al-4V Eli bar
	Shank length	-	Based on the volume fill
	Chamfer outer diameter	12	-
	Chamfer height	3	-
Hole, (45 degree 2 mm Chamfer) 	Hole diameter	6.5	Radial clearance of 0.25
	Outer diameter	10.5	-
	Hole depth	3.17	-
	Thickness of plate, t	3.17	Readily available Ti-6Al-4V sheets

The upset distance (consumable length) was calculated by considering the volume of material required to fill the bottom chamfer hole in the sheet. The bottom mechanical lock or rivet head will therefore need to be formed by plasticised material contained within the chamfered hole. A 120% volume fill was used to allow for a slight overflow and to compensate for any volume change during the forge/cooling phase. The axial and forge force was kept constant at 4 kN and 6 kN respectively.

After welding the FHPR joints, visual images were taken: the samples were then cut up for macrostructural analysis. The macrographs were prepared by grinding with a 600 grit paper, followed by a diamond wheel using 3 μ allegro. A suitable polishing cloth with OPU suspension was employed for polishing as the finishing step. For the macrostructure sample preparation, the etchant used was 2 ml HF (hydrogen fluoride 40 %), 5 ml H₂O₂ (Hydrogen peroxide 30 %) and 100 ml H₂O (distilled water).

The process energy and process energy per upset distance were calculated using the generic power formula as follows:

- Process energy E:

$$Power = \frac{Energy}{time\ interval} \quad 3.1$$

$$E = \frac{2\pi NT}{60} \times time\ interval \text{ (Joules)} \quad 3.2$$

Note: Where N is the rotational speed feedback, and T is torque feedback at that instant interval

- Process energy per upset distance:

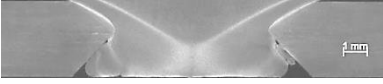
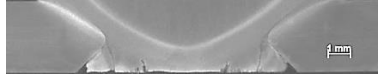


$$Energy\ per\ UP = \frac{process\ energy}{total\ Upset\ distance\ feedback} \quad 3.3$$

- Relative velocity, v :

$$velocity, v = wr \quad 3.4$$

Influence of rotational speed was quantified in terms of material flow. The process energy was calculated using a standard energy and power calculation formula as shown in Equation 1 (up until the stopping time without considering the peak brake torque). The effect of rotational speed on the bottom rivet forming process is illustrated by the cross sectional macrostructural appearance as revealed in Table 3-9.

Table 3-9: Rotational speed influence

Joint	Parameters set		Process Energy (kJ)	Energy / C. length (kJ/mm)	Joint cross section / macrostructure
	Rotational speed (rev/min)	Relative Velocity (m/s)			
B03	2000	0.63	2.01	0.70	
B04	4000	1.26	2.60	0.904	
B05	5000	1.57	3.41	1.19	
B06	7000	2.20	3.66	1.28	

As stated previously, in Rotary Friction Welding (RFW), a minimum peripheral velocity of 1.27m/s is required for sufficient bonding between the two work pieces [31]. For this experiment, peripheral velocity varied from 0.62 m/s (2000 rev/min) to 2.20 m/s (7000 rev/min) as a fusion bond between the rivet material and the side of the hole in the sheet was not considered critical. As indicated in Table 3-9, it was confirmed that with a lower peripheral velocity (0.62 m/sec at 2000 rev/min) at the outer periphery of the rivet, flow of the plasticised material was insufficient. This can be related to the quick completion of the joint at 2000 rev/min, as there was not enough heat generated at the faying surfaces to allow plasticised material to flow and form-fill the chamfered hole of the sheet. In relation to the process energy, the 7000 rev/min gave the highest value of 3.66 kJ.

From joints at 4000 rev/min and 5000 rev/min, it was observed that the material flow was acceptable although both showed deficiencies. Process time for a 5000 rev/min joint was longer than that of a 4000 rev/min joint, which relates to the tearing action being replaced by polishing with an increase in rotational speed. At 5000 rev/min, upset distance (plunge depth) rate slows down (which directly relates to cooling rate), increasing process time and producing a wider HAZ than at 4000 rev/min. Process torque response for the four welds is shown in Figure

3-18, with the straight black line showing the start of motor braking and also initiating the stopping of rotation.

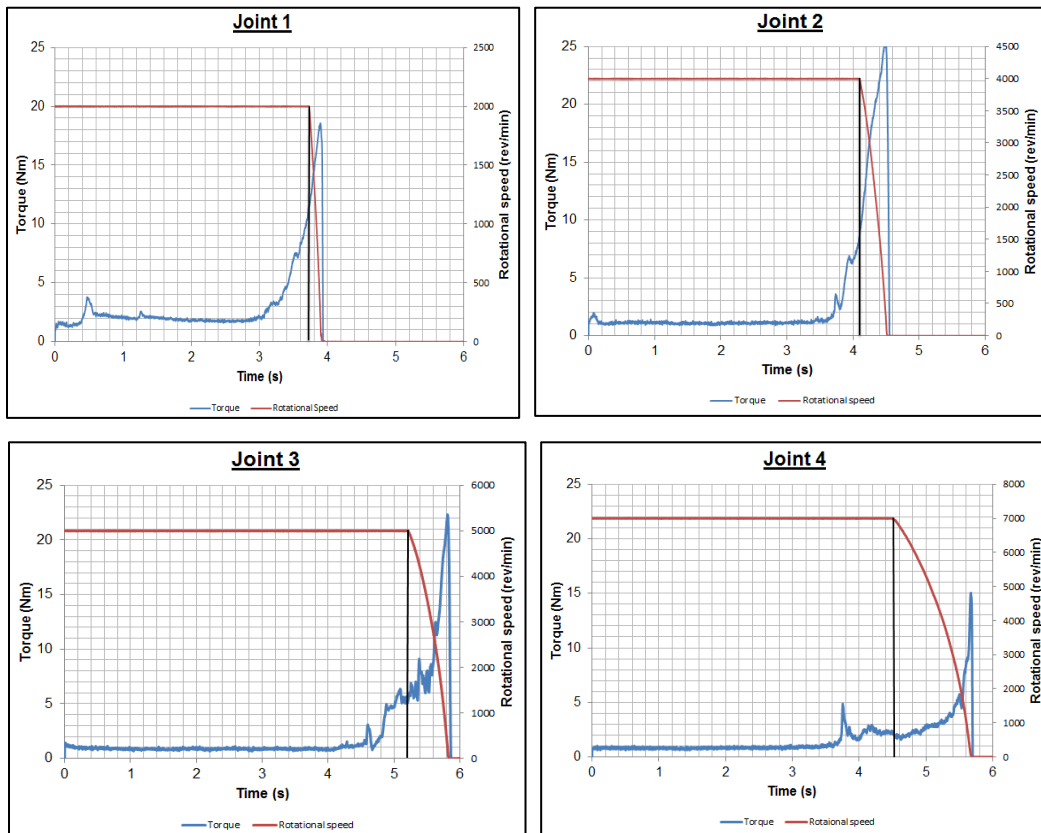


Figure 3-18: Process torque response curves

The torque curve contains important process information. Considering the 7000 rev/min (Figure 3-18:Joint 4), the torque curve stages can be identified; with the initial stage being the first stage of contacting (faying) surfaces, leading to the initial torque peak at approximately 3.92 seconds (4.6 seconds at 5000 rev/min). From the initial torque peak, the torque stabilises at 2N.m until the motor is stopped abruptly. When the motor is stopped, the torque remains constant and gradually peaks up to a brake torque (point of zero rotation) which is related to the braking time of the PDS platform and has been observed in all the joint trials. This is due to the large inertia of the welding head on the PDS platform and has been identified as a major challenge to be solved, allowing for production of optimal rivet head in the shortest time interval.

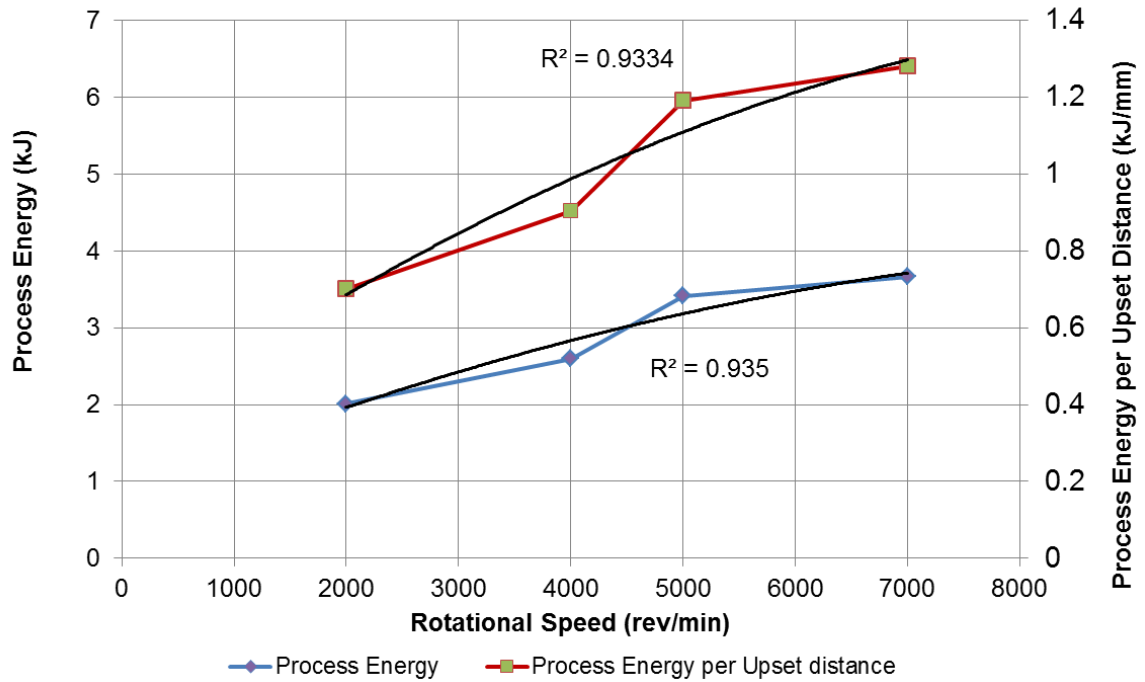


Figure 3-19: Process energy relationship to rotational speed

Figure 3-19 shows that the relationship between process energy and rotational speed which can be used to predict process energy at different rotational speeds. As the rotational speed increases, the feedback process torque decreases, which in turn causes a minimal difference to process energy at higher rotational speed of 5000 rev/min and 7000 rev/min. The gradient between two sets i.e. between 2000 rev/min and 4000 rev/min, of the rotational speed was quantified in Table 3-10.

- Sample calculation of gradient constant

$$\text{Gradient, } Q = \frac{\text{change in } y}{\text{change in } x}$$

$$Q = \frac{2598.55 - 2007.49}{4000 - 2000}$$

$$Q = 0.30 \text{ J}/(\text{rev}/\text{min})$$

Table 3-10: Gradient (Process Energy to Rotational Speed)

Rotational speed (rev/min)	Gradient, Q J / (rev/min)
2000 to 4000	0.30
4000 to 5000	0.81
5000 to 7000	0.12

This Q value showed that between 4000 rev/min and 5000 rev/min, there was a greater gradient compared to the other two. This signifies a change in the energy input into the FHPR process joining process. The high process energy difference between 4000 and 5000 rev/min is explained by an increase in overall process time (longer heating time for the 5000 rev/min joint than the 4000 rev/min joint). As explained in the literature review, at higher rotational speeds tearing is replaced by a polishing action which creates lower torques as shown in Figure 3-20.

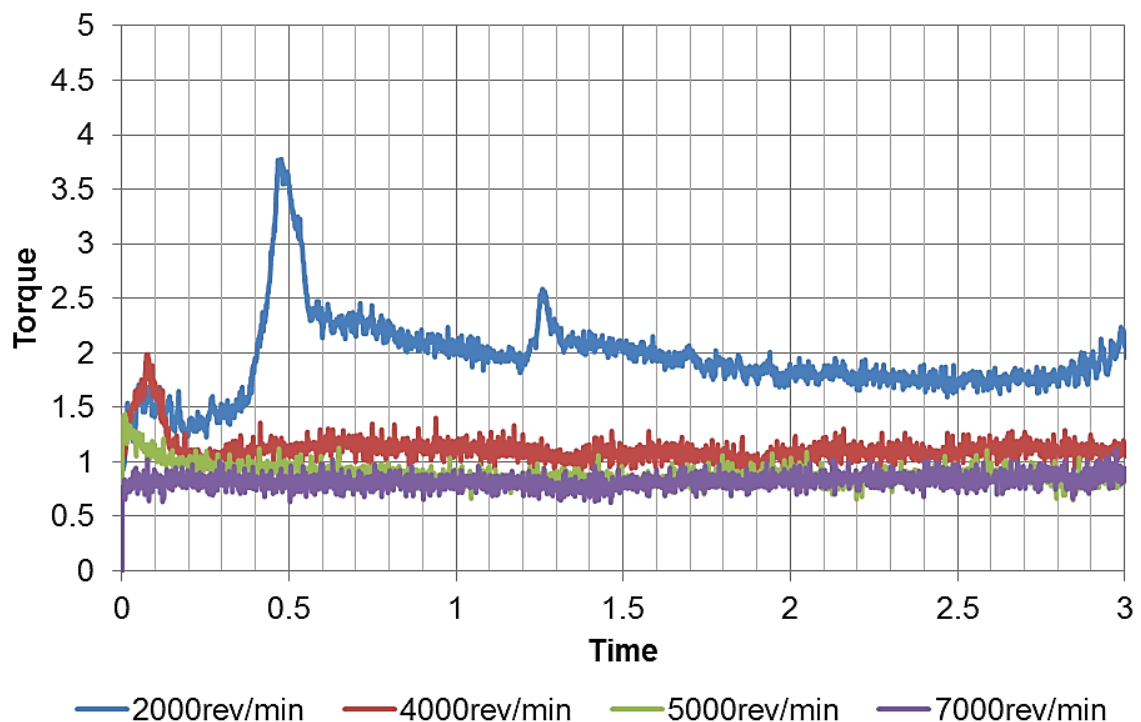


Figure 3-20: Influence of rotational speed on torque response

From here onwards, 4000rev/min and 5000rev/min joints were analysed in terms of hardness and also repeated with a full configuration of the two sheets and double chamfered holes of 45°. Hardness measurements were done 0.5mm from

the bottom of the plate in a horizontal direction with a 0.5kg load and 0.5mm spacing between indentations as shown below in Figure 3-21. Measurements of hardness were done close to the contacting surfaces of the rivet and backing plate as this is where frictional heat is generated and as these are the most likely points for introducing unwanted changes in terms of hardness.

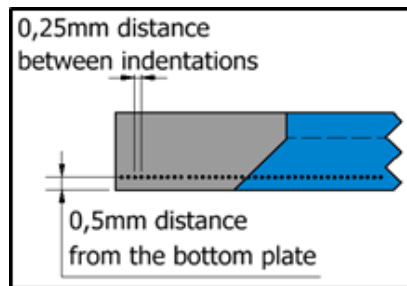


Figure 3-21: Hardness profile representation of half the sheet and rivet

The hardness profiles illustrated in Figure 3-22 shows the variations of hardness with location from the centre of the joint at approximately 0.5mm above the sheet (refer to Figure 3-21).

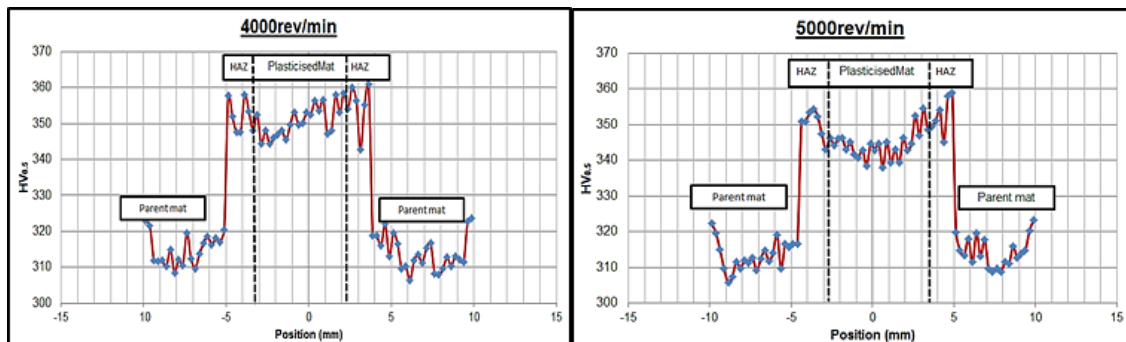


Figure 3-22: Horizontal hardness profile of 4000 and 5000 rev/min joints

Hardness values increase from the parent (310-325 HV) to the HAZ and the plasticized zone. An increase in hardness in the plasticised zone from the parent can be mainly attributed to forging force (this refines the grain size) and the temperature gradient during cooling.

The two joints at 4000 rev/min and 5000 rev/min were repeated with the full configuration of two (top and bottom) chamfered sheets and a countersunk 90°

rivet as shown in Figure 3-5. This was done so as to lock the two sheets together with a bottom and top chamfer as shown in Figure 3-23.

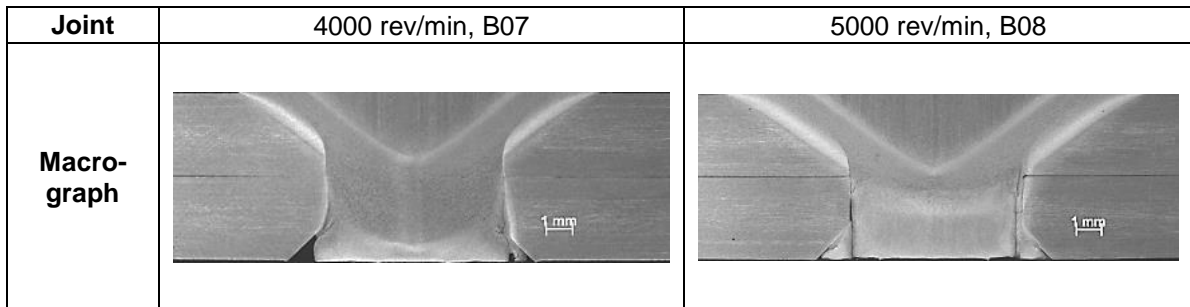


Figure 3-23: Full joint of 4000 rev/min and 5000 rev/min

Although it appears as if a proper fill of the bottom chamfer was achieved at 5000rev/min another phenomenon was identified raising some concerns. From macrostructural appearance, it appears that some diffusion or lack of fusion accrued along the original shank diameter and the newly formed plasticised material that formed the bottom rivet head as illustrated in Figure 3-24.

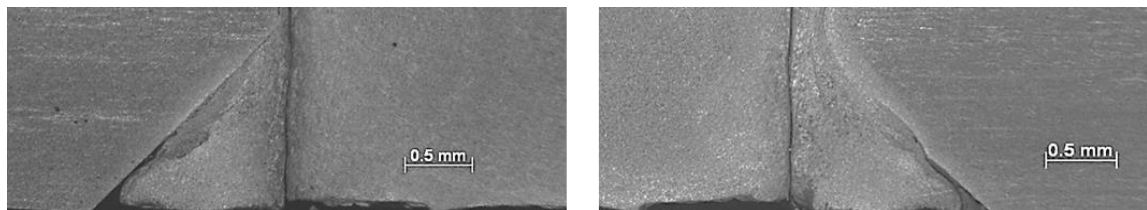


Figure 3-24: A clear separation line between plasticised material and rivet


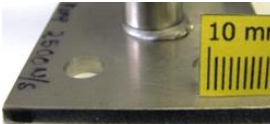




This is undesirable as it will not form the desired mechanical lock. It most probably occurred due to the result of plasticised material making contact with the side of the “cold” chamfered hole in the sheet, resulting in a stronger bond than that between the original stud and the displaced plasticised stud material, thereby forming a shear layer at this point. It is believed that this could be solved by stopping the process earlier and relying on a cold forge/form final.

As a result of this phenomenon, an investigation of how quickly the FP PDS platform stops was therefore initiated. As discussed earlier, the long stopping time is due to the large inertia head of the PDS platform, which necessarily is not an issue for FHPP welds where the process time is usually longer than 20

seconds. Solving the stopping time issue would allow for production of an optimal rivet head in the shortest time interval.

Constant rotational speed and upset distance - but varied axial force (4 kN; 5 kN and 6 kN) joints were FHPR processed. Stopping time in relation to axial force showed that with an increase in axial force, the FHPR joining process time decreased. The visual images presented in Table 3-11 of the FHPR joints showed that, an increased stopping time reduced the amount of flash formed.

Table 3-11: Influence of increasing axial force on braking time

Joint No.	B04	B09	B10
Force (kN)	4	5	6
Rotational speed (rev/min)	5000	5000	5000
Volume fill %	120	120	120
Joint top appearance			
Joint bottom appearance			

Although the flashed formed decreased with an increase in axial force, it was noted that from joints 5 kN and 6 kN, the FHPR joints would stick to Haynes 230 alloy insert. The sticking of the faying/contacting surfaces was mainly due to a large axial force keeping the surfaces intimate while the decrease in flash formed was due to a quicker stopping time which is affected by the large inertia of the FP head explained earlier. A force of 4 kN continuously used in the development of the FHPR process, did not exhibit any sticking between the rivet plasticised material and the Haynes 230 alloy. However separating the insert and joint became a problem as some material stuck on the backing plate insert thereby leading to a fairly rough surface on the bottom of the joint.

The rotational speed to time was also plotted for earlier joints done to quantify the influence of rotational speed on stopping time as shown in Figure 3-25.

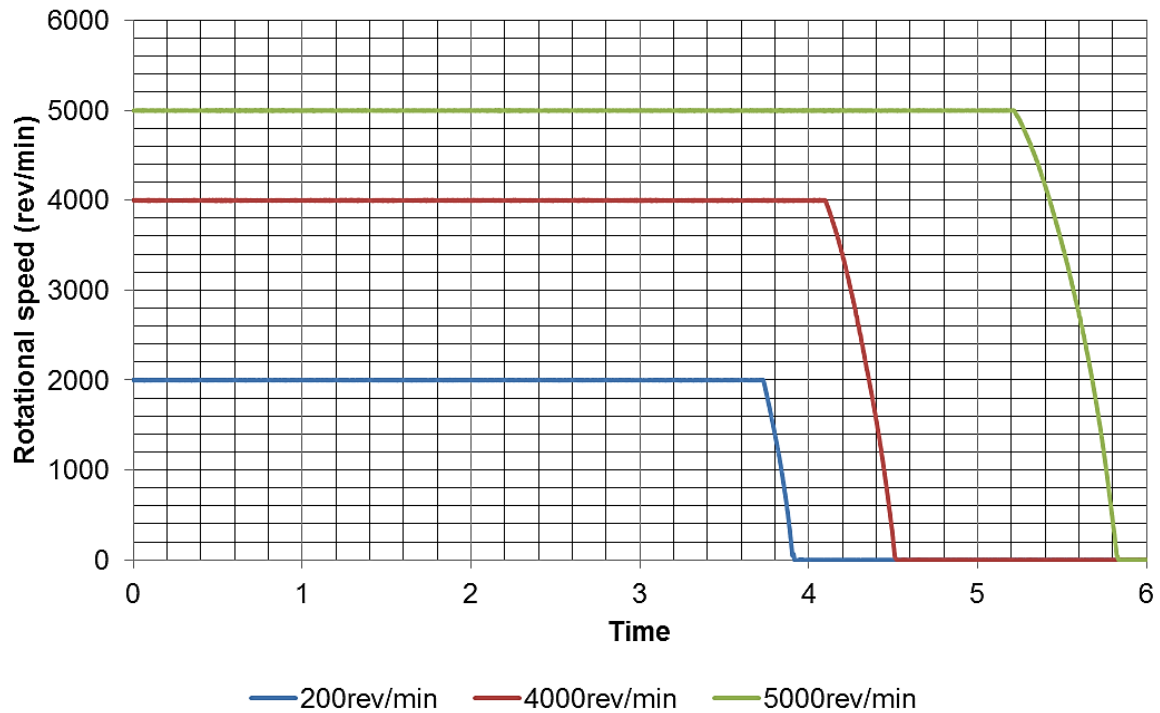


Figure 3-25: Increase in stopping/ braking time, PDS platform

Figure 3-25 shows 2000, 4000 and 5000 rev/min rotational speed feedback curves and from these a graph of rotational speed vs. stopping (refer to Figure 3-26 and Table 3-12) was plotted to characterise the platform when conducting diameter 6mm rivets for FHPR.

Table 3-12: Stopping time at different rotational speed

Rotational speed (rev/min)	Stopping time (s)
2000	0.190
4000	0.419
5000	0.618

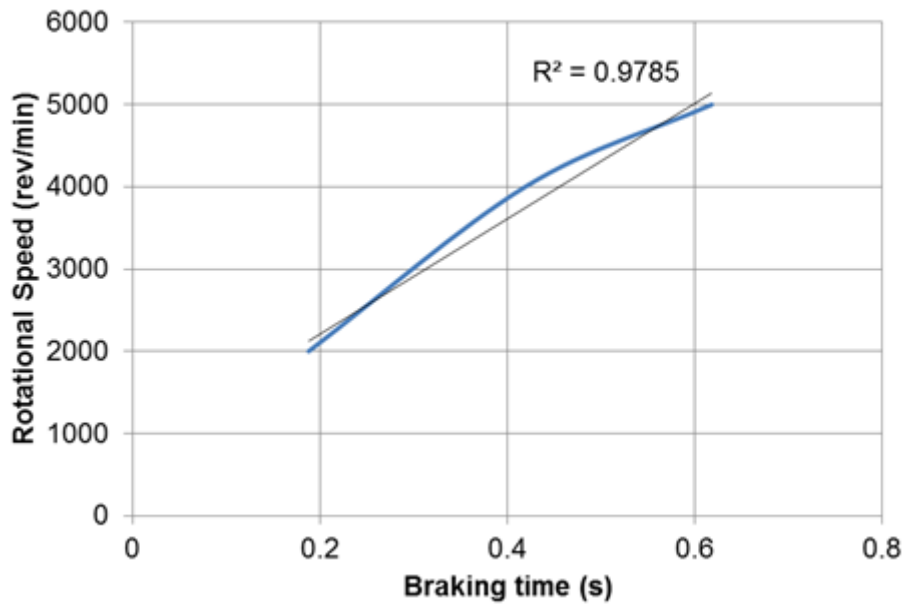


Figure 3-26: Rotational speed relationship to stopping time, PDS platform

The Weldcore platform has a maximum platform rotational speed of 5250 rev/min. At 5000 revm/min, it takes 0.05297seconds to come an abrupt halt from as shown in Figure 3-27. This decrease in stopping time has an effect on the flash formed as the process is easily controlled with the upset distance kept constant.

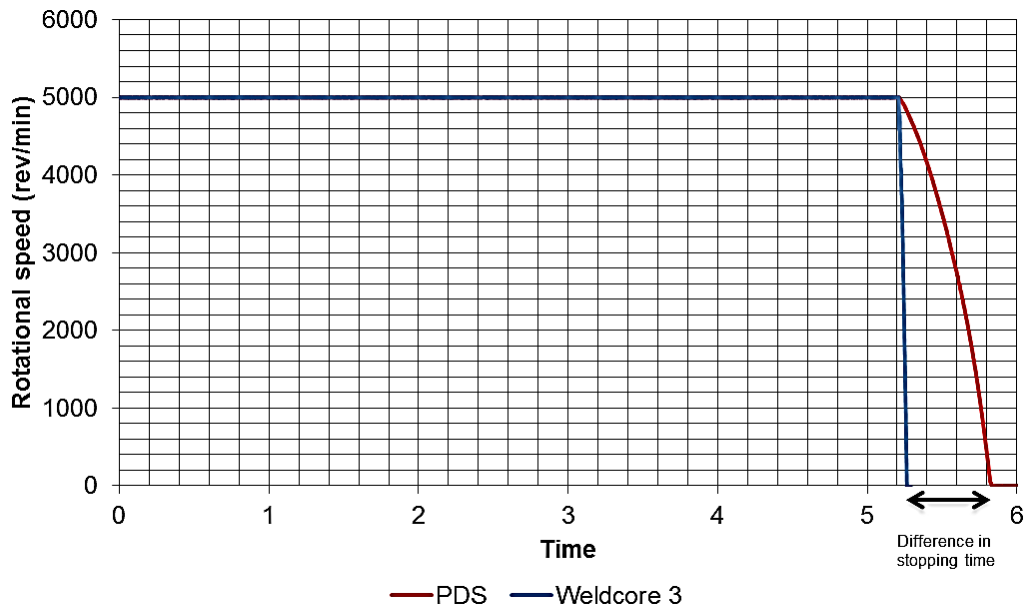


Figure 3-27: Rotational speed relationship to stopping time, PDS platform vs. Weldcore 3 platform

3.8 Summary

The results from the preliminary welding revealed important process relationships and evidence to show that FHPR can be used as a method for riveting Ti-6Al-4V sheets together. A drop in average process torque was experienced during rivet forming at higher speeds. This trend in turn is attributed to an associated increase in process temperature with the increase in rotational speed, reducing shear layer strength in the plasticised material and thereby resulting in the drop in process torque. Increased heat input on the other hand reduced the cooling rate due to a greater volume of material being heated up. As the cooling rate decreased, a wider HAZ was observed. Therefore, rotational speed contributes to the frictional heating and influences the joining speed of FHPR process.

This chapter also describes the two different platforms used in the initial and final development of the FHPR process. The difference in the platforms is in their stopping times with the Weldcore which is utilised more quickly in the final stopping due to a decrease in the inertia of the welding machine.

From this preliminary work, the required process stages have been defined with a clear indication that the final process will have to tend more to a cold forge/form stage rather than a traditional FHPP stage. The clear separation between plasticised material pushed to fill the bottom hole chamfer and the rotating rivet, needs to be discussed further. Stopping the process quickly and adjusting the bottom hole chamfer angle might play a role in eliminating this problem.

Chapter 4: Results and Discussion

4.1 Introduction

This chapter details the final development of Friction Hydro Pillar Riveting (FHPR) where the bottom hole chamfer was varied (15° , 30° and 45°) and a blind hole geometry introduced as shown in Table 4-1 and Figure 4-1. Macrographs of the joints were studied and linked to the pull off strength of the FHPR joints. The FHPR joining process was done using the Weldcore 3 platform at 5000 rev/min (maximum rotational speed of the platform is 5250 rev/min) and 4 kN axial force while the forging force was increased by 150% to the axial force.

The preliminary work detailed for FHPR was used for the initial process development as there were no prior developments in FHPR of Ti-6Al-4V. From the established set of process parameters, the final matrix was developed by involving a varying of the bottom chamfer angle (15° , 30° and 45°) in the bottom sheet hole. This variation of chamfer angle allowed for results' quantification in terms of material flow (macrographs) thereby determining which geometry adequately fills the bottom hole chamfer. The idea behind the introduction of varied chamfer angle bottom hole sheets was to try to eliminate the problem discussed in section 3.7.2 FHPR Matrix B (refer to Figure 3-23) where a clear separation was visualised. The pull off test would then be used to quantify the joint strength in the axial direction.

From the logged feedback data, upset distance, rate of upset distance, heating time and frictional torque were determined and subsequently analysed. Frictional torque was used to identify the different stages of the FHPR process. The final matrix finished off with shear testing of the best configuration and microstructure evaluation of all the FHPR joints from the parent material, heat affected zone (HAZ) to the weld zone. This could then lead to the development of a new and exciting way of riveting Ti-6Al-4V sheets for the Aerospace industry via Friction processing.

Table 4-1: FHPR of Ti-6Al-4V Final Matrix

Description	Joint Number,	Joint description	Rotational speed (rev/min)	Axial Force (kN)	Upset distance (mm)
Macro/ Microstructural	01	45°	5000	4	3.6
	02	30°	5000	4	2.5
	03	15°	5000	4	1.8
	04	Blind Hole 5000 rev/min	5000	4	1.3
Pull off test	05	15°	5000	4	3.6
	06	30°	5000	4	2.5
	07	45°	5000	4	1.8
	08	BH 5000 rev/min	5000	4	1.3
	09	Blind Hole 2500 rev/min	2500	4	1.3
Shear test	10	15°	5000	4	1.8
	11	Blind Hole 5000 rev/min	5000	40	1.3

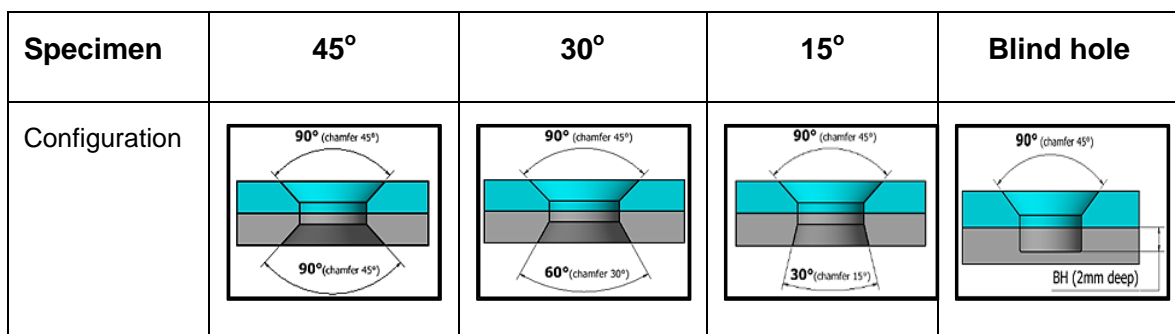


Figure 4-1: Geometry of the plate with varying chamfer angles and the blind hole

Figure 4-2 shows the final matrix rivet (consumable tool) design. For research purposes only, the rivet overall length was longer than actual “would be” design for commercial integration so that it could accommodate the numerous tests that were conducted (i.e. the pull off test required at least the back part to be 15 mm in length before clamping it with the jaws of the Instron tensile tester machine).

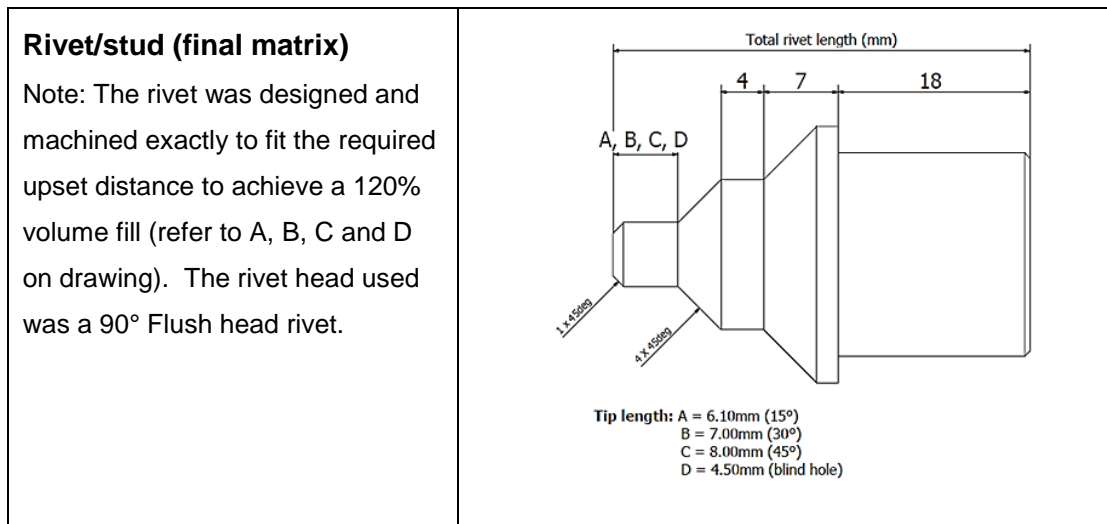


Figure 4-2: Rivet design for final matrix using the Weldcore 3 platform

4.2 FHPR process model

The torque curve of FHPR, as discussed in Chapter 3, contains important information that can be used to model the FHPR process: this was discussed and the stages of the FHPR process were detailed. There are many configurations and various possible joint geometries that can be used in making a FHPR joint. The geometry that has been discussed thus far is of the bottom hole chamfer scenario. It has shown characteristics that allow it to be an alternative joining technique for riveted joints and will be studied further with the blind hole configuration.

It is the author's opinion that the FHPR process has five important process stages can be defined for the FHPR process by using the friction process torque curve. Initially the process involves a pre-machined rivet / stud and two Ti-6Al-4V sheets with the top sheet having a rivet hole and chamfer which is of the same size as the rivet being utilised. In this case, a 90° rivet was used with a top sheet having a 45° chamfer. The bottom chamfer can be varied from 45° to 15° or to a blind hole as has been suggested in this work. The sheets being joined are firmly clamped together onto a backing plate with a Haynes plate insert.

The rivet is rotated into the aligned holes of the sheets being joined together combined with a small axial force. At the start of the FHPR process, the combination of rotational speed and axial force generates frictional heat which

increases the temperature at the faying or contacting surfaces of the rivet and the backing plate. In the initial stage, as with RFW and FHPP, the FHPR has a rubbing and seizure stage which is quickly completed - and is not easily visible on the torque curve due to the smallness of the rivet size compared to normal FHPP and RFW processes. After this rubbing and seizure stage has been completed, accompanied by a temperature increase at the faying surfaces, upsetting of the rivet starts. For this to begin, the temperature needs to increase until it reaches the plasticisation temperature of the material. Due to low thermal conductivity of Ti-6Al-4V alloy, the plasticisation temperature is quickly reached and the material then starts to flow, gradually filling the bottom hole chamfer. Upsetting or rivet shortening is governed by the amount of upset distance required to fill the bottom hole chamfer, thereby enabling the formation of a mechanical lock.

Unlike Friction Taper Stud Welding [38], the FHPR, as with its sister FHPP, involves a rapid formation of a pillar of shear layers as the whole rivet is plasticised: this then leads to plasticised material flowing to fill the bottom hole chamfer during the rivet consumption/upset. When the set upset distance is reached, rotation is stopped abruptly, thus leading to the beginning of the final stage of forging/forming and consolidation. The forging force refines the grain size and material consolidates as temperature decreases. During this forging stage, some of the plasticised material is pushed out as flash, while the rest cools down and fills the bottom hole chamfer.

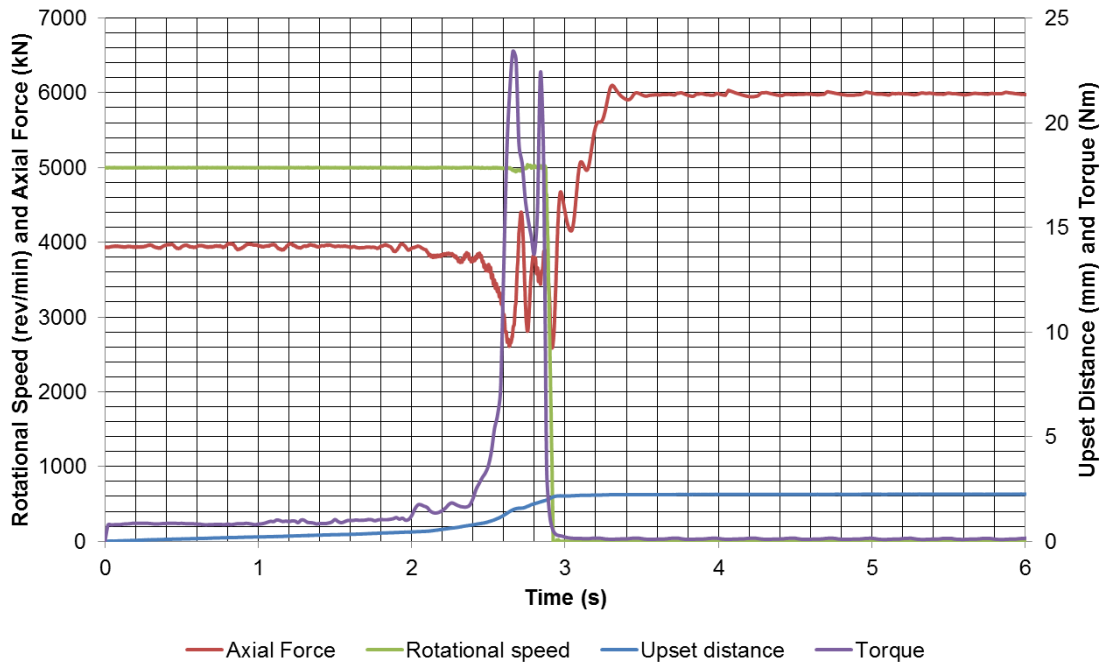


Figure 4-3: FHPR process curve for Bottom hole chamfer (15°)

From this process curve, Figure 4-3, the stages of the FHPR process can be determined and the torque curve is divided into five FHPR stages (i, ii, iii, iv, v) as shown in Figure 4-4.

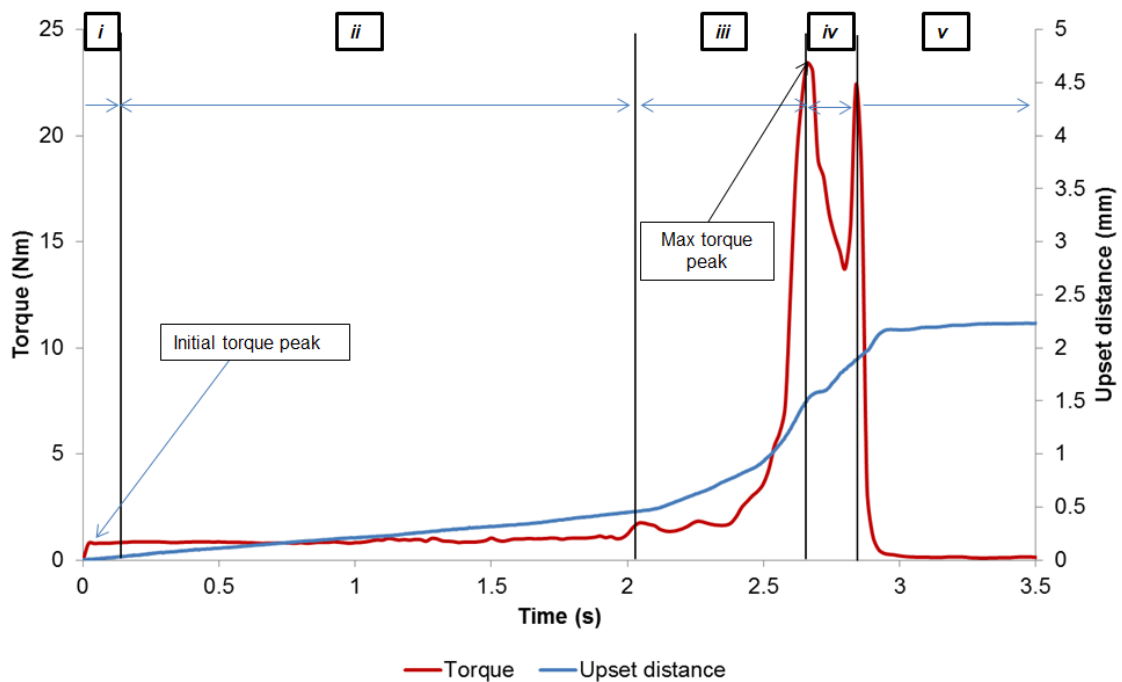


Figure 4-4: Torque curve stages

It is imperative to discuss the stages represented by the torque curve for the full configuration. Earlier discussion in the preliminary development stage focussed on a single sheet process torque curve prior to changing platform from the PDS to the Weldcore 3 platform. The stages of a full configuration FHPR joint are now identified and discussed as follows:

Stage i: This stage involves the rubbing and seizure stage. The rivet contacts the faying surfaces leading to an initial torque peak. Temperature in this stage increases with upsetting distance still close to zero as rubbing and seizure is completed.

Stage ii: This stage is characterised by the increase in upset distance at a fairly constant torque as the rivet is being plasticised and is forming shear layers. With low rotational speed the torque feedback will be higher than at higher rotational speed. In this stage, there is a relationship between the plasticisation of material and material flow with upset distance: this is because upset increases linearly over process time. However further investigation is required to understand this phenomenon better.

Stage iii: This stage is a continuation of stage ii, but now sees a gradual increase in torque due to the whole rivet head gradually coming into contact with the top chamfer hole, hence leading to an increase in torque up to a maximum: this is caused by the diameter of the rivet head increasing, with an increase in contact area as the rivet depletes or is consumed, thereby leading to a torque increase.

Stage iv: It is the author's opinion that at this stage, the rotating rivet under an axial force is apparently now into holes of the two sheets being joined, at which point, a 100% volume fill has been achieved. The torque decreases as the flash is being formed due to the 20% additional upset distance (120% volume fill set), and then rapidly increases again as the stopping of the platform's motor starts.

Stage v: This is characterised by the third torque peak which is due to the abrupt braking of the Friction Processing platform motor the forging and material consolidation starts.

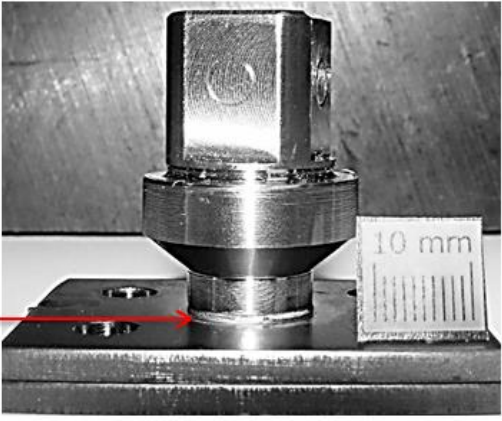
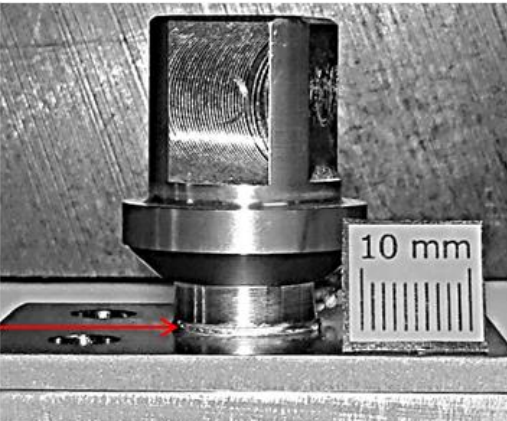
Table 4-2 (see below) lists the process parameters with their functions as investigated in the preliminary work where an emphasis was set on quantifying the influence of rotational speed and axial force on joint formation and material flow behaviour.

Table 4-2: Process Parameters that in FHPR

Parameter	Function
Rotational Speed	Contributes to the frictional heating. Influences the joining speed.
Axial Force	Controls the distribution of pressure on the joining area. Contributes to frictional heating and joining speed.
Forging Force	Contributes to grain refinement and consolidation of the rivet plasticised material.
Upset distance	Indicates the level of rivet penetration and deformation (consumption).
Temperature	Influences the properties of titanium (plasticising and material flow behaviour).
Frictional Torque	Associated with material plasticizing. Identification of process stages.

Table 4-3 shows two joints (45° bottom hole chamfer configuration for pull off and macro-analysis) which display uniformity in the flash formed between joints of the same bottom hole chamfer angle. From the FHPR process feedback curve, important information was collated as shown in Table 4-4 for feedback data analysis (refer also to Appendix C: Visual images of Joints).

Table 4-3: Visual appearance of same process parameter joints

Joint description	Visual image
15° bottom hole chamfer (Macro analysis joint)	 <p data-bbox="518 645 699 678">Flash formed</p>
15° bottom hole chamfer (Pull off analysis joint)	 <p data-bbox="518 1104 699 1137">Flash formed</p>

One of the advantages of FP is that it is easily repeatable, thereby giving this same process feedback within experimental error [2] [26]. For repeatability purposes and quality control of the FHPR process, the input upset distance and the feedback upset distance data was analysed. Upset distance was analysed because the FHPR process is a joining process which is governed by upset distance considering rotational speed and axial force are kept constant. An upset distance governed joining process means the upset distance is used as one of the inputs to control process time by setting the required upset into the Friction Welding machine. Table 4-4 shows the analysis of upset distance. From the feedback data, it was noted that the process was repeatable before testing could commence.

Table 4-4: Upset distance analysis

Joint description	Set upset distance (mm)	Feedback upset distance				Mean	Uncertainty
		Macro/ Micro	Pull off test	Shear Test 1	Shear Test 2		
BH 5000rev/min	1.3	1.517	1.511	1.623	1.588	1.56	0.09
15°	1.8	2.274	2.123	2.237	2.105	2.18	0.13
30°	2.5	2.74	2.559	X		2.65	1.15
45°	3.6	3.768	3.751			3.76	0.11

The process torque curve was also used to analyse the repeatability of the FHPR process by calculating the amount of process energy required for the FHPR process. The 45° bottom hole chamfer process curve shown in Figure 4-3 has a torque feedback and rotational speed which are used in the generic power formula to quantify the amount of process energy. Figure 4-5 shows an example of two similar joints (blind hole configuration) which were completed at the same process parameters.

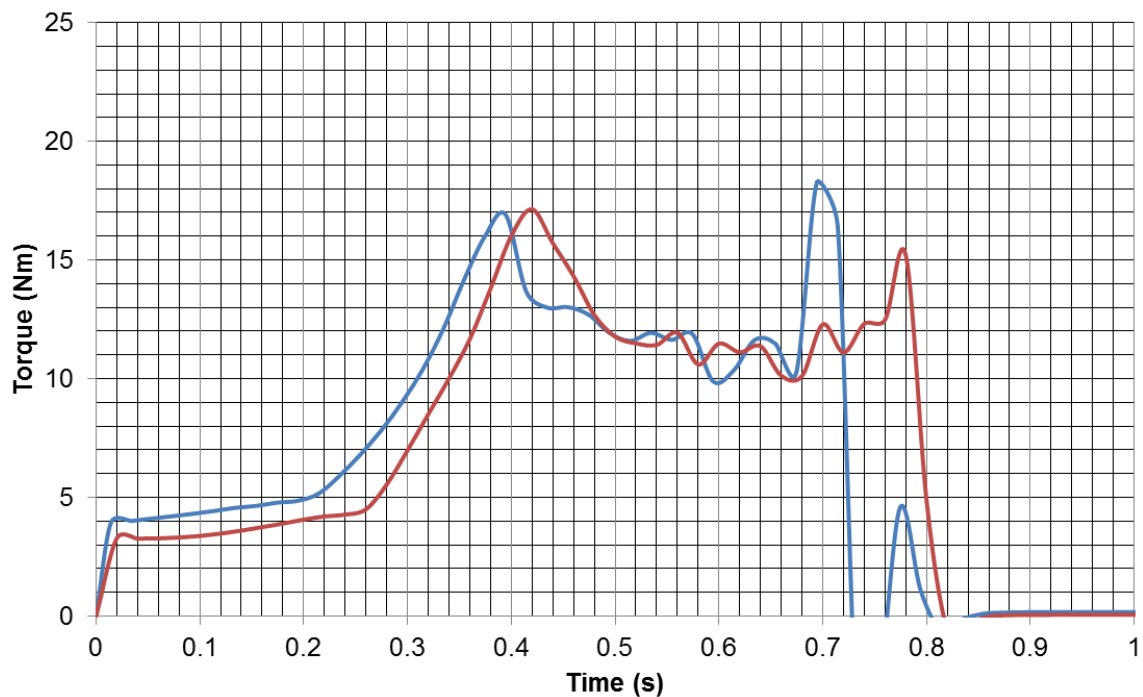


Figure 4-5: Same process parameter FHPR joints process torque

From the set of samples done for pull off testing and for micro/macro analysis the process torque was quantified and tabulated as illustrated below in Table 4-5.

Table 4-5: Calculated process energy

Joint type	Energy 1.(J)	Energy 2.(J)	mean
45°	5725	5791	5758
30°	4732	4701	4716
15°	3750	3720	3735
Blind hole 5000rev/min	3458	3433	3445

From the data tabulated in Table 4-5, a Means Graph with 95% error bars of process energy versus joint type was plotted in Figure 4-6: Process energy. As shown here, the error bars for 45°, 30° and 15° do not overlap: this means there is a significant difference in process energy, i.e. the energy values for the different geometries are not equal within experimental error (it is important to note this for the following process energy and pull off energy absorbed relations). If the 15° bottom hole chamfer is compared to blind hole, there is an overlap (error bars) which is attributed to the reduction of the chamfer angle, leading to less process energy being required for 15° geometry.

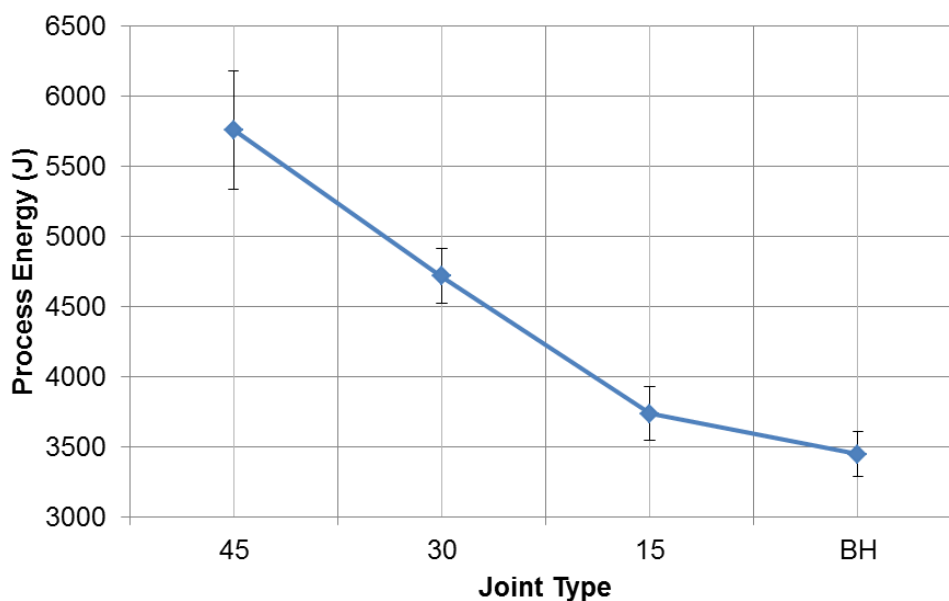


Figure 4-6: Process energy vs. Joint Type

4.3 Macrostructural analysis

The idea behind the variation of chamfer angle of the bottom sheet was to fully understand and obtain a material optimum angle of flow which is the angle at which material flows to adequately fill the bottom hole chamfer. As was discovered in the preliminary work with the 5000 rev/min joint, an undesirable clear separation existed between plasticised material ‘pushed’ to the side which contacts the cold sheet chamfer and the rotating rivet. A decision was made to repeat the 45° bottom hole chamfer geometry using the Weldcore 3 platform (quicker stopping time) and from the macrograph try to visualize the difference in the joint at a quicker stopping time. Figure 4-7 therefore shows the 45° bottom hole chamfer joint repeated. The process parameters for the two joints are the same although different platforms were used (refer to Figure 3-23).

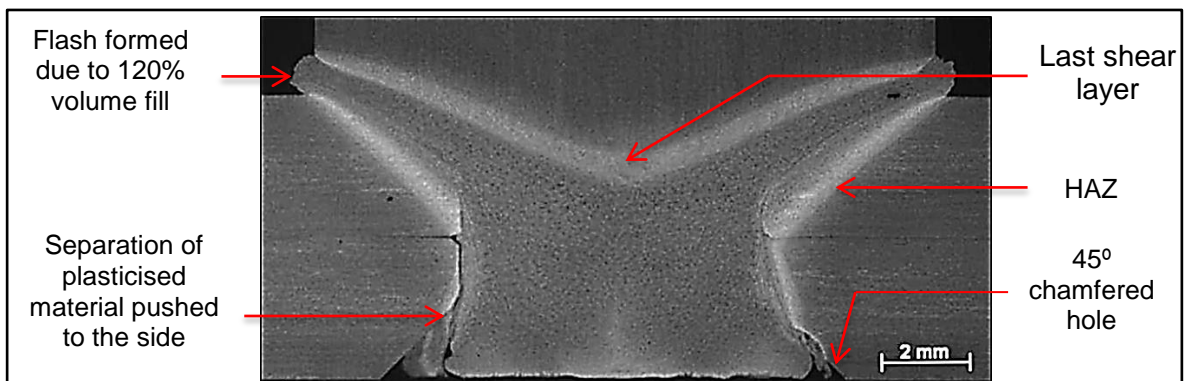


Figure 4-7: 45° bottom hole chamfer macrograph

As visualised from the 45° bottom hole chamfer macrograph, an improvement in the bottom hole filling was visible although a clear “separation” was still evident which led to the introduction of bottom hole chamfer varying. The 30° and 15° bottom hole chamfer configurations were then done to quantify the difference in macrographs with a subsequent decrease in chamfer angle. Figure 4-8 shows the gradual progression in the filling of the bottom hole chamfer including the 45° bottom hole chamfer joint and blind hole.

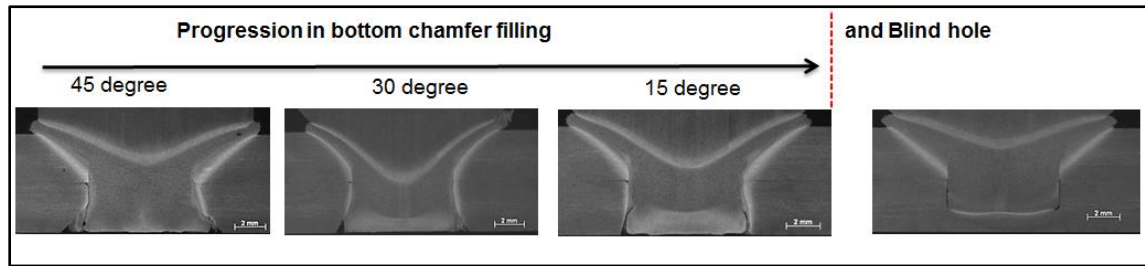


Figure 4-8: Macrographs of FHPR joints with varying angles and the blind hole

From the macrographs, there is gradual progression in the optimum fill of the bottom chamfer. The blind hole (BH 5000 rev/min) showed great potential as there was bonding of the sheet to the rivet (ref to Figure 4-4) at the bottom faying interface.

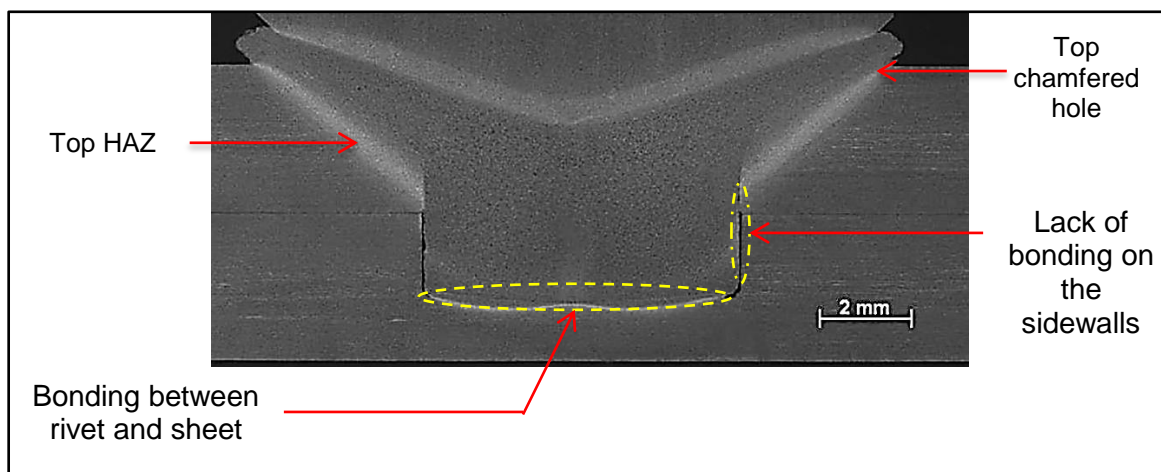


Figure 4-9: Blind hole 5000rev/min macrograph

Lack of bonding on the sidewall for joint blind hole 5000rev/min could be solved by reducing the clearance between the rivet and hole. For all the FHPR joints discussed, bonding to the side wall was not necessary a requirement for a good FHPR joint, only to be able to form a mechanical lock by joining the two sheets together.

4.4 Pull off Test

As had been discussed in the preliminary process development and illustrated by Figure 4-7, the clear separation line of material plasticised to fill the chamfer and the rivet would affect the mechanical lock strength of the FHPR joint. Therefore, the pull of test was established. The pull off test was performed according to a modified ASTM 7322 standard, which was used to develop a pull off test method for the FHPR joints as discussed in section 3.6.1. The pull off test was done due to the need to quantify the amount of force required to pull the rivet out of the two sheets joined.

4.4.1 Pull of test results

From the pull off tested samples, a force vs. displacement graph for all the joints was plotted as shown in Figure 4-10. The pull off tests results are tabulated in Table 4-6 indicating the first fracture force/load and displacement. The first fracture force is defined as the position of the first slip on the force vs. displacement graph.

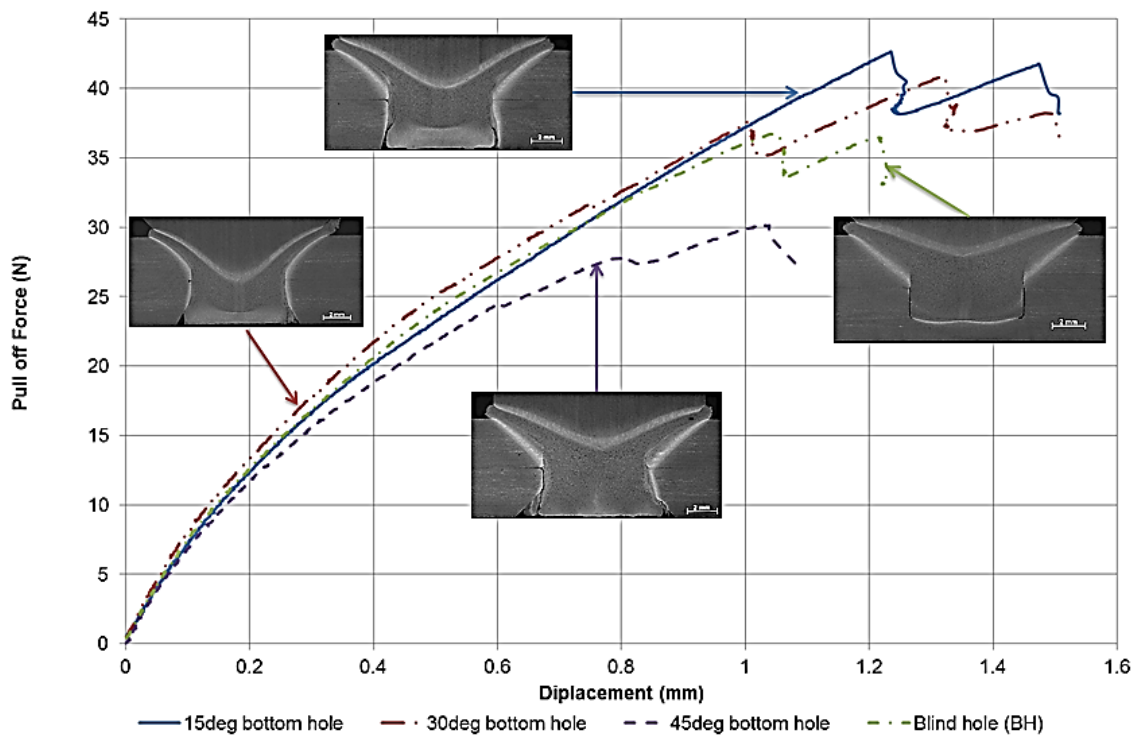


Figure 4-10: Pull off test results

Table 4-6: Pull off results

Joint description	First Fracture Force (kN)	Displacement (mm)
45° bottom hole	30.709	1.038
30° bottom hole	37.568	1.005
15° bottom hole	42.643	1.235
Blind hole (BH)	36.709	1.041

Figure 4-11 shows the pull off joints fracture surfaces for tested joints of different bottom hole chamfer (15°, 30°, 45° and BH 5000 rev/min). The shiny surface shown on the pulled off rivets is plasticised material that fills the bottom chamfer hole. The 15° showed that with a decrease in chamfer angle, a bond was formed at the bottom chamfer hole therefore forming a strong mechanical lock as compared to the others. The rivet fractured in half without the whole rivet being pulled off as shown from Figure 4-11 (15° bottom hole visual images).

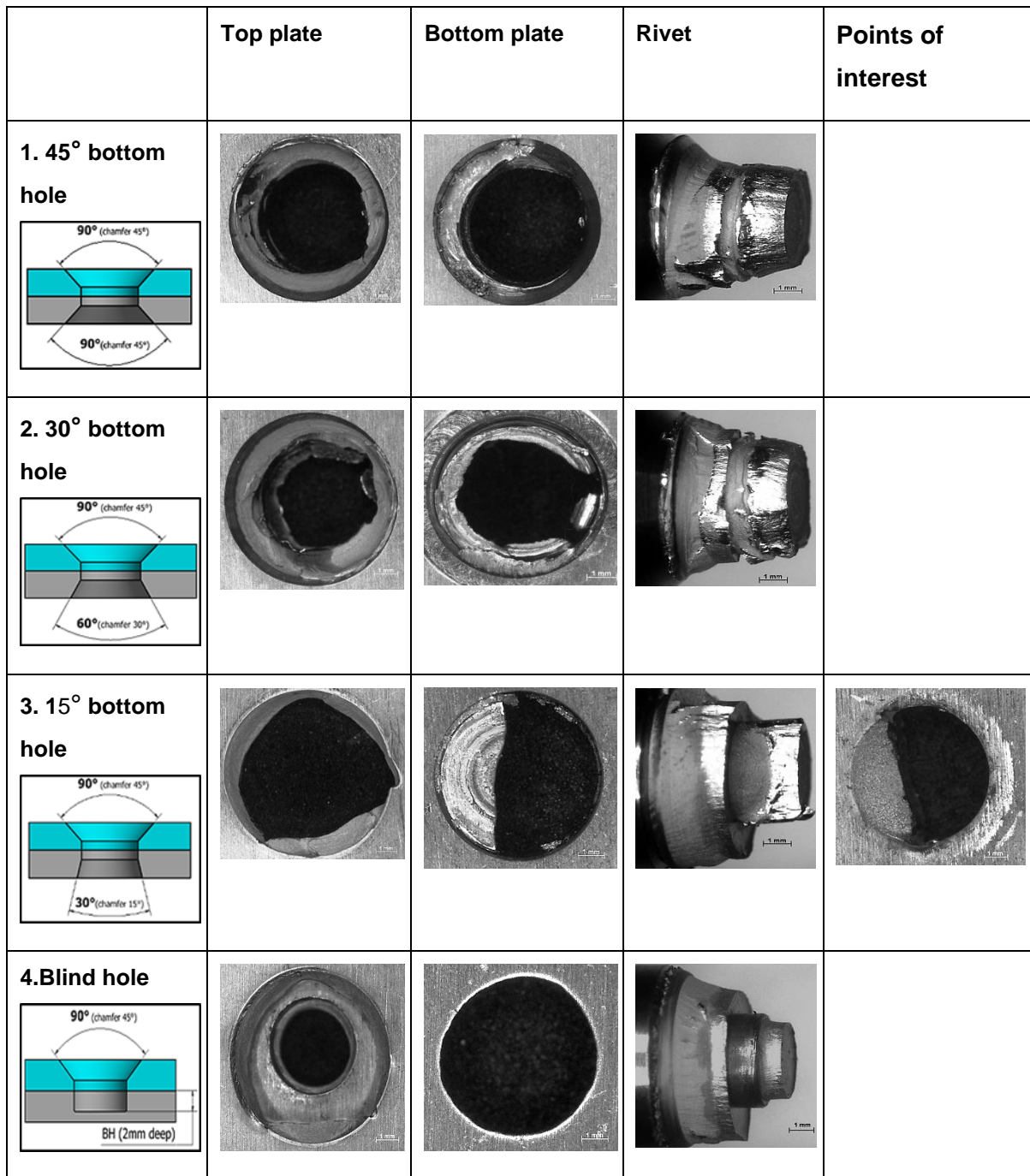


Figure 4-11: Pull off fracture surfaces

From the pull of results the following was deduced:

45° bottom hole chamfered: From the pull off result (force and displacement curve), it was clear that a low pull off force and displacement was recorded because of the failure to adequately fill the bottom hole chamfer. As discussed earlier, the clear separation line which is still visible on the 45° macrograph had an impact on the first fracture force (defined as the position of the first slip on the

force vs. displacement graph) which was lower than the other 3 tested geometries.

30° bottom chamfered hole: The 30° macrograph is almost a similar to the 15° macrograph. With an increased angle of 30°, the pull off force is lower than that of the 15° configuration.

15° bottom chamfered hole: It has the highest pull off force and leads to the conclusion that, with a decrease in the chamfer angle, the pull strength increases which will be elaborated further in the following sections.

Blind hole (BH 5000 rev/min): The blind hole setup configuration eliminated the need for a Haynes insert backing support (refer to Figure 4-1). The faying surfaces were between the Ti-6Al-4V sheet and rivet. Pull off results showed that the bond between the sheet and rivet at the bonding interface was strong therefore leading to the fracture of the 1mm sheet at the bottom as shown in Figure 4-11. Bonding at the interface of the rivet and sheet formed the desired mechanical lock.

4.4.2 Pull off energy absorbed

From the pull off vs. displacement graph, the amount of energy absorbed can be calculated as the area under pull off vs. displacement graph. The energy absorbed allows to the quantification of the joint energy absorbed by looking at the both the displacement and the pull off which allows for choosing of the best geometry with better energy absorption qualities. Energy absorbed is termed as the amount of energy required to break the joint or for failure to occur (in this case the first fracture force). The energy absorbed is similar to toughness of a material.

Energy absorbed = Force x displacement at an interval (Joules) Equation 4.1

Figure 4-12 shows the energy absorbed graph of the FHPR joints conducted for pull off testing at the point of first fracture. Two sets of the data are shown, the first being from the preliminary work (initial Tested FHPR joints) which were done

at 100% volume fill and were used to characterise the Instron machine pull-off testing capabilities. A few set-up problems that were identified during initial testing were adjusted (i.e. avoiding any slipping of the FHPR joints when being tested) thereby leading to the final matrix testing results which are detailed in this section. The initial and final results (refer to Figure 4-12) show a similar trend in the energy absorbed to the bottom chamfer angle considering that there were riveted at different volume fill % (100% and 120% volume fill for initial and final testing respectively).

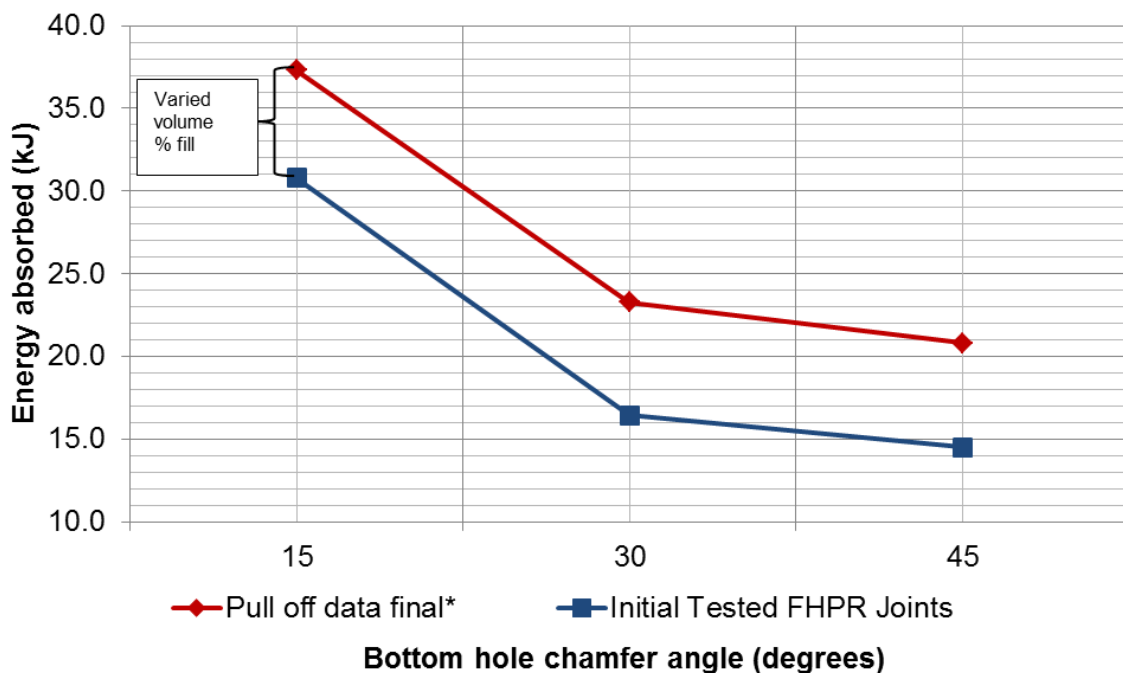


Figure 4-12: Energy absorbed at differing angles; Pull off test; (* data discussed in this section)

Note: Initial test done at 100% volume whilst the Final volume was done at 120% volume fill

15° bottom hole chamfer outperformed the other two geometries by more than 10kJ of absorbed energy as compared to the second nearest (30° bottom hole chamfer). From this data it was noted that there is a decrease in the energy absorbed from the 15° to 45° chamfered angles. This in turn relates with the pull off data which showed that the 15° had outperformed both in terms of first fracture force and displacement.

The FHPR joints can be easily repeated within the experimental error allowing for the use of only one tested sample for pull off data with close monitoring of the

upset distance and the process energy input. The process energy from feedback data and the pull off energy absorbed energy were plotted against each other in Figure 4-13. This graph also takes into account the blind hole as it was done at the same process parameters as the bottom chamfered sheets.

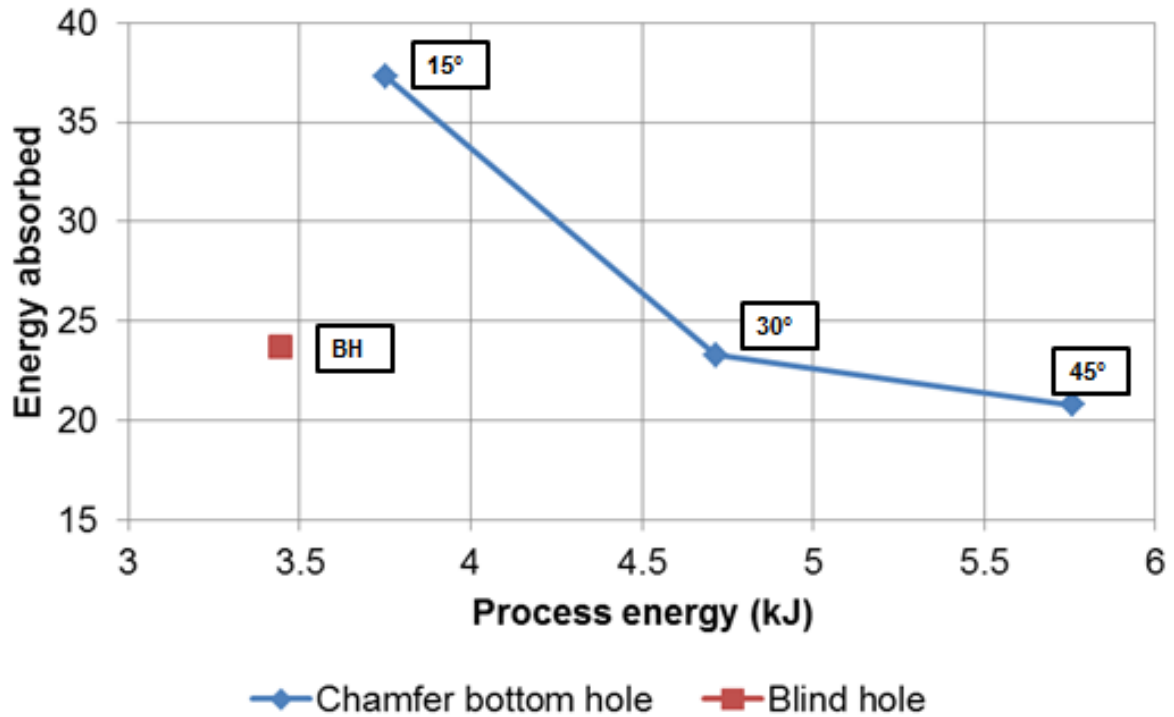


Figure 4-13: Energy absorbed and process energy relationship

Although the joints are done at the same process parameters, the difference bottom hole sheet configuration determines the amount of upset distance whilst the volume fill (%) is kept constant. The blind hole has the least process energy compared to the bottom hole chamfered sheets followed by 15° bottom hole chamfer due to its geometry having a blind hole instead of through hole, leading to a decrease in require upset distance to fill the hole.

4.5 Shear testing

The shear testing was conducted as illustrated in section 3.6.2. Shear strength of mechanical fasteners is critical especially in the aerospace industry. Typically in aircraft structures, fasteners are responsible for transfer of force or load in joined sheets in terms of shear. For this research, the shear samples consisted of single riveted specimen as shown in Figure 4-14. For the shear testing, the 15° FHPR

bottom hole chamfer joint which outperformed the 30° and 45° in terms of pull off strength was tested in shear. 15° bottom hole chamfer was only tested as there was expected uniformity of shear strength results of all the joints and also it was the best performing joint according to the pull off results. The blind hole 5000 rev/min joint was also tested to quantify its shear strength with change in joint configuration.

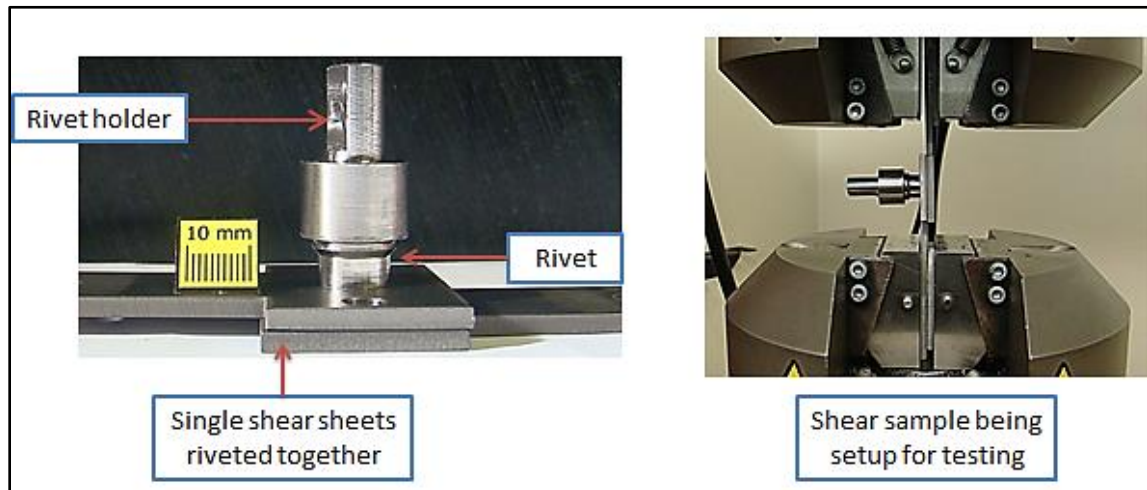


Figure 4-14: Shear testing sample

To quantify the results both the blind hole and 15° bottom hole chamfer joint were repeated twice and an unprocessed rivet was also tested. The unprocessed rivet was used for comparison purposes to the shear strength capabilities of FHPR processed joint. The testing procedure and sample geometry were described in section 0.

4.5.1 Shear testing results

The unprocessed rivet achieved an averaged result of 16.4 kN which related to 578.8 MPa ($\varnothing 6$ mm rivet). This was in the range specified by the material supplier of between 480 MPa and 690 MPa for Ti-6Al-4V ELI bar shear strength. As for the FHPR joints shear test results, Figure 4-15 and Figure 4-16 shows graphs of the 15° and blind hole joints. For 15° bottom hole chamfer test one at position labelled A, a noticeable slippage occurred which is similar to a common occurrence in shear strength testing of self-piercing riveting, then the rivet continued to elastically deform until failure occurs.

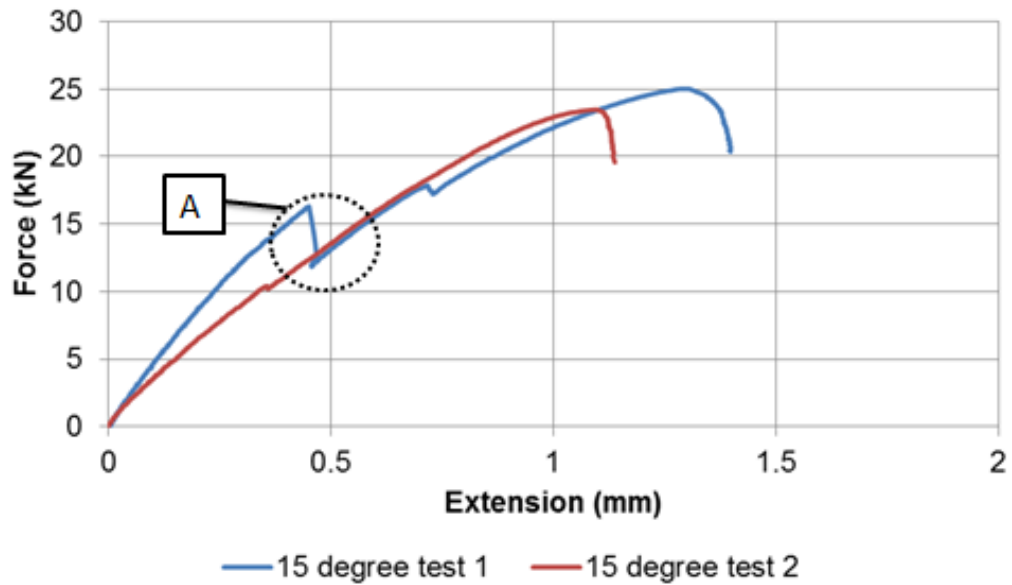


Figure 4-15: Shear test results: 15° bottom hole chamfer

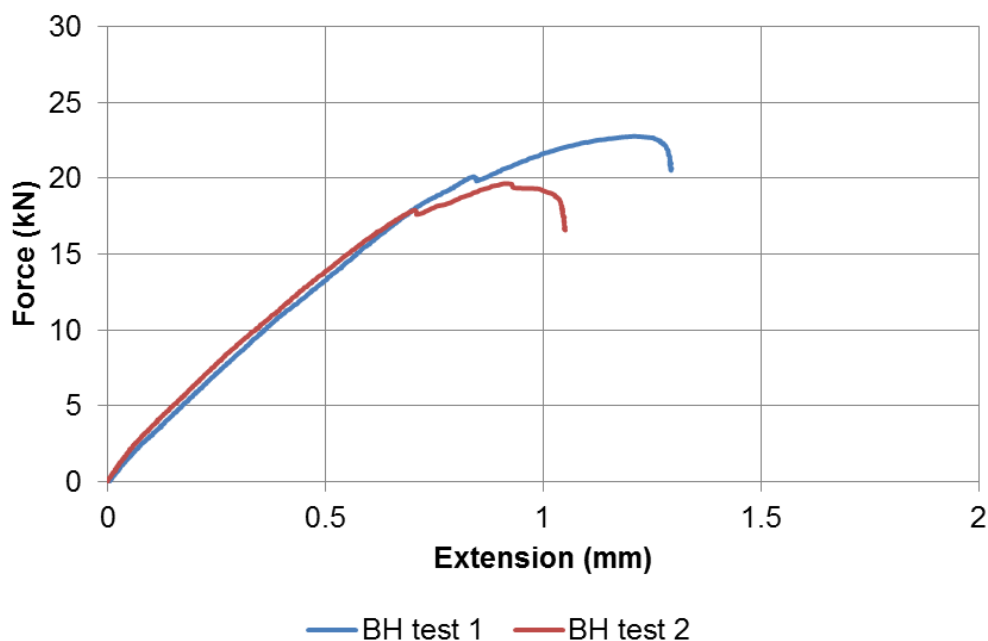


Figure 4-16: Shear test results: Blind hole geometry

At the start of shear testing the joints deform elastically as shown in both Figure 4-15 and Figure 4-16, showing a linear increase on the force-extension graph. Due to an inability to visualise a transition point on the shear test results, the ultimate shear fracture force was used to conduct shear strength analysis. For the blind hole configuration, a transition point was noticeable for both curves before rivet fracture which was related to the pulling out the bottom sheet that had formed a bond with rivet being pulled out slightly before the rivet eventually failed.

That point as shown in Figure 4-17 was then used as the point of interest in characterising the joint quality, even though the rivet goes on to further fracture at a high shear force. The average shear test results are presented in Table 4-7.

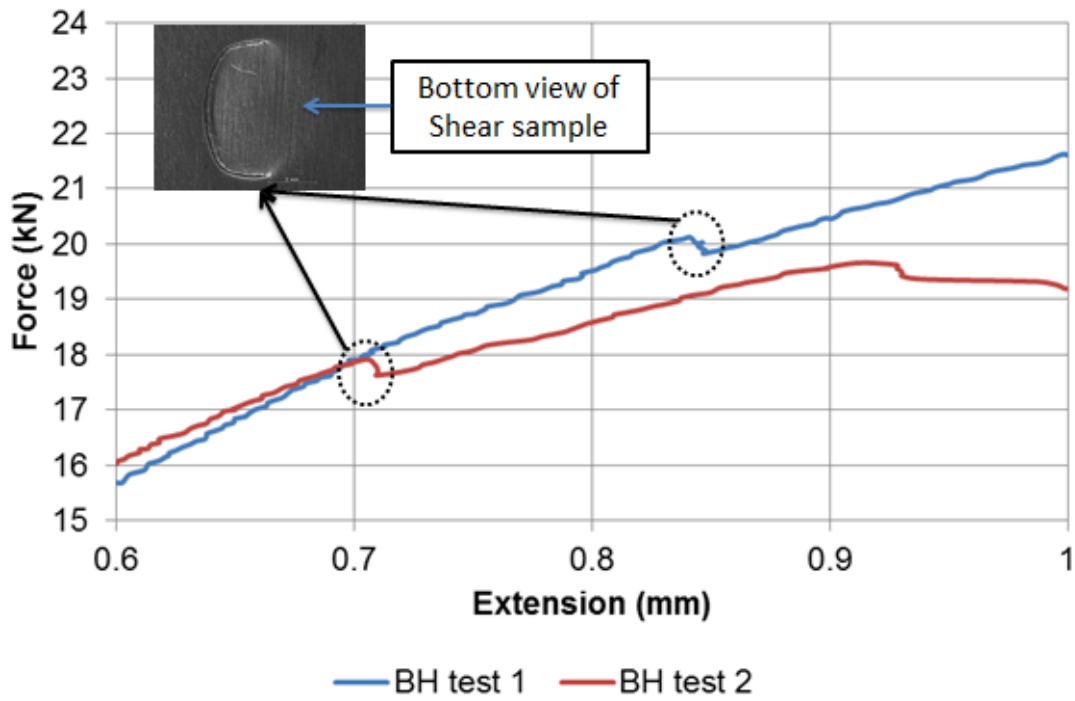


Figure 4-17: Blind hole, Rivet pulling off the bottom sheet

Table 4-7: Shear testing results calculated using an unprocessed rivet diameter

Joint description (Ø6 mm rivet)	Maximum Fracture force (kN)			Stress (MPa)	Point of pulling of bottom sheet (Average stress, MPa)
	Test 1	Test 2	Average		
Rivet	15.4	17.3	16.4	578.8	-
FHPR 15° bottom chamfer	25.0	23.5	24.2	857.3	-
FHPR Blind hole	22.8	19.7	21.2	750.5	671.9

Although no data to compare with was found for Ø6 mm Titanium rivet, the unprocessed rivet results showed that the FHPR joint shear strength gives a joint efficiency of above 100% which is positive. The joint efficiency is termed as ratio of FHPR joint shear strength to unprocessed rivet shear strength.

4.5.2 Shear Fracture surfaces analysis

Fracture surfaces of the shear samples were analysed to determine type of failure mode using the Scanning Electron Microscope (SEM). Figure 4-18 and Figure 4-19 show the fracture surfaces at highlighted points. The failure surface showed a dimple-cuplike fracture surface which suggests a ductile failure for both the 15° and blind hole joints. The fracture surfaces showed elongated dimples. The dimples observed are not shallow but rather deep and conically shaped. The characteristics of elongated dimples are that the dimples are not entirely surrounded by a rim and one end of the dimple is open as stated in the Metals Handbook on Fractography [24]. The failure is purely ductile with no visible evidence of brittle failure.

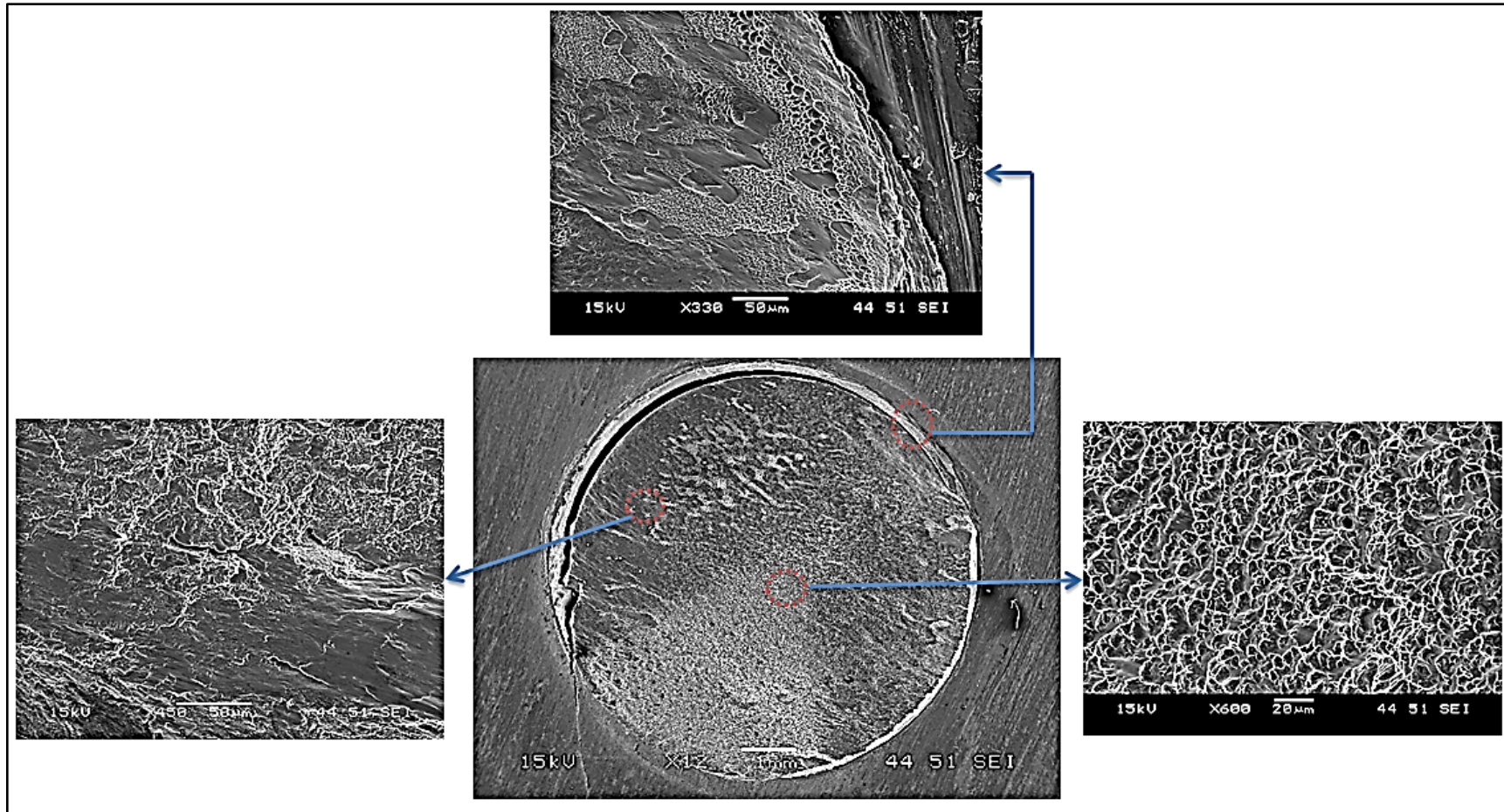


Figure 4-18: 15° bottom hole chamfer fracture surface

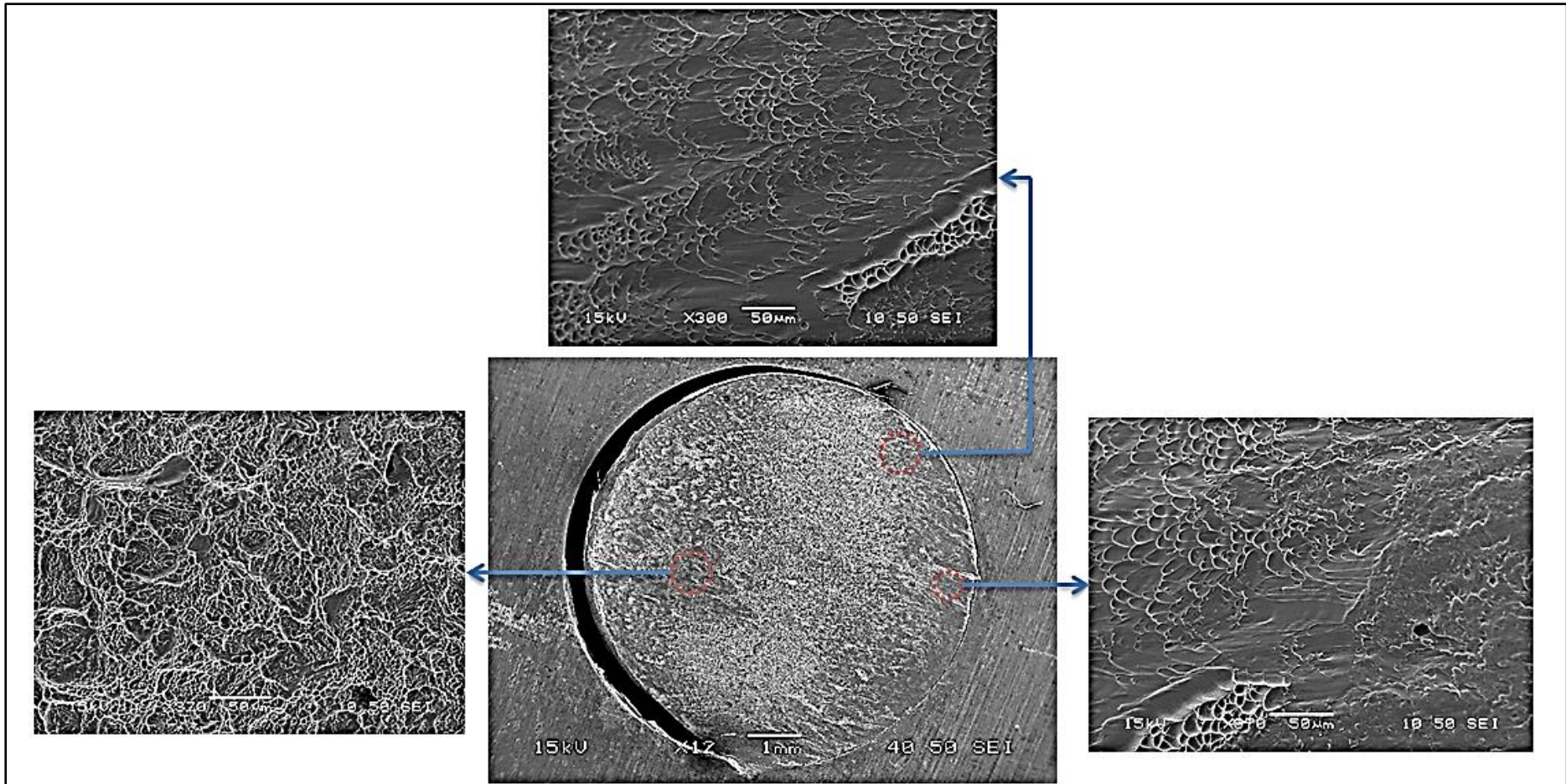


Figure 4-19: Blind hole shear fracture surface

From the 15° bottom hole chamfer, it was observed that the sheet had secondary cracks during the shear testing. A high fracture force meant that the rivet was strong enough to withstand a higher force, leading to crack initiation of sheet before the rivet finally sheared off as shown in Figure 4-20. This was discovered during the shear fracture analysis of the FHPR joints.

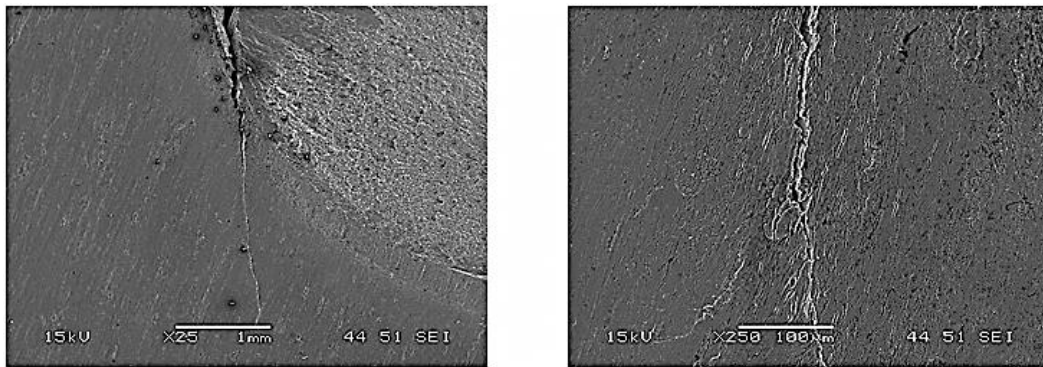


Figure 4-20: Crack initiation on the Ti-6Al-4V FHPR joined

4.6 Hardness analysis

The Micro-hardness profile of the two joints quantified in shear strength (15° bottom hole chamfer and blind hole) was done. It was noted that the Micro hardness of the FHPR joints changed from different zones due to the thermal and mechanical processing. From the parent material across to the weld zone, there was general increase in hardness values with the average hardness of the parent sheet was 316 HV.

As the 15° degree had the best results in terms of pull off strength and was tested for shear strength, it was decided to do hardness profile of the joints to determine the influence of FHPR processing on formation of the riveted joint. The 15° bottom hole chamfer joint at rotational speed 5000rev/min, axial force 4kN and a forge force of 6kN hardness' profile is shown in Figure 4-21.

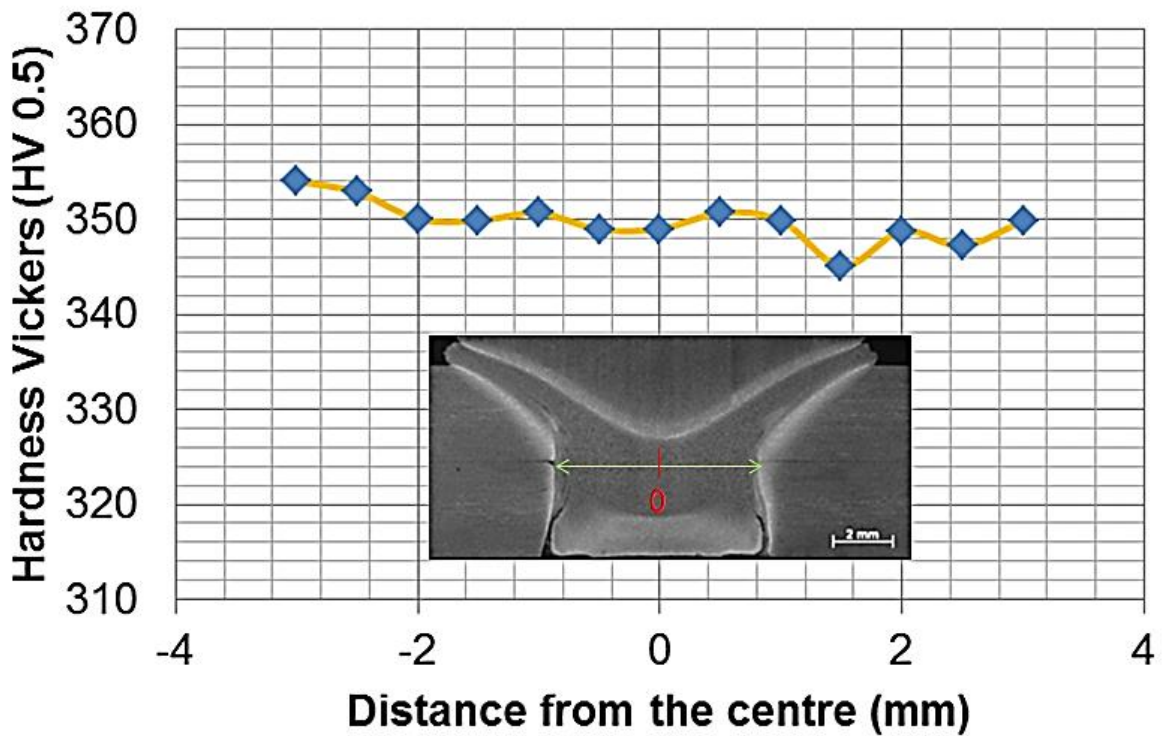
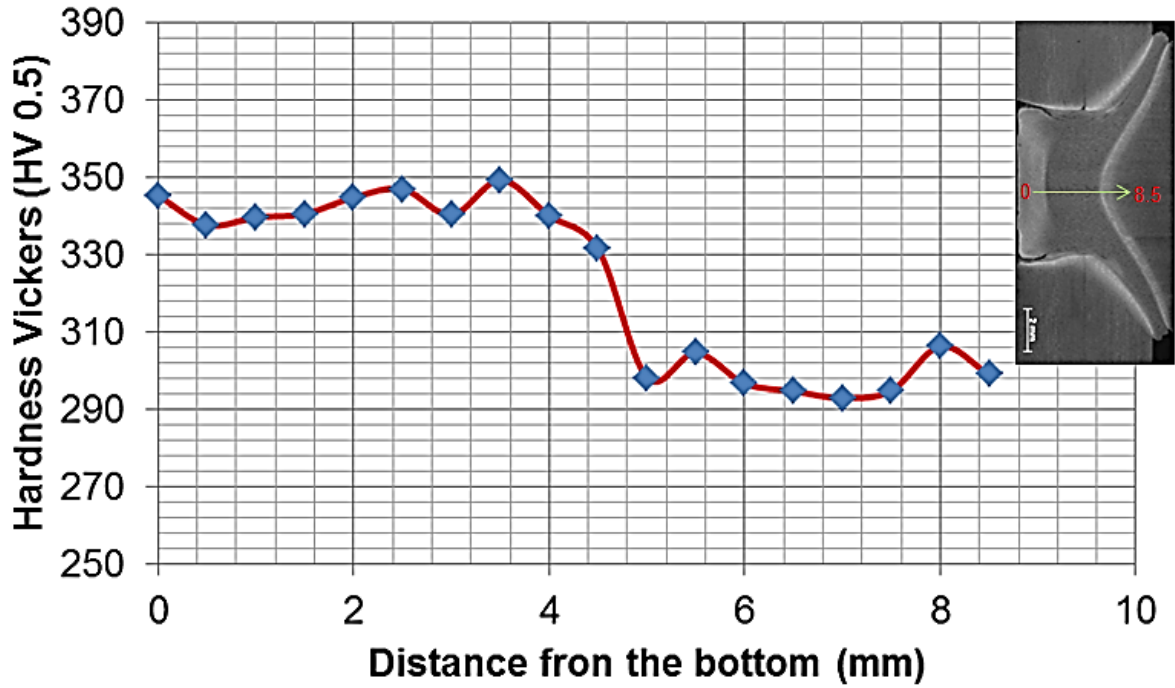


Figure 4-21: Micro-hardness 15° bottom hole chamfer, bottom and centre

The micro-hardness distribution in the 15° bottom hole chamfer showed interesting variations. The hardness values in the vertical direction from the bottom are similar up until the last shear layer where hardness decreases to about a value close to the parent material. Plasticisation and grain refinement in the weld zone led to hardness increase which positively affects the shear strength with a decrease in grain size altering the preferential shear slip plane. The average horizontal hardness across the joint was 350HV which is above the hardness of the tested parent rivet material and sheet material hardness

Figure 4-22 illustrates the hardness of the blind hole at process parameters of rotational speed, 5000 rev/min, axial force, 4 kN and a forge force of, 6 kN.

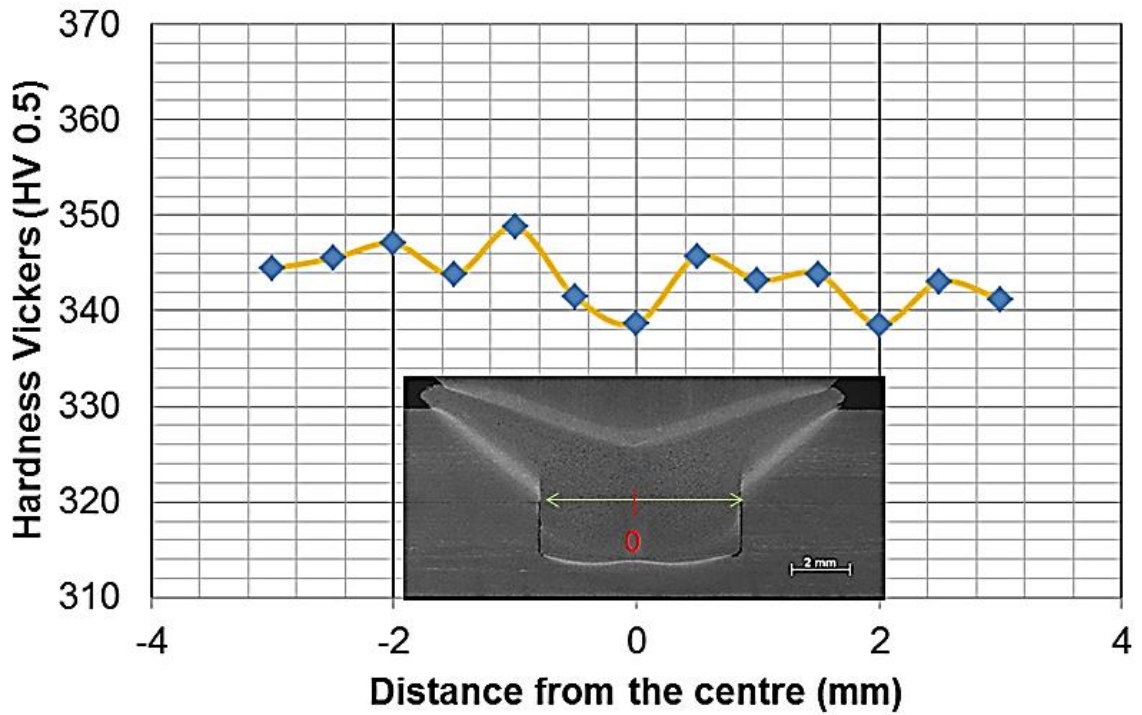
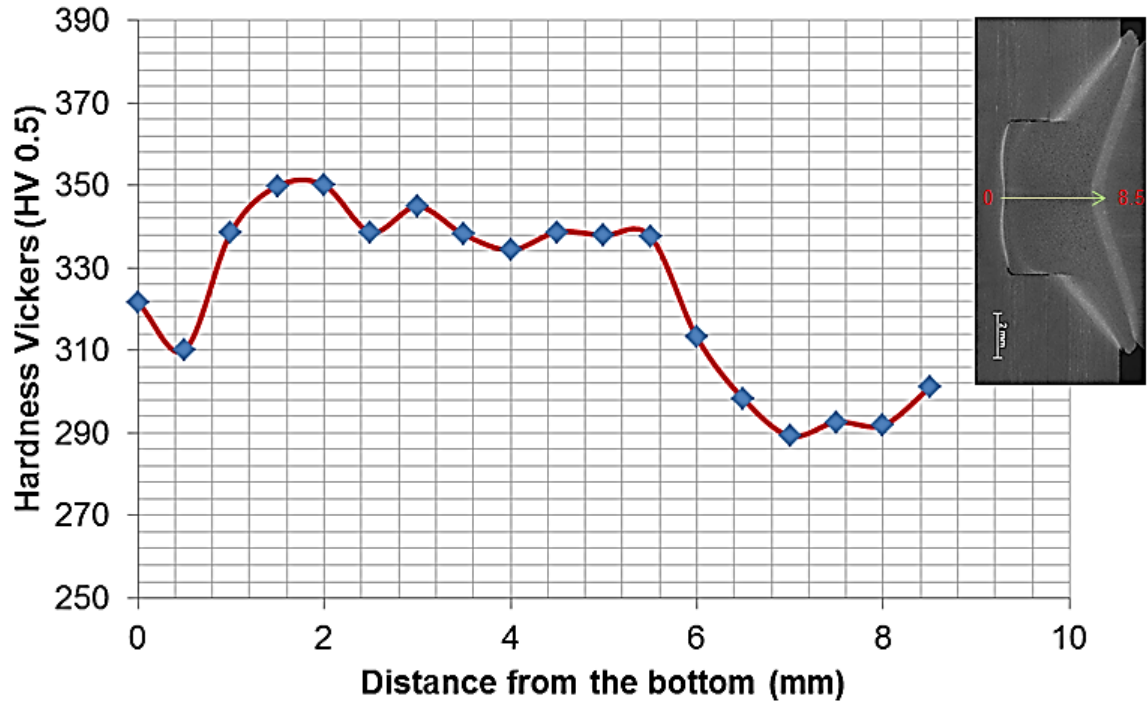


Figure 4-22: Micro-hardness blind hole, bottom and centre

As expected hardness values increased from the bottom HAZ into the weld zone then decreasing after the last shear layer. The average horizontal hardness across the blind hole was 340HV which to lesser extent explains the low shear strength values compared to the 15° bottom hole chamfer joint.

4.7 Microstructure analysis

Although the final matrix joints were done at the same process parameters, the influence of these process parameters on the microstructure needed to be quantified. Figure 4-23 and Figure 4-24 illustrates the microstructure of the rivet and sheet material.

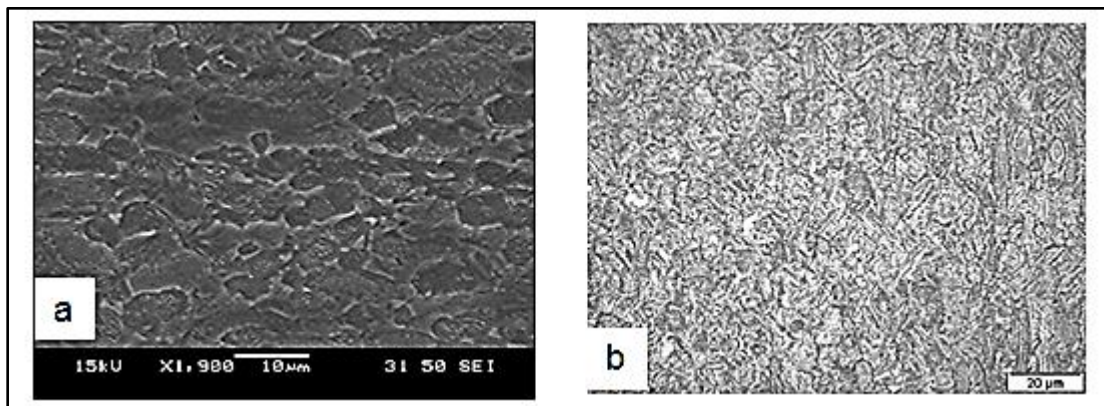


Figure 4-23: Parent sheet material (a. SEM X1900 and b. Optical Microscope)

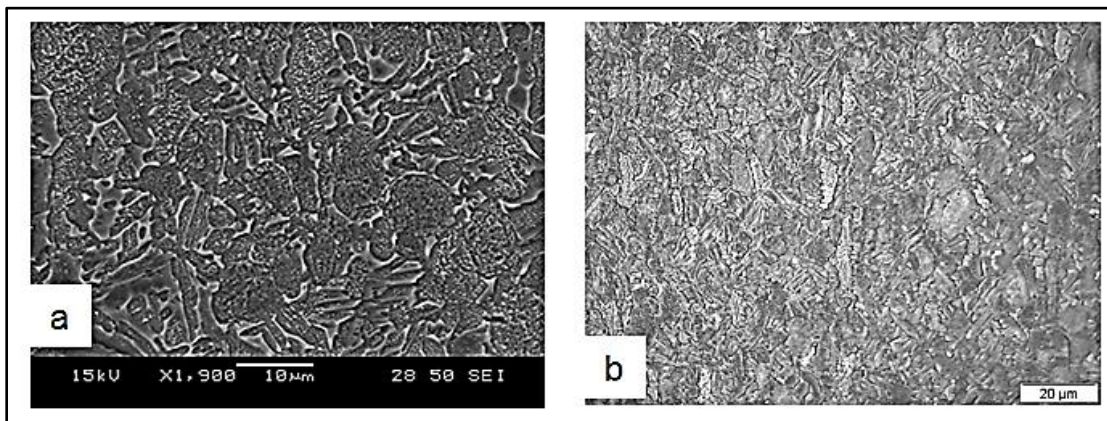


Figure 4-24: Parent rivet material (a. SEM X1900 and b. Optical Microscope)

The microstructure of both the rivet and the sheet are similar with the rivet material being Ti-6Al-4V Eli. The microstructure of the sheet and rivet shows α -phase (dark) surrounded by β -phase light (light). This correlates to the specified α

+ β mill-annealed titanium microstructure. The evaluated microstructure of the 15° and BH 5000rev/min is shown in Figure 4-25 and Figure 4-26 (for 30° and 45° refer to Appendix E: Microstructure variation (30° and 45°). These were the joints tested in shear using the same process parameters as the other bottom hole chamfer configuration joints. Figure 4-25 and Figure 4-26 shows the full micrographs done on an optical microscope.

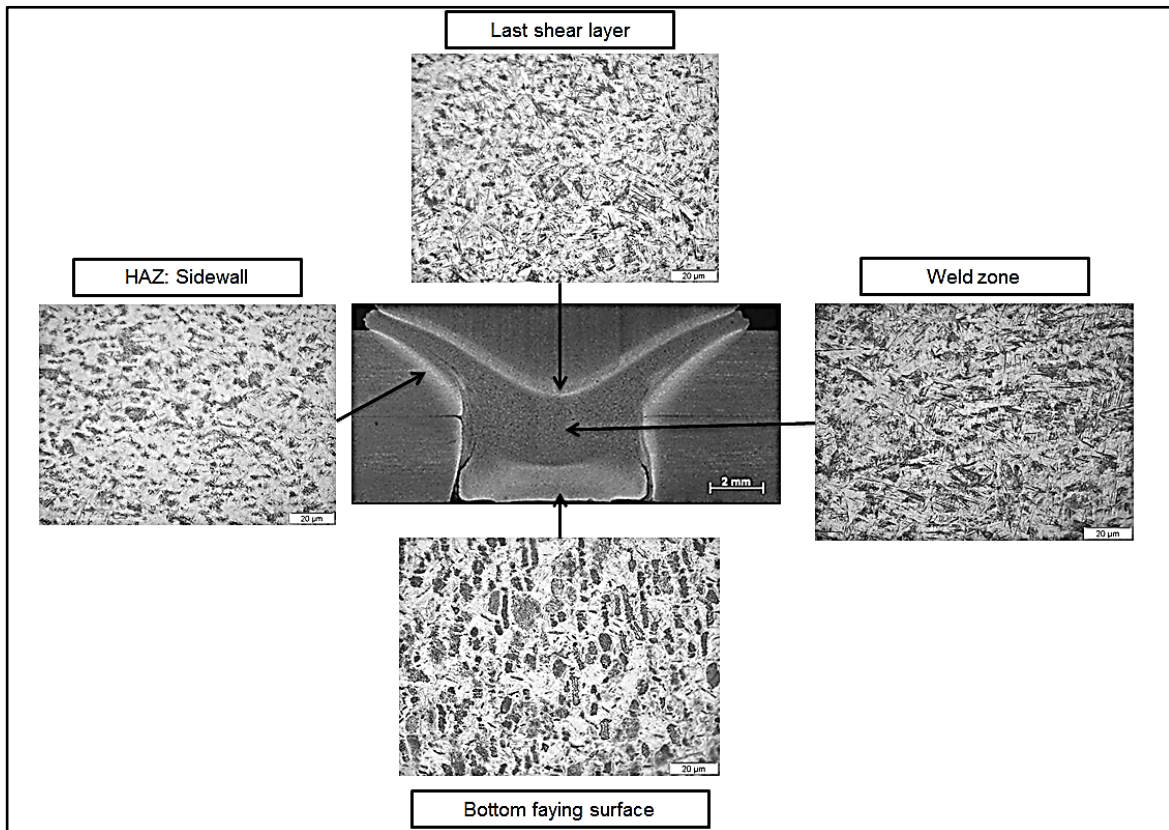


Figure 4-25: 15° bottom hole chamfer microstructure analysis

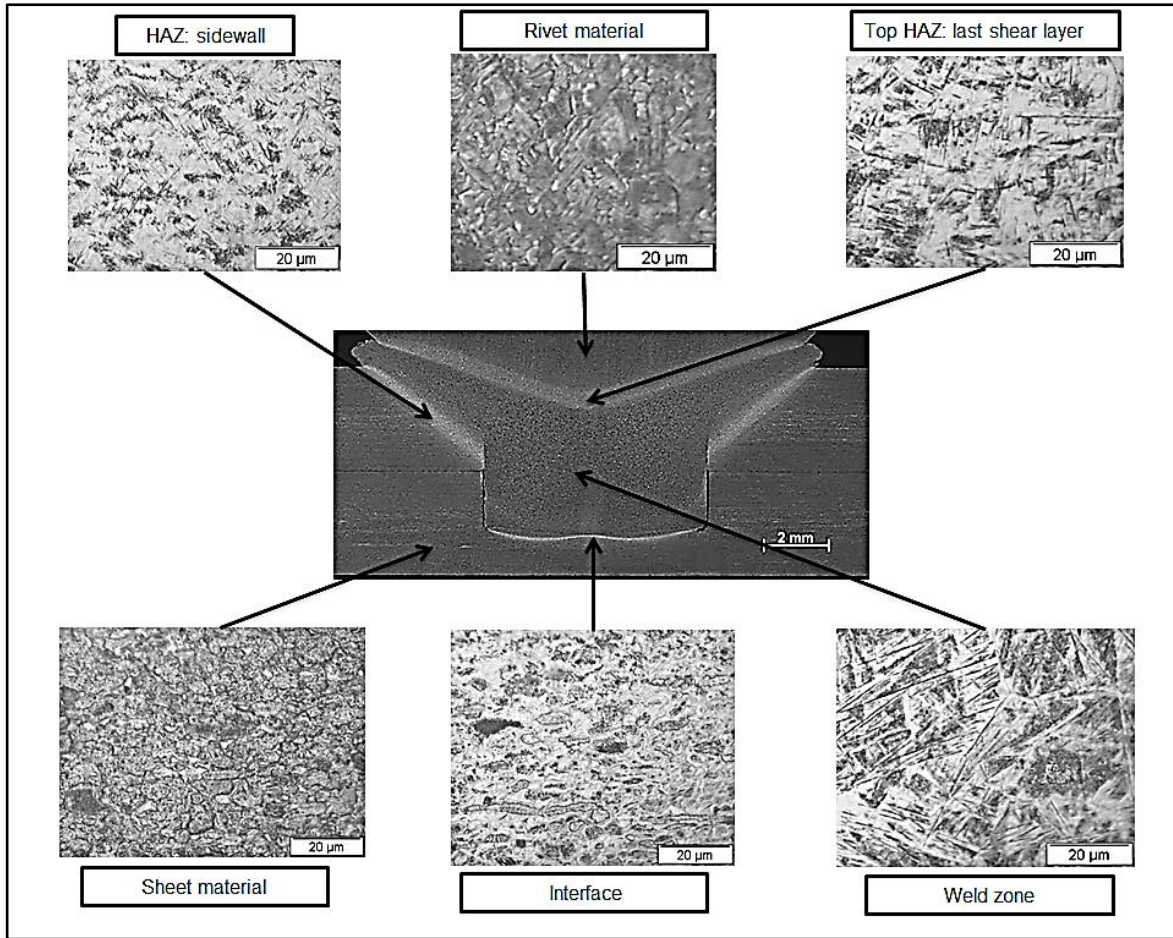


Figure 4-26: Blind hole: (5000rev/min) microstructure analysis

The microstructural analysis was conducted to characterise the different zones of FHPR joints in the determination of a preliminary window of FHPR. From the micro-analysis, it was noted that there are distinct zones in the FHPR joints. The identified zones were the HAZ, weld zone and the interface between the faying /contacting surfaces. These zones are described in detail as follows:

4.7.1 Weld zone

The weld zone micro-analysis showed that the structure formed after FHPR processing was more of primary equiaxed α and acicular $\alpha + \beta$. Using the Titanium technical guide, the weld zone microstructure relates to a process maximum temperature of 955°C which is then rapidly cooled, forming the microstructure illustrated in the blind hole and 15° bottom hole chamfer micro-analysis figures.

4.7.2 Heat Affected Zone (HAZ)

From the HAZ, the material had an equiaxed α phase or embedded α' martensite (transformed β) which is similar to what was observed by Mashinini [23].

4.7.3 Interface between the faying surfaces

As this was the region where frictional heat was generated, the microstructure looks similar to the HAZ for both the blind hole and the 15° joints.

To conclude this section on microstructural analysis, more work needs to be done to understand the phase change and effect of process parameters on the microstructure change/ evolution. The microstructural zones are similar due to the same process parameters being used in the preliminary development of the FHPR process. The cooling rate of Ti-6Al-4V after FHPR processing which was not investigated in this research but if done, could help in the explanation of the microstructure formed after FHPR process. Selected points were evaluated on the SEM and are shown in Figure 4-27 and Figure 4-28. The SEM images showed that there was grain refinement in the weld zone as compared to the parent in both the 15° bottom hole chamfer and blind hole geometry configurations.

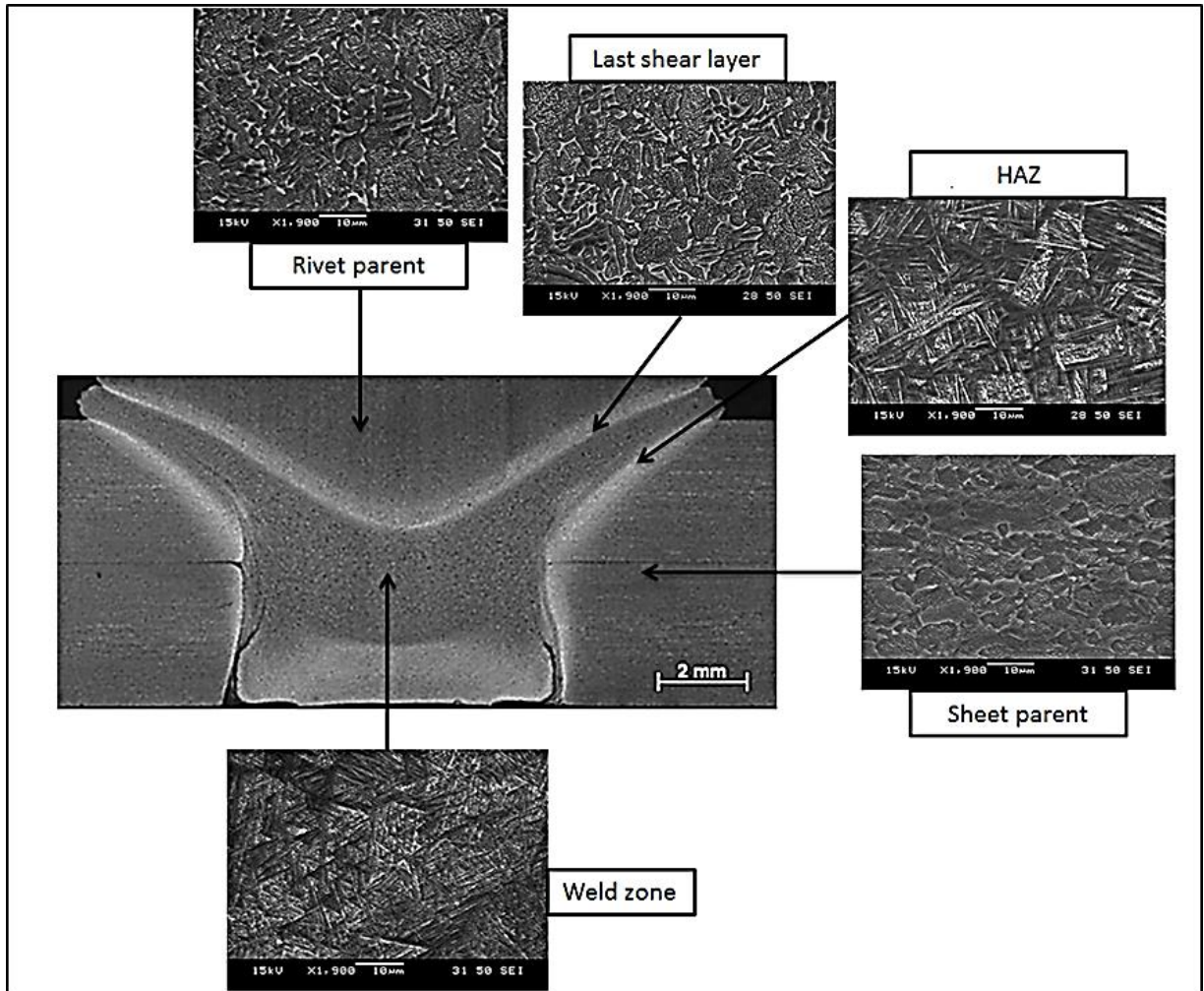


Figure 4-27: 15° Bottom hole chamfer microstructure; SEM x1900

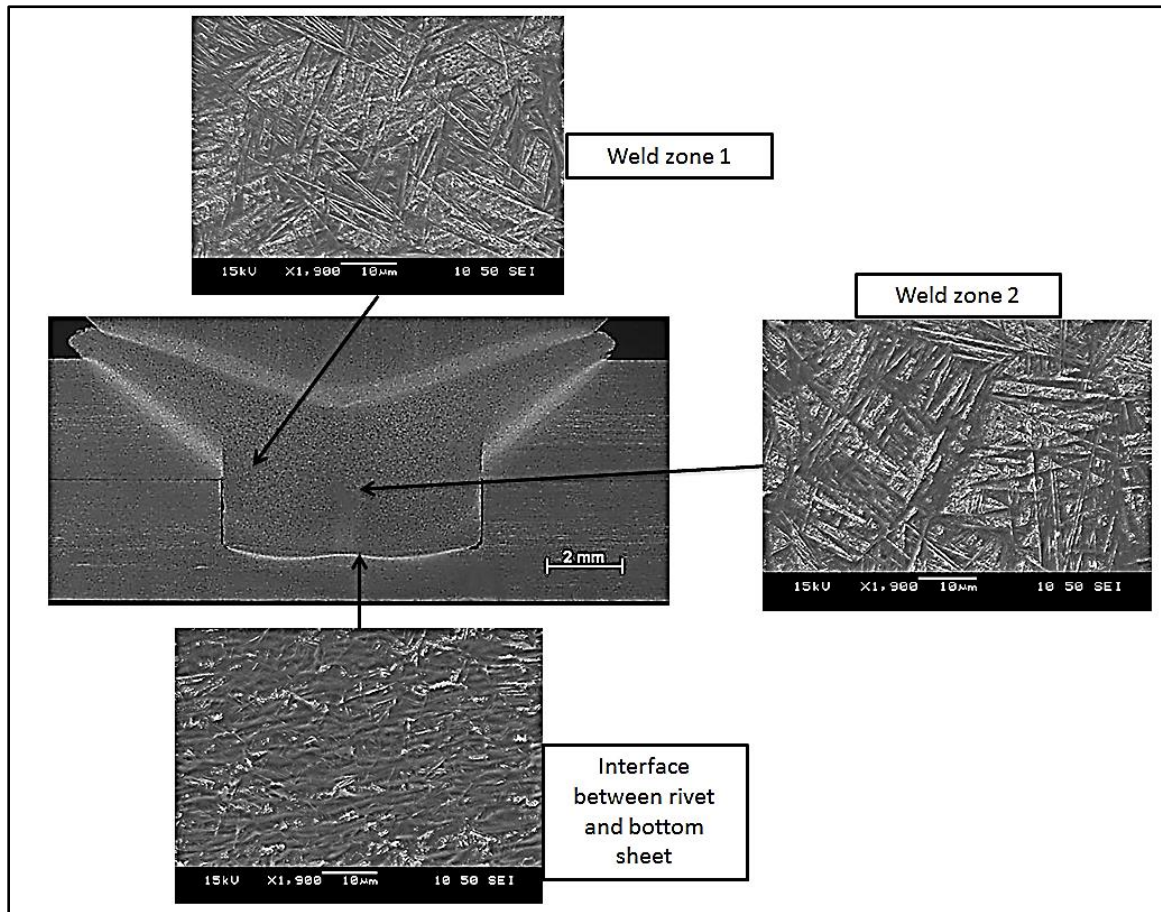


Figure 4-28: Blind hole (5000 rev/min) microstructure SEM x1900

4.8 Effect of rotational speed on FHPR joints

To further analyse the effect of rotational speed on joint formation of the FHPR process, the effect of rotational speed was analysed with the introduction of the blind hole at 2500 rev/min joint. From the blind hole geometry joints of 5000 rev/min and 2500 rev/min, it was decided to conduct a pull off test, microstructure and hardness analysis on the weld zone to establish the effect of rotational speed. A blind hole joint at 5000 rev/min (discussed earlier) was conducted using the same process parameters as the 15°, 30° and 45° bottom hole chamfer geometries. The second blind hole (BH2500 rev/min) was repeated with same process parameters with the exception of rotational speed which was reduced to 2500 rev/min. The resulting influence of the change in rotational speed is shown in Figure 4-29 and Figure 4-30 macrographs of the pulled off rivets.

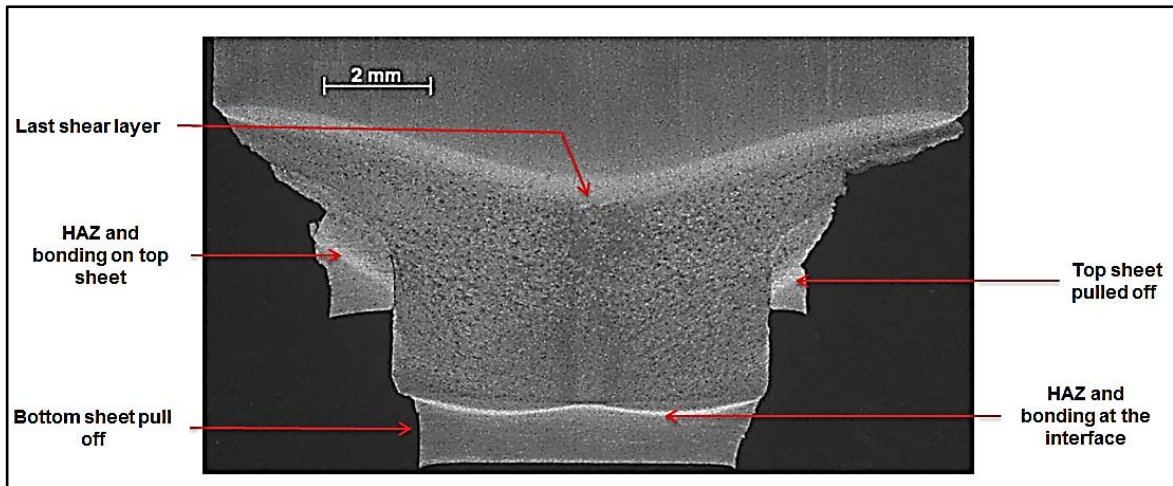


Figure 4-29: Blind hole 5000rev/min macrograph of pulled off rivet

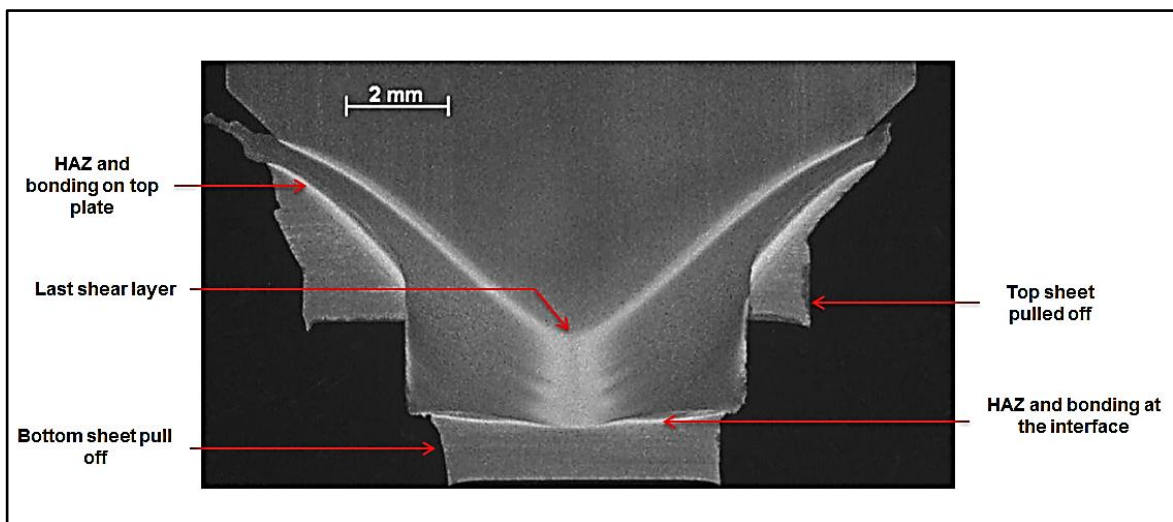


Figure 4-30: Blind hole 2500rev/min macrograph of pulled off rivet

The two curves for both 5000 rev/min and 2500 rev/min blind hole configurations are shown in Figure 4-31. From the two curves, there is definite decrease in process torque due to the increase in rotational speed. The effect of rotational speed showed that with an increase of rotational speed, the process energy input increased, leading to a higher up shear layer as visualised in Figure 4-29. Whilst at the interface of the faying / contacting surfaces, the HAZ increased.

At higher rotational speed, the upset distance rate is reduced, meaning a longer heating time leading to lower hardness values. By considering the position of the last shear layer on the blind hole joints, 2500 rev/min and 5000 rev/min, it was observed that greater volume of material was displaced due to the low heating

time for the 5000 rev/min blind hole. Low heating time allows for the propagation of thermal energy along the axial direction of the workpieces being friction processed.

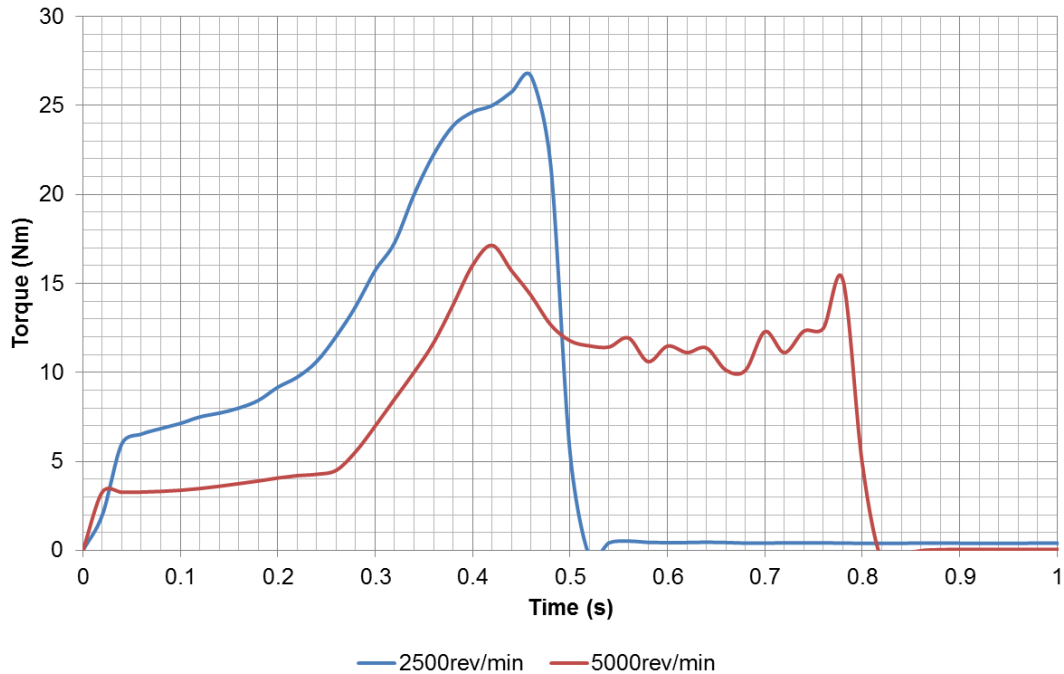


Figure 4-31: Blind Hole, Rotational speed influence on torque curve

The difference in rotational speed, which meant a reduction in peripheral velocity from 1.57 m/sec to 0.78 m/sec, had an effect on pull off strength as illustrated in Figure 4-32. It is the author's opinion that the amount of displaced material contributed to the difference in the pull off results.

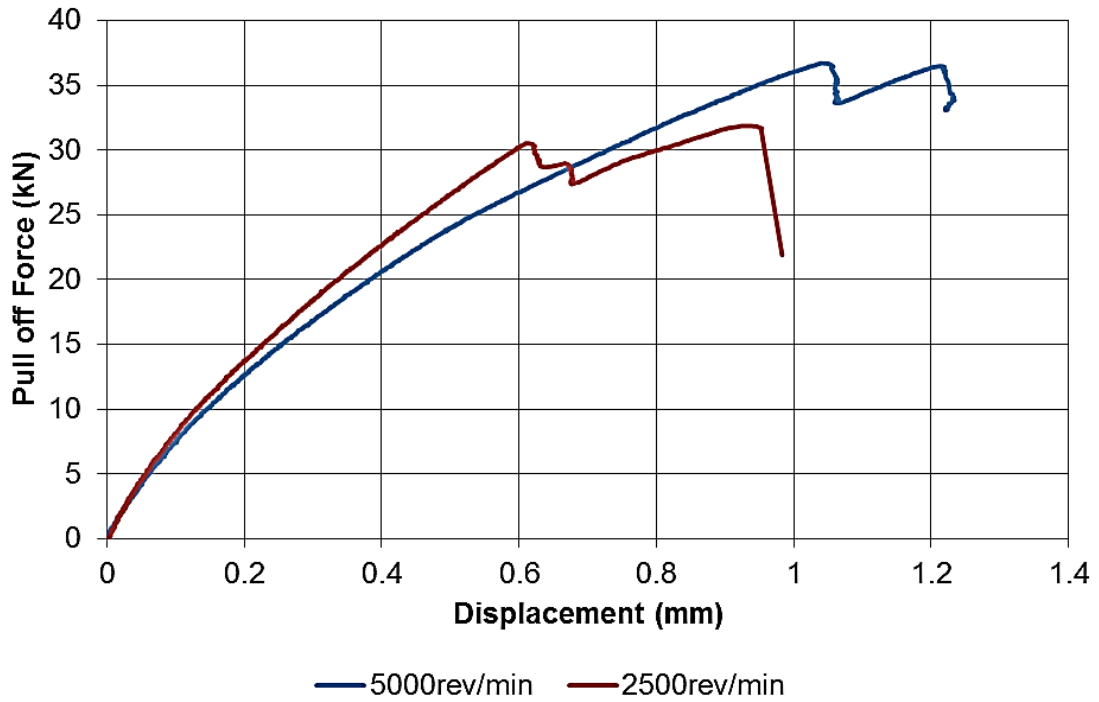


Figure 4-32: Pull off results of 2500rev/min and 5000rev/min

Figure 4-33 shows the microstructure analysis of the 2500 rev/min blind hole joint. The microstructure analysis was conducted on the pulled off rivet whilst microstructure for blind hole 5000 rev/min is illustrated in Figure 4-26.

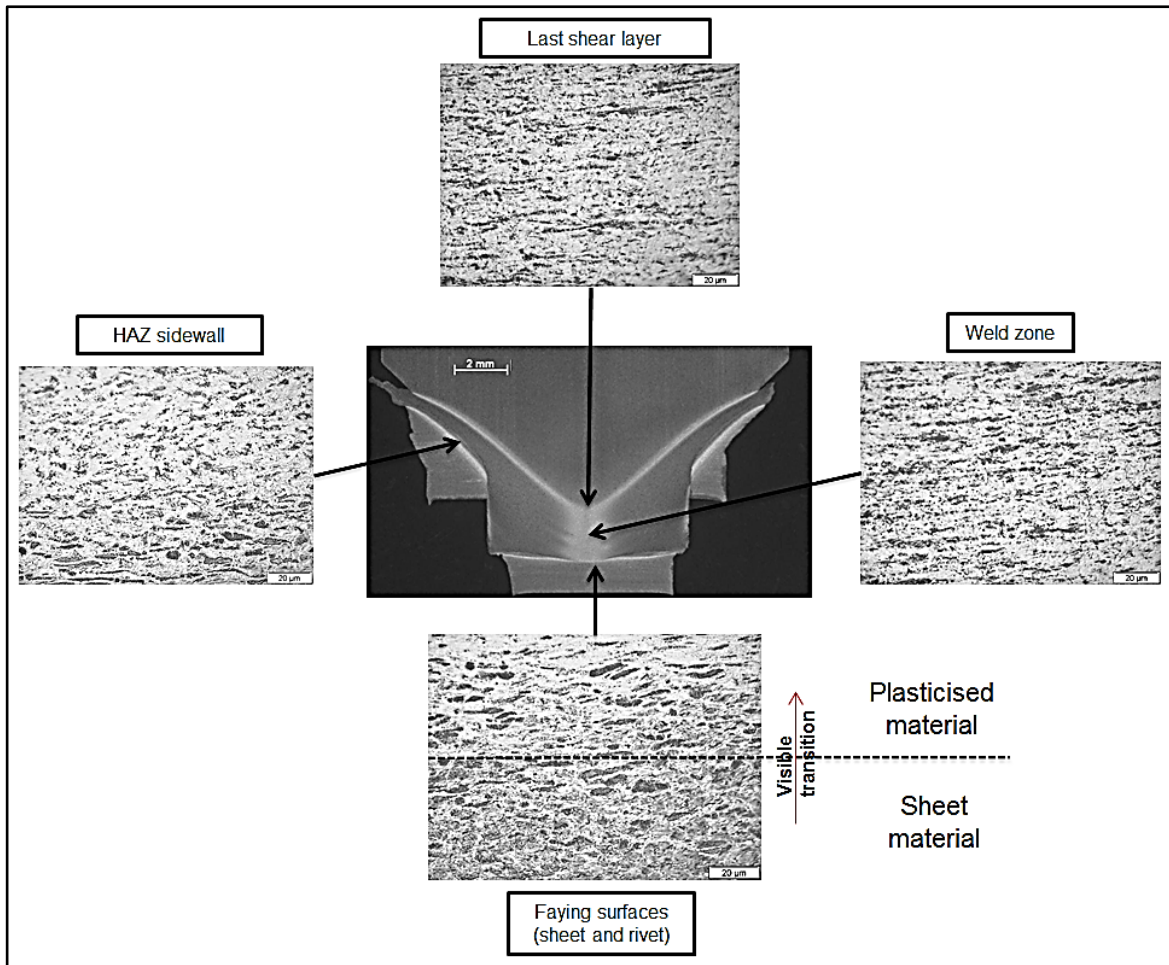


Figure 4-33: 2500rev/min Blind hole

The microstructure of the 2500 rev/min compared to the 5000 rev/min one, showed that at the middle section of the weld zone, the 2500 rev/min blind hole had a more refined microstructure. This tends to agree with the fact that at low rotation speed, the grain structure formed is finer than in high rotational speed (5000 rev/min). To verify this, hardness was also done for both blind hole joints to quantify if there is major difference in the hardness values (refer to Figure 4-34).

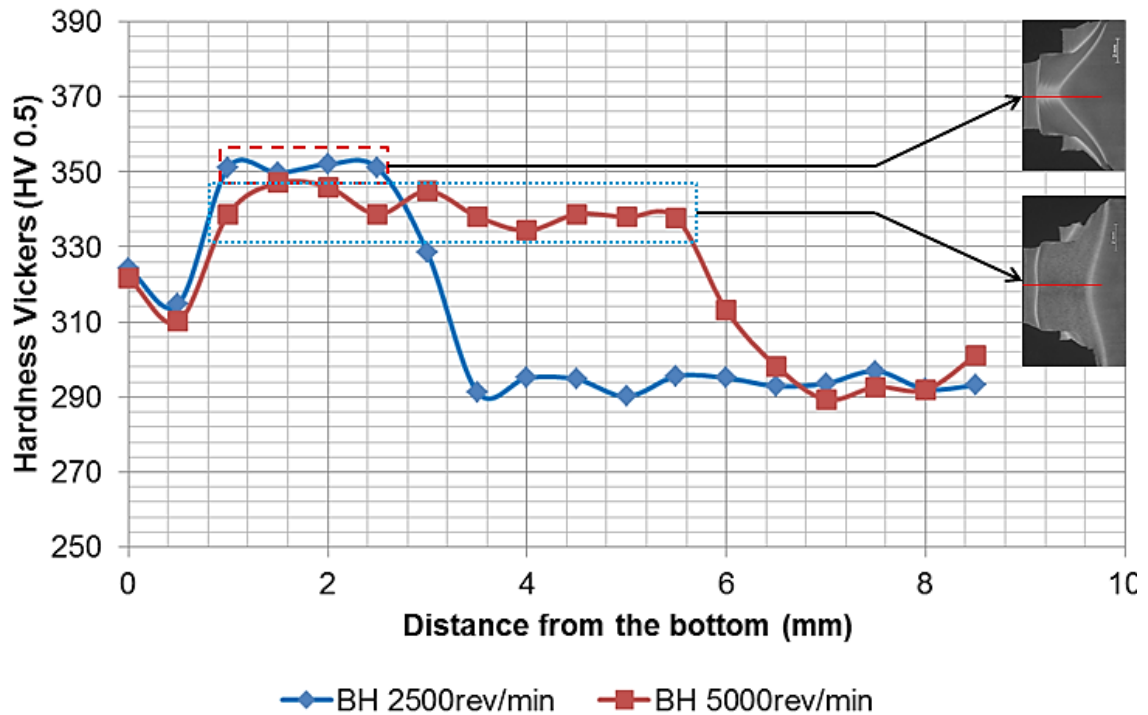


Figure 4-34: Hardness profile of varied rotational speed blind hole joints

Hardness measurements were done across the joint with position zero being the bottom sheet were parent material registered a Hardness value of between 310 to 325HV. The hardness values of 2500 rev/min compared to the 5000 rev/min showed that the BH 2500 rev/min hardness values are just above 350HV in the weld zone compared to an approximate average of 340HV for the BH 5000 rev/min (average calculated over the whole entire range). This relates to the microstructure refinement in the weld zone.

4.9 Summary

It is necessary to state that this chapter was not a process parameter optimisation but used to understand and establish the process of FHPR. The influence of changing the chamfer angle from 45° to 15° showed that by decreasing the chamfer angle at the bottom hole, material fills the chamfered hole better due to dynamic flow of plasticised material. The reduction of the chamfer angle also had a positive effect on the pull off results with a decrease in angle relating to increase in pull off strength. These pull off tests dispelled any questions as to whether a

fully mechanical lock had formed, which would be able to firmly clamp the sheets together.

It can be concluded that the FHPR process is fairly repeatable from the torque data and upset distance feedback analysis. The process torque as discussed is a valuable piece of information which was used to characterise the FHPR process. The curve itself was divided into 5 stages which explained what happened at each stage. The microstructure analysis showed that for both 15° and blind hole 5000 rev/min joints the structure was similar. The hardness values of the two in the maximum shear plane showed that the 15° joint had a marginally higher hardness compared to blind hole at 5000 rev/min.

Chapter 5: Conclusion and Future work

5.1 Introduction

This research was done to determine the feasibility of riveting Ti-6Al-4V overlapping sheets together with the emphasis on providing a joint that would be able to provide an alternative joining technique. Based on FHPP, FHPR used the same principles which allowed for the quick development of this joining process. Analysis was conducted on the process data feedback of all the FHPR joints and a select few joints were analysed in pull off strength, shear strength, hardness and micro/macro-structural analysis. The varied chamfer angle geometry was tested by pulling the joints so as to determine the effect of varying the bottom hole chamfer angle (pull off test).

5.2 Discussion and Conclusion

Ti-6Al-4V overlapping sheets were successfully joined together using a Ø6 mm rivet made of Ti-6Al-4V rod in two different joint geometries (bottom hole chamfered sheet and blind hole). These two geometries were tested and exhibited good mechanical properties in terms of the pull off and the shear strength. Initially in the preliminary work, the effect of rotational speed and axial force were quantified. It was noted that rotational speed played a role in the generation of frictional heat and the joining speed which translated to the overall process time. From a series of rotational speeds tested, it was observed that an adequate rotational speed for easily displacing of material to fill the chamfered hole at the bottom should be at least 5000 rev/min. Due to the machine capabilities (maximum speed of 5250 rev/min) and the preliminary work results, it was decided to use 5000 rev/min for the final matrix tests.

Axial force which is responsible for the keeping of the faying surfaces in contact and the temperature gradient was also quantified in the preliminary work. The effect of axial force on the FHPR joint was that with low axial force, the material flow was not adequate to fill the bottom hole chamfer whilst a high force pushed material under the backing plate as well as causing sticking between the backing plate and the rivet. From the axial force tests, it was decided to use a force of 4

kN with a 150% increase on the forge force. The increase in forge force refined the grain structure and consolidated the plasticised material as it cooled down. The forging force was kept constant at 150% which is deemed not too high so as to minimise the amount of material that flowed as flash.

Due to the clear “separation” line that was comprehensively detailed in the preliminary work findings, it was decided that the following joints be tested in their capacity to withstand a pull off force. This allowed the quantification of how much force would pull apart the sheets which are FHPR mechanically locked together. With the decrease in the bottom hole chamfer angle, it was noticed that the pull off force increased. This was explained by the fact that the clear separation line was eliminated while bonding was visualised at the bottom hole chamfer therefore forming a stronger mechanical lock. A blind hole configuration was tested in its pull off force capabilities and it was observed that the joint did not fail at the bonding interface of the rivet and bottom hole sheet material, but that the sheet was pulled out. This scenario suggested that by decreasing the blind hole depth, it would increase the pull off strength although it was not tested in this work.

The shear testing was related to the hardness results for the 15° and the blind hole configurations. From the shear strength deduction, the 15° bottom hole chamfer had the best shear strength results compared to the blind hole although both were done at the same process parameters. A possible explanation was the decrease in hardness in the blind hole which in turn was related to the difference in joint configuration. Comparing the shear fracture surfaces, it was observed that failure was due to ductile for both tested joints.

The microstructure after FHPR processing was the same for all the joints due to no change in the process parameters. In the weld zone, the microstructure was refined and more of primary equiaxed α and acicular $\alpha + \beta$. The microstructure observed is similar to the microstructure after duplex annealing with heat treatment where the alloy is heated to 955°C then air cooled [17]. The blind hole had two variations in rotational speed, and the microstructure of the 5000rev/min to 2500rev/min was compared and it was noticed that the 2500rev/min had a

refined microstructure in the weld zone which translated to an increase in the average hardness although marginally.

Friction Hydro Pillar Riveting “a new riveting technique” developed, characterised and explained in this work has proved to be a feasible alternative joining technique for Titanium alloys. For commercial purposes, its shear strength puts it in good stead as alternative joining process for Ti-6Al-4V sheets. The bottom hole chamfer can be used where accessibility of the both sides is not an issue while the blind hole caters for where only one side is accessible for joint preparation.

To conclude the main observations from this research are as follows:

- Rotational speed plays an important role in frictional heating and thereby generating enough heat for material plasticisation and flow to adequately fill the bottom chamfered hole.
- An adequate axial force is required to keep the contacting surfaces intimate as the plasticised material is pushed to fill the bottom hole chamfer.
- Joint pull off strength of the FHPR joints is related to the bottom hole chamfer angle, with a decrease in chamfer angle leading to an increase in pull off strength.
- The shear fracture surfaces of the FHPR joints exhibited ductile failure.

5.3 Future work

The development of the FHPR process identified certain areas which will require further study. Suggested areas are as follows:

- The process window needs to be optimised with an in-depth analysis on the upset distance and volume fill to allow for a FHPR joint where the amount flash is minimal.
- An analysis on the effect of radial clearance on the joint formation leading to improved pull off strength.
- A temperature analysis to verify the type of microstructure formed with the cooling rate.
- Increasing the shear area of blind hole, could in turn have an effect on pull off strength and allow for ease of manufacture.

- The fatigue life and residual stress of FHPR joints due to different process parameters, needs to be investigated before the process can be applied to the Industry.
- The use of a hollow rivet should be investigated and what impact it has on the formation of the bottom head to lock the sheets together.

The knowledge generated in this study can be used as a basis for further development of the FHPR process. The work done on FHPP regarding process parameters and geometries can fully be enhanced by FHPR.

References

1. Nicholas ED. Friction Processing Technologies. *Welding in the World*. 2003 47 (11-12): p. p.2-9.
2. Meyer A. Friction Hydro Pillar Processing: Bonding Mechanism and Properties. PHD Thesis. ; 2003.
3. Sahin M, Erol Akata H. An experimental study on friction welding of medium carbon and austenitic stainless steel components. 2004: p. 122-129.
4. Thomas W, Nicholas D. Leading Edge - Friction Hydro Pillar Processing. *TWI Connect*. 1992 June.
5. Kaifu Z. Riveting Process Modeling and Simulating for Deformation. *Chinese Journal of Aeronautics (Science direct)*. 2010;; p. 9.
6. Houldcroft PT. *Welding Process Technology*: Cambridge University Press; 1977.
7. *Fastener Engineering and Design Support. Bolted Joint Design*. ; 2009.
8. Hartley PJ. Friction Plug Weld Repairs for the Space Shuttle External Tanks. *Welding and Metal Fabrication*. September 2000.
9. Anon. *Will the Joint Hold?: Aerospace Engineering*; 1987.
10. Thomas W, Wictorowicz R, Nicholas D. The need for gas shielding - Positive advantages for two friction processes. *TWI Bulletin*. Sep/Oct 1997: p. 84 - 88.
11. Hera Innovation in Metals. Hera Innovation in Metals website. [Online]. [cited 2013 June 30. Available from: <https://www.hera.org.nz>.
12. The Titanium Information Group. *Welding Titanium: A designers and users andbook*. World Center for Materials Joining Technology (TWI). 1999 May.
13. Macintosh H. *Aircraft Wing Design*; 2013.
14. Department of Defense. *Military Handbook (Metallic Materials and Elements for Aerospace Vehicle Structures)*; 1998.
15. Soul F, Hamdy N. Numerical Simulation of Residual Stress and Strain Behavior After Temperature Modification. [Online].; 2012 [cited 2014 October 12. Available from: <http://http://www.intechopen.com>.
16. Deng J, Tang C, Zhan Y, Xingying J. Effect of die forms on rivet deformation

References

- and microstructure. *Advanced Materials Research*. 2013 January; 634-638.
17. Donachie MJ. *Titanium: A Technical Guide*. 2nd ed. Ohio: ASM International; 2000.
 18. RMI IMC. *Titanium Alloy Guide*. ; 2000.
 19. Kingsley-Jones M. *Flight Global Aviation Connected Web site*. [Online].; 2007 [cited 2013 March 24. Available from: <http://http://www.flightglobal.com/>.
 20. Smith. *The Boeing 777. Advanced Materials and Processes*. 2003.
 21. Arcam EBM system. *Ti6Al4V ELI Titanium Alloy*. [Online]. Available from: www.arcam.com.
 22. Sha W. *Titanium alloys: Modelling of microstructure, properties and applications*: Woodhead Publishing; 2009.
 23. Mashinini M. *A process window for titanium FSW*. Masters Dissertation. Port Elizabeth: Nelson Mandela Metropolitan University, Department of Mechanical Engineering; 2011.
 24. ASM. *Metals Handbook; Fractography*. 9th ed. Mills k, editor. Ohio: ASM International; 1987.
 25. Nicholas ED. *Friction Processing Technologies*. *Welding in the World*. 2003; 47((11-12), p.2-9).
 26. Ambroziak A. *Investigations of underwater FHPP for welding steel overlap joints*. *Archives of Civil and Mechanical Engineering*. 2007; 7(2).
 27. Amancio S. *Friction Riveting: development and analysis of a new joining technique for polymer-metal multi-materials structures*. PhD Thesis. Geesthacht: GKSS; 2007.
 28. Stol I, Thomas WM, Threadgill PL, inventors; *Friction Plunge Riveting*. United States of America patent US 2002/0125297. 2002 September 12.
 29. Gao D, Ersoy U, Stevenson R, Wang PC. *Friction Stir Blind Riveting*. *Manufacturing Science and engineering*. 2009 November; 13 (16)(061002).
 30. Abstract AWS. [Online]. [cited 2013 June 27. Available from: <http://www.nctfrictionwelding.com/process.php>.
 31. Kimura M, Seo K, Kusaka K, Fuji A. *Observation of joining phenomena in friction stage and improving friction welding method*. *Journal of Solid*

References

- Mechanics and Materials Engineering. 2009 August; 3(2).
32. Avinash M, Chaitanya VK, Giri DK, Upadhya S, Muralidhara BK. Microstructure and Mechanical Behaviour of Rotary Friction Welded Titanium Alloys. World Academy of Science, Engineering and Technology. 2007 December.
33. Samuel D. Characterization of joint integrity of Friction Stud Welding as Applied to AISI 304L Stainless steel. Masters' Dissertation. Port Elizabeth: Nelson Mandela Metropolitan University, Department of Mechanical Engineering ; 2009.
34. Thomas W, Nicholas D. Leading Edge - Friction Hydro Pillar Processing. TWI Connect. 1992 June.
35. Bulbring D. Characterization of Friction Hydro Pillar Process Weld Properties as Applied to 10CrMo910 Creep Resistant Steel for Application in the Power Generation Industry. PhD Thesis. Port Elizabeth: Nelson Mandela Metropolitan University, Department of Mechanical Engineering ; 2013.
36. Thomas W, Nicholas D. On trail - a new thick plate joining technique. TWI Connect. 1993 April.
37. Pentz W. Development of Repair Procedure for Rotor Steel Material (26NiCrMoV145) by Friction Hydro Pillar Processing. Masters Dissertation. Port Elizabeth: NELSON MANDELA METROPOLITAN UNIVERSITY, Department of Mechanical Engineering; 2012.
38. Bulbring D. Characterization of Friction Taper Stud Weld Properties as Applied to AISI 4140 High Tensile Steel. Masters' Dissertation. Port Elizabeth: Nelson Mandela Metropolitan University, Department of Mechanical Engineering; 2009.

Appendix A: Loadcell calibration

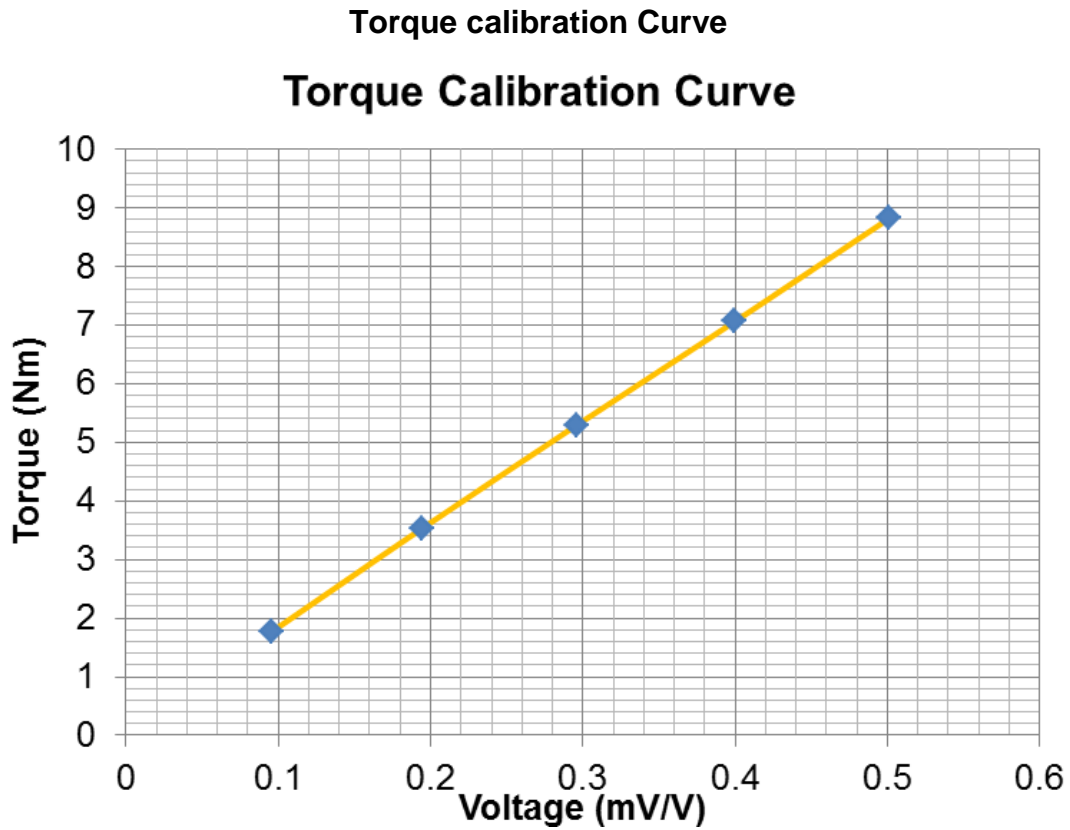


Table of Recorded data

Mass (kg)	Torque (Nm)	Recorded voltage (mV/V)			average	uncertainty
		1	2	3		
1	1.766	0.102	0.094	0.090	0.09536	0.015
2	3.532	0.198	0.191	0.194	0.19436	0.009
3	5.297	0.299	0.297	0.293	0.29616	0.006
4	7.063	0.401	0.400	0.398	0.3998	0.003
5	8.829	0.504	0.504	0.496	0.50148	0.011

Appendix B: Paper submitted to the Advanced Metals Initiative, Light Metals Conference

Friction Hydro Pillar Riveting – Alternative joining technique for 3.17mm Ti-6Al-4V sheet

D.G. Hattingh^{1, a} and D.S. Tsikayi^{b *}

¹ Nelson Mandela Metropolitan University,

Department of Mechanical Engineering

Port Elizabeth, South Africa

^a danie.hattingh@nmmu.ac.za, ^b davies.tsikayi@nmmu.ac.za

Keywords: Friction Hydro Pillar Processing, Friction Hydro Pillar Riveting, process energy, process parameters.

Abstract. This paper reports on preliminary results obtained during exploratory research, investigating the feasibility of employing Friction Hydro Pillar Processing principles as an alternative technique for producing riveted joints in 3.17mm Ti-6Al-4V sheets. Influence of process parameters was investigated to understand material flow during the plasticisation phase. An understanding of joint performance from a macrostructural and hardness point of view was established and forms part of the data presented. Process energy was quantified in relation to rotational speed. The data presented will assist in guiding the overall research objective to determine the feasibility of Friction Hydro Pillar Riveting as a suitable alternative high integrity joining process for the Aerospace industry.

Introduction

Mechanical fasteners are used extensively in the joining of two or more metal plates or sheets. For most applications of mechanical fasteners a pre-drilled hole is fitted in with the fastener (i.e. rivets, bolts and etc.). The fastener is inserted into two or more aligned holes of plates or sheets being joined. Riveting is one of the more viable methods to fasten thin wall sheets permanently. Rivets have many advantages, such as simple joining process, reliable joining intensity and high working efficiency, and are used profusely in the aircraft industry. Ti-6Al-4V accounts for 50% of titanium usage in the aircraft industry [1, 2]. Due to material type and thickness of sheets used in aircraft skins and other components, welding processes tend to degrade fuselage skin structures and the skins are not easily welded. With the emergence of friction processing as an alternative method of joining components together in the aerospace industry, emphasis has been placed on understanding and quantifying the impact of this new technological advancement as a potential joining process. Research is currently being carried out on the feasibility of joining Ti-6Al-4V sheets using Friction Stir Welding (FSW) [2, 3, 4]. The Welding Institute (TWI) describes Friction Hydro Pillar Processing (FHPP) as involving rotating of a consumable cylindrical shaft under an applied load inside a blind hole of nominal diameter and generating friction between the shaft and the material at the bottom until sufficient heating, causing a temperature increase. Material plasticises and bonding occurs forming a metallurgical bond [5, 6, 7, 8]. Friction Hydro Pillar Riveting (FHPR) as proposed by this research project provides an alternative joining technique and is based on

the same principles as FHPP. The significant parameters that influence FHPR are axial force, rotational speed and consumable length (plunge depth) as stated by Sahin et al. for FHPP [7]. Consumable length is the distance that the rivet plunges to allow for adequate filling of the bottom sheet chamfer before the top of the rivet head is forced into the rivet location hole of the top sheet. Rotational speed is the least sensitive process parameter and individual materials have their optimum rotational speed [8]. Axial force controls temperature gradient in the weld zone for FHPP [8]. Hattingh et al. showed how these parameters strongly affect the strength of AISI 4140 steel joint in Friction Taper Stud Welds (FTSW) [9]. This paper reports preliminary work on FHPR, ‘a new riveting’ technique under development at Nelson Mandela Metropolitan University (NMMU) for joining of thin wall overlapping Ti-6Al-4V sheets. Currently it is envisaged that a typical FHPR process will involve a rotating pre-machined rivet-stud into aligned holes of two overlapping sheets onto a backing plate under a small axial force. On initial contact with the backing plate, the temperature of the stud material will rise sharply with an associate torque peak due to rubbing of the faying surfaces (,-rivet and backing plate). When the pre-set consumable length (plunge depth) to form the bottom rivet head is achieved, rotation is stopped abruptly and the final forge/forming sequence is completed allowing the plasticised material to form the bottom rivet head during consolidation.

Experimental procedure

Material used in this investigation was 3.17mm Ti-6Al-4V alloy and Ti-6Al-4V *Extra Low Interstitials* (Eli) bar for the rivets. The sheet material chemical composition (wt. %) is Al 6, V 4.04, Fe 0.19, N 0.018, O 0.18 and remaining Ti while the rivet is Al 6.25, V 4.04, Fe 0.1, N 0.01, O 0.18, C 0.03 and remaining Ti. The Eli bar material has improved toughness and ductility as compared to the sheet material [10].

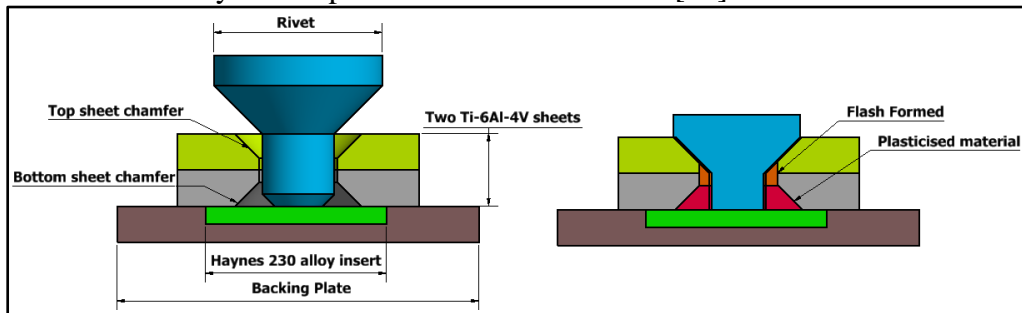


Figure 1: Schematic of FHPR

In the preceding process development phases, several setup combinations were considered to evaluate the influence, for example of rivet diameter, clearance and rivet “end face” geometry, however for this paper only the geometry and set up as illustrated in Fig.1 was considered. Material used for the backing plate was Haynes 230 alloy. With reference to Fig. 1, the function of the backing plate insert is to act as a support face or anvil for forming the bottom head of the rivet. Haynes 230 alloy is commonly used as a backing material in FSW of Ti-6Al-4V due to the material’s high melting point and ability to withstand high forces at these elevated temperatures, allowing for the non-sticking of the titanium rivet at the faying (contacting) surface. The platform used for this research was a NMMU developed ‘Process Development System’ (PDS), friction processing machine purposely designed for process research on FSW and FHPP. The PDS platform allows the researcher to independently control axial force, forge force, consumable length, forging time and rotational speed. As one of the considerations during the work was to limit ‘total time’ to form a rivet, the influence of axial force and consumable length were closely

controlled as they were identified as the main contributors to joining time. By increasing axial force, process time decreases whilst increasing consumable length has the opposite effect as more material is displaced [2]. For this investigation, rotational speed is varied from 2000rev/min to 7000rev/min while other process parameters, axial and forge force and forging time were kept constant in reference to preceding work not covered in this paper. The set up used in this matrix was that of a single bottom sheet (instead of a double sheet configuration). The dimensions and geometry of the rivet and sheet is shown in Fig. 2.

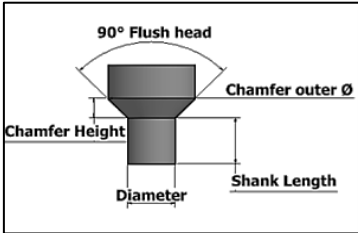
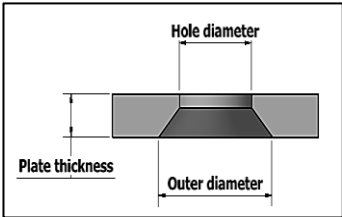
Configuration	Description	Size (mm)	Comments
90 degree Flush rivet 	Diameter	6	Machined to size Ti-6Al-4V Eli bar
	Shank length	-	Based on the volume fill
	Chamfer outer diameter	12	-
	Chamfer height	3	-
Hole, (45 degree 2 mm Chamfer) 	Hole diameter	6.5	Radial clearance of 0.25
	Outer diameter	10.5	-
	Hole depth	3.17	-
	Thickness of plate, t	3.17	Readily available Ti-6Al-4V sheets

Figure 2: Geometry utilised

Consumable length was calculated by considering the volume of material required to fill bottom chamfer hole in the sheet. The bottom mechanical lock or rivet head will therefore be formed by plasticised material contained within the chamfered hole. A 120% volume fill was used to allow for a slight over fill and compensate for any volume change during the forge/cooling phase. The axial and forge force was kept constant at 4kN and 6kN respectively. A shielding mechanism was integrated into the setup of the machine due to the need to shield Ti-6Al-4V from oxidation during joining. Although FHPR can be considered a solid state joining process meaning that the process does not exceed the melting temperature, a need for shielding was observed. A brown colour or blue purge was observed on the flash with no shielding while with shielding, shiny metallic flash was formed. For the macrostructure sample preparation, the etchant used was 2ml HF (40 %), 5ml H₂O₂ (30 %) and 100ml H₂O. Hardness was done 0.5mm from the bottom of the plate in a horizontal direction with 0.5kg load and 0.5mm spacing between indentations as shown in Fig. 3.

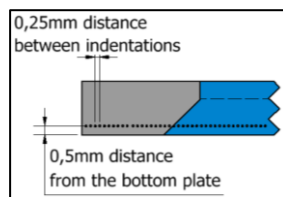


Figure 3: Hardness profile representation of half the sheet and rivet

Results

Influence of rotational speed was quantified in terms of material flow. The process energy was calculated using standard energy and power calculation formula shown in Equation 1 (up until the stopping time without considering the peak brake torque). The relative velocity formula is illustrated in Eq. 2.

$$\begin{aligned} \text{Energy} &= \text{Power} \times \text{Time interval} \\ E &= 2\pi/60 NT \times \text{time interval} \end{aligned} \tag{1}$$

$$\begin{aligned} \text{Relative velocity} &= \text{rotational speed} \times \text{radius} \\ v &= \omega r \end{aligned} \tag{2}$$

The effect of rotational speed on the bottom rivet forming process is illustrated by the cross sectional macrostructural appearance as revealed in Fig. 4.

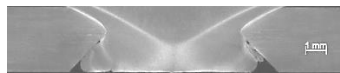
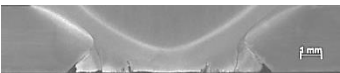


Joint	Parameters set		Process Energy (kJ)	Energy/ C. length (kJ/mm)	Joint cross section / macrostructure
	Rotational speed (rev/min)	Relative Velocity (m/s)			
1	2000	0.63	2.01	0.70	
2	4000	1.26	2.60	0.904	
3	5000	1.57	3.41	1.19	
4	7000	2.20	3.66	1.28	

Figure 4: Rotational speed influence

In Rotary Friction Welding (RFW), a minimum relative velocity of 1.27m/s is required for sufficient bonding between the two work pieces [8]. For this experiment, relative velocity varied from 0.62m/s (2000rev/min) to 2.20m/s (7000rev/min) as bonding between the plasticised material and the side of the hole in the sheet was not considered critical. From the Figure 4, it was confirmed that with a lower relative velocity at the outer periphery of the rivet, flow of the plasticised material was insufficient. This can be related to the quick completion of joint at 2000rev/min, as there was not enough heat generated at the faying surfaces to allow plasticised material to flow and form-fill the chamfered hole of the sheet. In relation to the process energy, the 7000rev/min gave the highest value of 3.66kJ.

From joints at 4000rev/min and 5000rev/min, it was observed that the material flow was acceptable although both showed deficiencies. Process time for 5000rev/min joint was longer than that of 4000 rev/min joint, which relates to the tearing being replaced by polishing with an increase in rotational speed [2]. At 5000rev/min, consumable length (plunge depth) rate slows down (which directly relates to cooling rate), increasing process time and producing a wider HAZ than at 4000rev/min. Process torque response for the

four welds is shown in Fig.5 with the *black straight line* showing the start of motor braking and initiating the stopping of rotation.

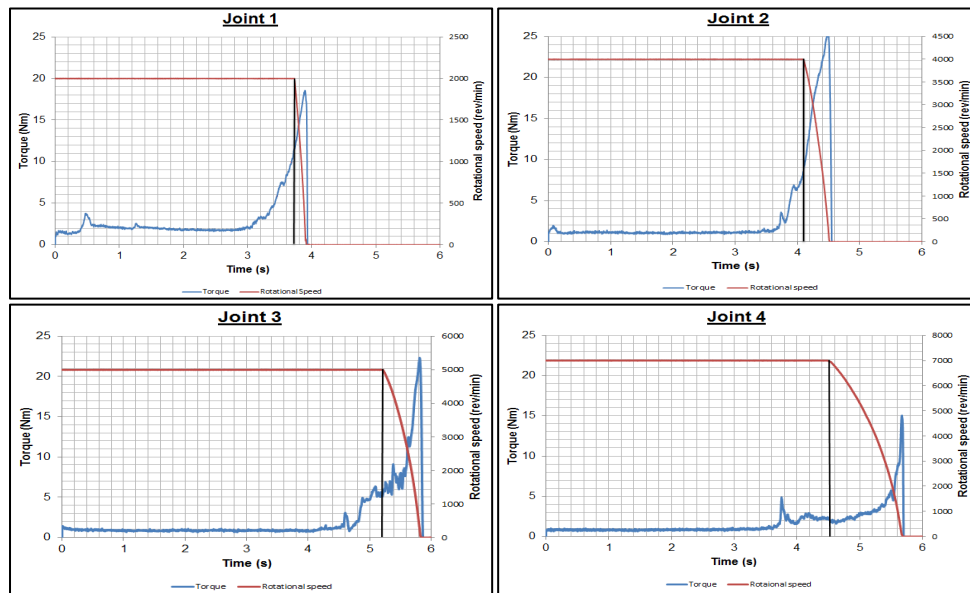


Figure 5: Process torque response curves

The torque curve contains important process information. Considering the 7000rev/min (Figure5:Joint 4), the torque curve stages can be identified; with the initial stage being the first stage of contacting (faying) surfaces, leading to the initial torque peak at approximately 3.92 seconds (4.6 seconds at 5000rev/min). From the initial torque peak, the torque stabilises around 2N.m until the motor is stopped abruptly. When the motor is stopped, the torque remains constant and gradually peaks up to a brake torque (point of zero rotation) which is related to the braking time of the PDS platform and is observed in all the joint trials. This is due to the large inertia of the welding head on the PDS platform and has been identified as a major challenge to be solved, allowing for production of optimal rivet head in the shortest time interval.

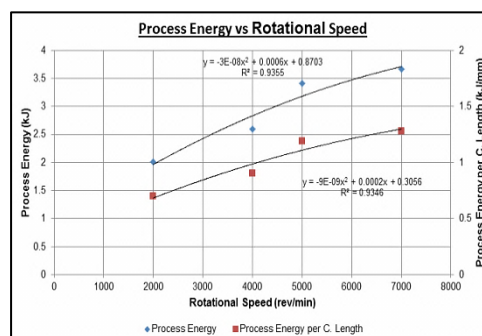


Figure 6: Relationship between Process Energy and Rotational speed

Figure 6 shows that there is a non-linear relationship between process energy and rotational speed which can be used to predict process energy at different rotational speeds. As the rotational speed increases, the torque decreases which in turn causes minimal difference to process energy at higher rotational speed of 5000rev/min and 7000rev/min.

The hardness profiles illustrated in Figure 7 shows the variations of hardness with location from the centre of the joint at approximately 0.5mm above the sheet (refer to Fig. 3).

Measurements of hardness were done close to the contacting surfaces of the rivet and backing plate as this is where frictional heat is generated and are the most likely points for introducing unwanted hardness changes.

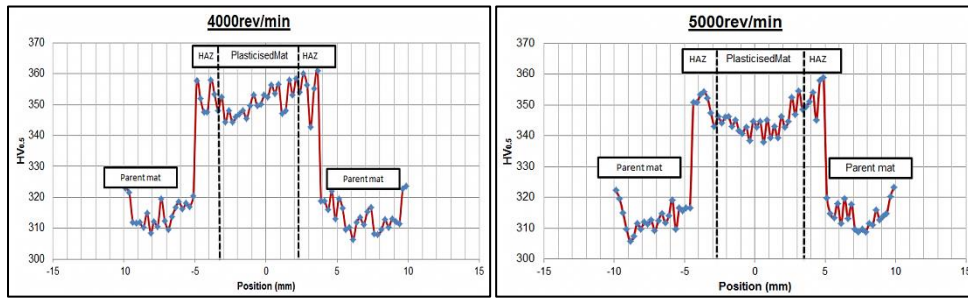


Figure 7: Horizontal hardness profile of 4000 and 5000 rpm joints

Hardness values increase from the parent (310-325HV) to the HAZ and plasticized zone. Increase in hardness in the plasticised zone from parent can be mainly attributed to forging force (refines the grain size) and the temperature gradient.

The two joints at 4000rev/min and 5000rev/min were repeated with the full configuration of two (top and bottom) chamfered sheets and a countersunk 90° rivet as shown in Fig. 8. A mechanical lock was formed as illustrated in the macrographs shown in Fig. 8.


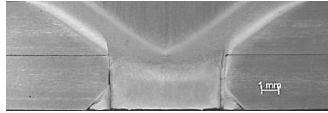
Joint	4000rev/min	5000rev/min
Macrostructural		

Figure 8: Full joint of 4000 rpm and 5000 rpm

Although it appears as if a proper fill of the bottom chamfer was achieved at 5000rev/min another phenomenon was identified raising some concerns. From macrostructural appearance, it appears that some diffusion or lack of fusion accrued along the original shank diameter and the newly formed plasticised material that formed the bottom rivet head as illustrated in Fig. 9.

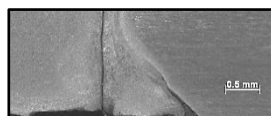


Figure 9: A clear separation line between plasticised material and stud

This is undesirable as it will not form the desired mechanical lock. It most probably occurred due to the result of plasticised material making contact with the side of the “cold” chamfered hole in the sheet, resulting in a stronger bond than that between the original stud and the displaced plasticised stud material, forming a shear layer at this point. It is believed that this could be solved by stopping the process earlier and relying on a cold forge/form final stage and will be investigated further.

Conclusion

The results from this study revealed important process relationships and evidence to show that FHPR can be used as method for riveting Ti-6Al-4V sheets together. The results further showed that rotational speed has a non-linear relationship to process energy. This

non-linear relationship can be attributed to the drop in average process torque experienced during rivet forming at higher speeds. This trend in turn is attributed to an associated increase in process temperature with the increase in rotational speeds, reducing shear layer strength in the plasticised material resulting in lower process torque required. Increased heat input on the other hand reduced the cooling rate due to greater volume of material being heated up. As the cooling rate decreased, a wider HAZ was observed. Therefore rotational speed contributes to the frictional heating and influences the joining speed. From this work the required process stages have been defined with a clear indication that the final process will have to tend more to a cold forge/form stage rather than a traditional FHPP stage.

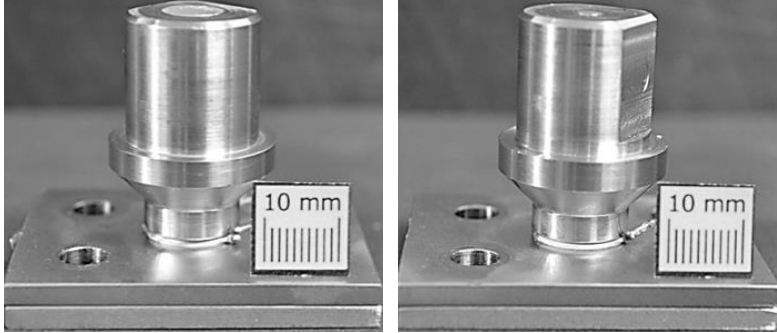
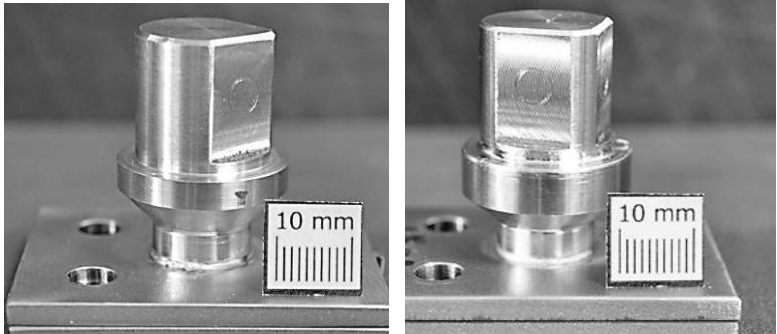
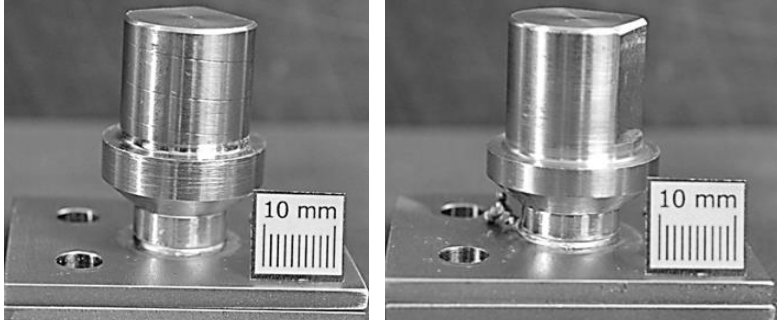
Acknowledgements

The authors would like to express their sincere gratitude to the Nelson Mandela Metropolitan University, Titanium Centre of Competence and Advanced Metals Initiative for their continued support.

References

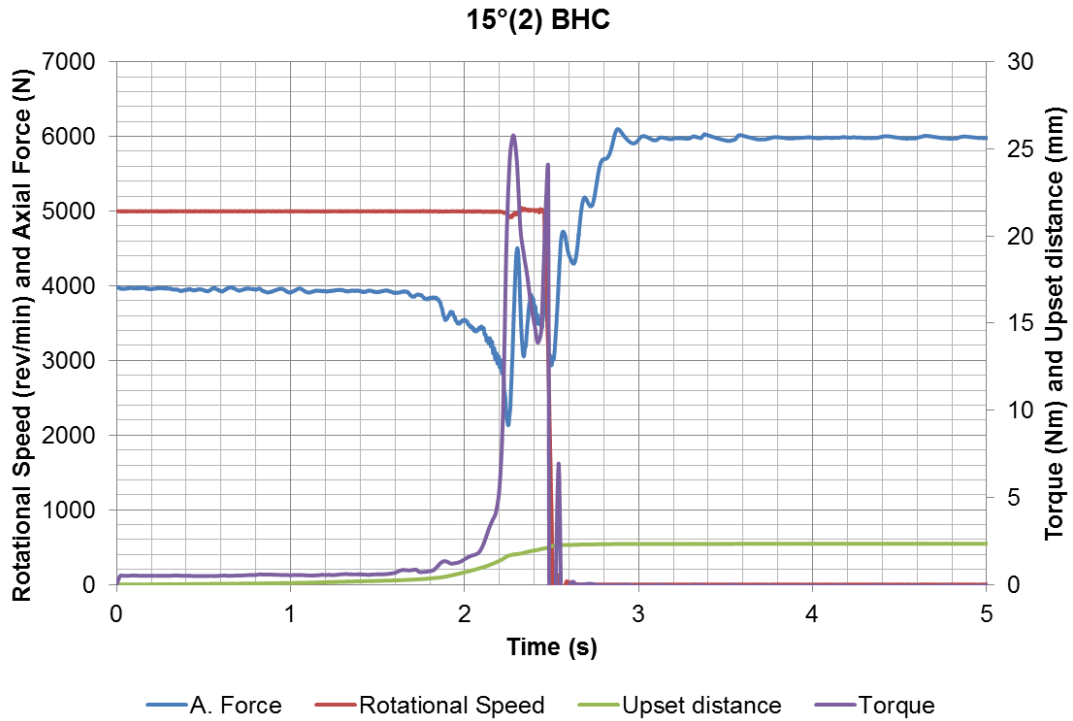
- [1] I. Stol, W.M. Thomas, P.L. Threadgill, U.S. Patent 6769595,
- [2] Information on <http://www.alliedtitanium.com/technical/Titanium%20-%20The%20Ultimate%20Choice.pdf>
- [3] P.M. Mashinini, Process window for FSW of 3mm Titanium (Ti-6Al-4V), Masters dissertation, Nelson Mandela Metropolitan University; 2011.
- [4] Titanium Information Group (TIG), World Center for Materials Joining Technology (TWI), Welding Titanium, a designers and users handbook, 1999.
- [5] W.M. Thomas, D. Nicholas, Leading Edge - Friction Hydro Pillar Processing. TWI Connect, 1992.
- [6] D.H.L. Bulbring, D.G. Hattingh, A. Botes. Feasibility of coring and plugging dissimilar steel welds by using Friction Taper Stud Welding, International Friction Processing seminar, 2011.
- [7] M. Sahin, H. E. Akata, An experimental study on friction welding of medium carbon and austenitic stainless steel components: submitted to Journal of Industrial Lubrication and Tribology 2004.
- [8] A. Meyer, Friction Hydro Pillar Processing Bonding Mechanism and Properties, PHD Thesis, GKSS-Forschungszentrum Geesthacht GmbH Geesthacht, 2003.
- [9] D.G. Hattingh, D. Bulbring, A. Botes, M.N. James, Process parameter influence on performance of friction taper stud welds in AISI 4140, Submitted to Journal of Materials and Design, 2011.
- [10] Information available at <http://www.arcam.com/wp-content/uploads/Arcam-Ti6Al4V-ELI-Titanium-Alloy.pdf>

Appendix C: Visual images of Joints

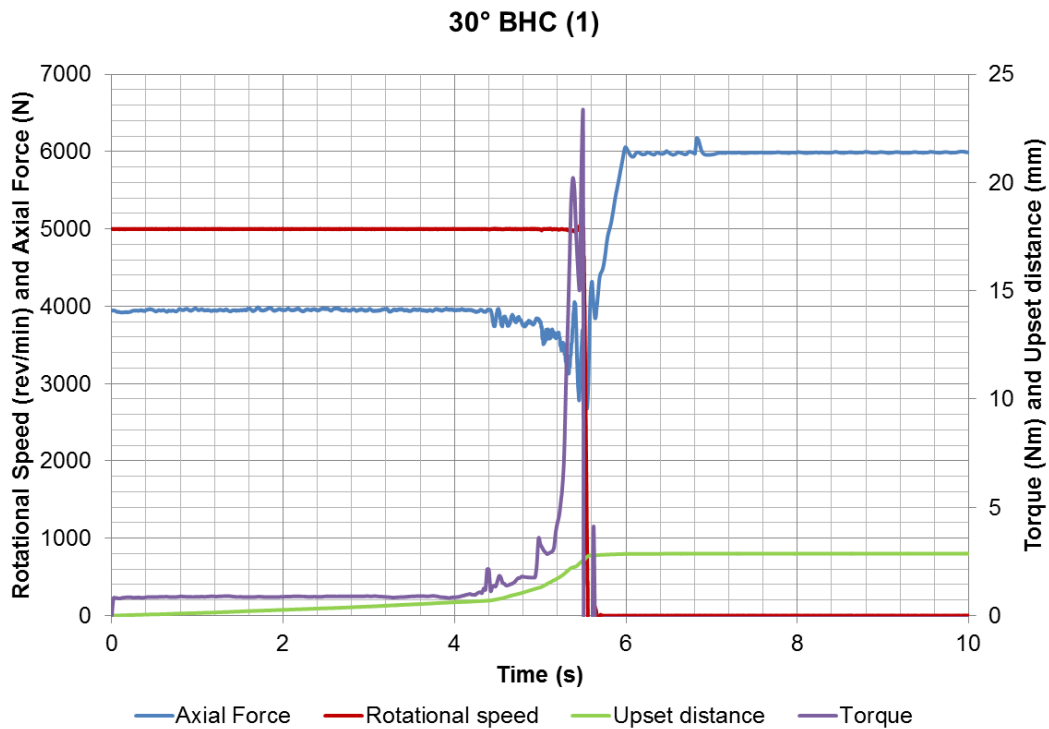
Joint description	Visual Image
15° Bottom hole chamfer	Shown in Table 4-3
30° Bottom hole chamfer	
45° Bottom hole chamfer	
BH 5000rev/min	

Appendix D: Process curves (15°, 30° and 45° joints)

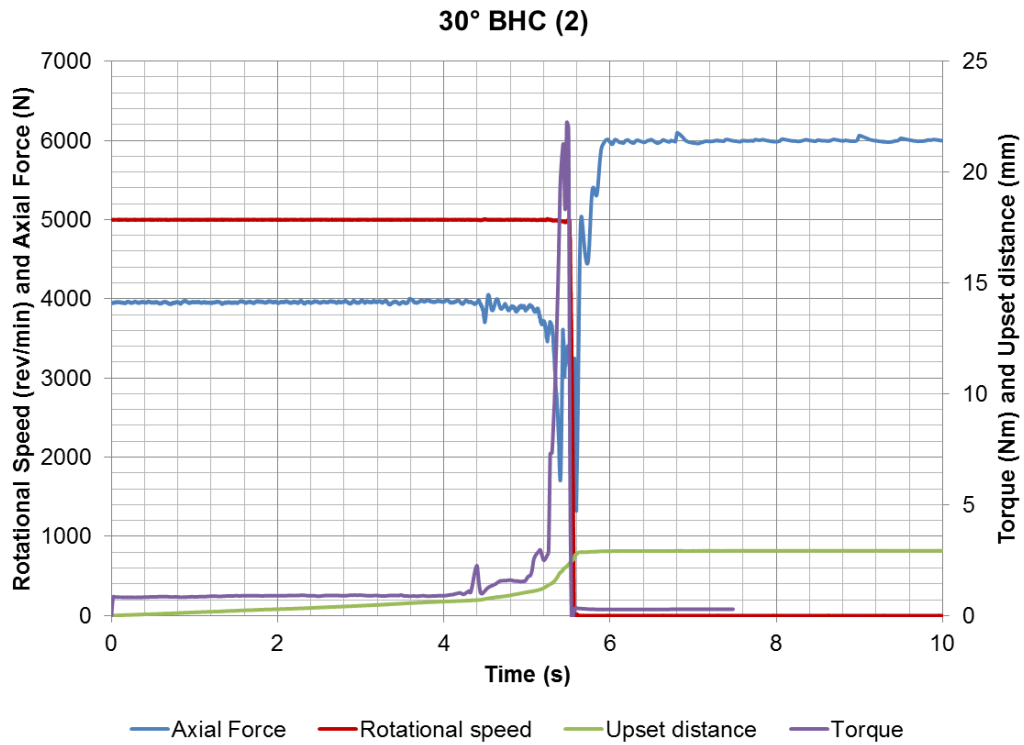
15° Bottom hole chamfer process curve (similar to that shown in Figure 4-3 (1) at the same process parameters)



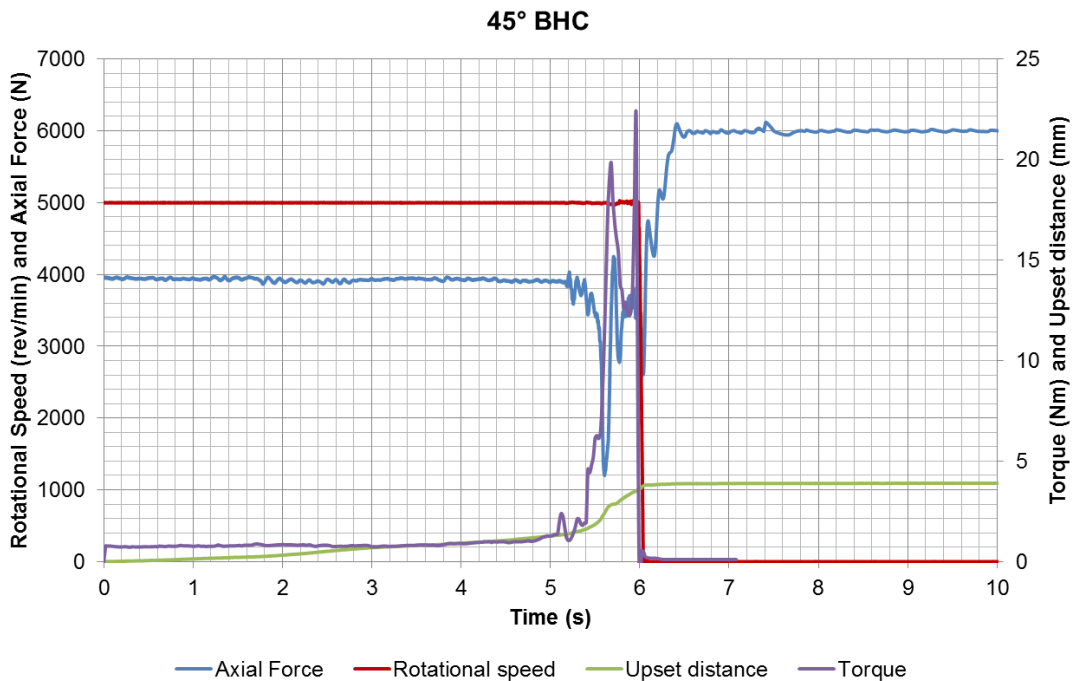
30° Bottom hole chamfer process curves



Appendices



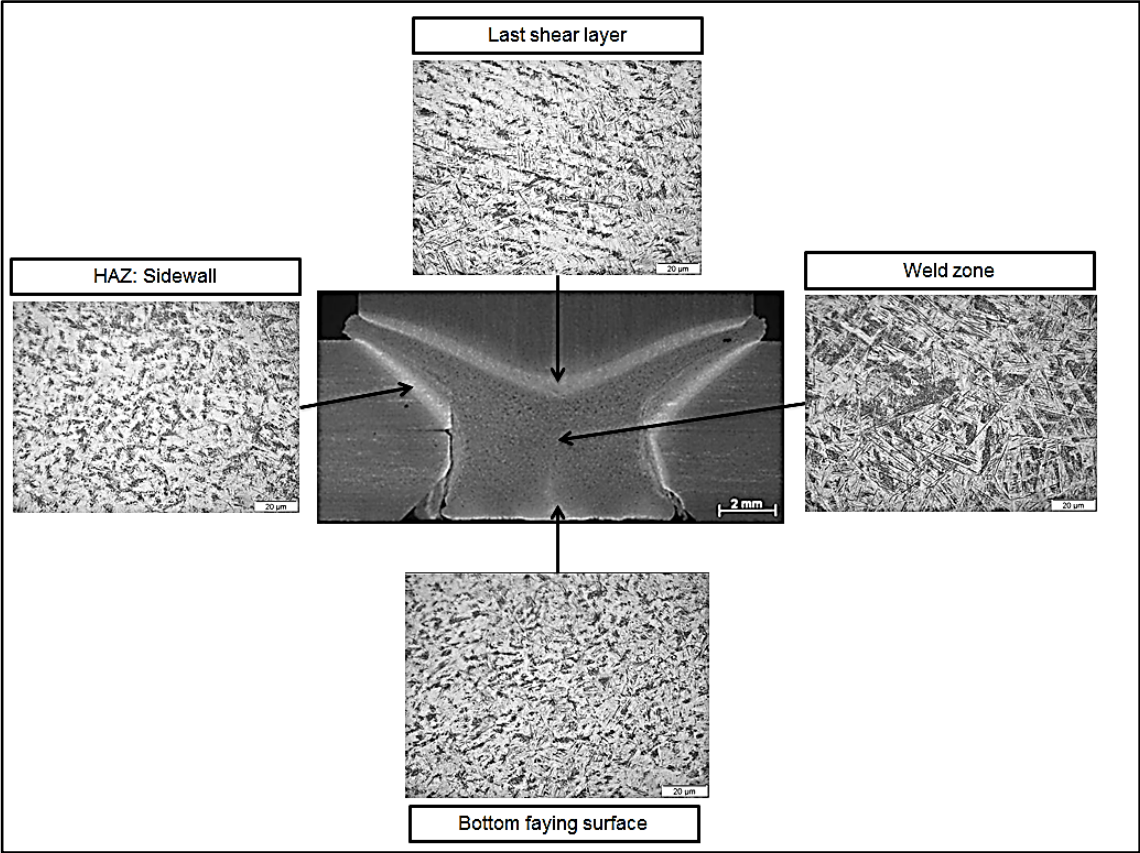
45° Bottom hole chamfer representative process curve



Note: The average feedback axial force and rotational speed was 4000N and 5000rev/min respectively at steady state.

Appendix E: Microstructure variation (30° and 45° joints)

30° Microstructure analysis



45° Microstructure analysis

